UCLouvain

École polytechnique de Louvain

Towards the design of a paper-based microfluidic sensor for water quality monitoring and comparative life cycle assessment

Author: **Odile CRAHAY**
Supervisor: **Jean-Pierre RASKIN**
Readers: **Karine GLINEL, Grégoire LE BRUN**
Academic year 2019–2020
Master [120] in Chemical and Materials Engineering

Acknowledgements

First, I wish to express my deepest gratitude to Grégoire Le Brun for his invaluable help and availability all year long. Thank you for your support and your enthusiasm. Many thanks also for your readings and interesting remarks.

I would like to thank my supervisor, Professor Jean-Pierre Raskin, for his attentive listening, advice and trust during this master thesis.

I also acknowledge Professor Karine Glinel for accepting to be part of my master thesis jury and for her precious help at the start of my lab work.

I would like to thank Audrey Leprince and Jacques Mahillon for the great and productive collaboration even tough it was cut short beyond my control. A special thank to Audrey for the relecture of the biological parts.

I would also like to thank Professor Tristan Gilet for his reading of the chapter dedicated to microfluidics and his helpful comments.

I wish to warmly thank Paul Rouster and Eléana Somville for their help and the many tips and advice during my lab work.

Many thanks to Margo Hauwaert without whom this master thesis would not have been so enriching thanks to our technical and friendly interactions.

Finally I would like to sincerely thank my family and my friends for their listening and continuous encouragements during this year. I wish especially to acknowledge my family for her support and great time together despite the lockdown.

Abstract

Point-of-care devices have the potential to revolutionize public health care in both developing and developed countries. In today's society, rapid, relatively inexpensive, disposable tests are becoming an important necessity, particularly for tracing the sources of infectious diseases. On the other hand, these devices can be a key to the development of developing countries where access to safe and sufficient water is not yet assured. In recent years, interest in point-of-care screening devices has increased and is expected to continue to grow, in particular due to changes in the need for health care.
The project that led to this master's thesis aims to create a prototype point-of-care screening device suitable for use in developing countries. This affordable, portable and sensitive biosensor will consist of a disposable paper-based platform that will allow microflow of a water sample and electrical detection of harmful *E. coli* bacteria. Although the detection of *E. coli* in a developing country is the intended application, these devices may have different uses. The emergence in 2019 of the new coronavirus disease (COVID-19) has highlighted one of them. The biosensor to be studied could meet the need for detection of various viruses in the coming years through appropriate modifications.

In this work the use of a nitrocellulose membrane as biosensor substrate for the detection of *E. coli* bacteria from a water matrix is discussed. It is conducted by the study of microfluidics in the nitrocellulose through a discussion of design parameters impact on the biosensor response, and by the introduction of membrane biofunctionalization by phage receptor binding proteins (RBPs) and cell binding domains (CBDs).
The test sensitivity is mainly affected by the capillary flow rate of the water sample at the specific test line location. Even if smallest pores sizes lead to a smaller flow rate, high ones allow an easiest displacement of target particles through the device so that this type of membrane should be preferred. The capillary flow rate could be controlled by adapted sudden change in the strip width.
The volume of analyzed sample is also a parameter playing a role on the sensitivity of the device. It is related to the void volume downstream the capture line and the addition of an absorbent pad (i.e. a chromatography paper) at the top of the strip can be used to increase the volume of sample flowing through the test line.
Nitrocellulose is of high interest as biosensor substrate thanks to its very good properties of immobilizing biomolecules. In this work the first biofunctionalization experiences are done with receptors specific to the *Bacillus* cereus group. This approach "proof-of-concept" highlights that phages RBPs and CBDs are good candidates to be used as bioreceptors.
The choice of the nitrocellulose support for microfluidics needs compared to the PDMS one is confirmed thanks to a comparative life cycle assessment (LCA) comparing their embodied energy and their carbon footprint.

Acronyms and abbreviations list

Ab	Antibody
Ag	Antigen
Al	Aluminium
ASSURED	Affordable, sensitive, specific, user-friendly, rapid and robust, equipment-free and deliverable to end-users
AuNP	Gold nanoparticle
BSA	Bovine serum albumin
CBD	Cell binding domain
CFU	Colony-forming unit
CN	Cellulose nitrate
COVID-19	Coronavirus disease 2019
DNA	Deoxyribonucleic acid
EAD	Enzymatically active domain
E. coli	*Escherichia coli*
EIS	Electrical impedance spectroscopy
ELISA	Enzyme-linked immunosorbent assay
Fc	Fragment crystallizable
GFP	Green fluorescent protein
gp	gene product
GWP	Global warming potential
Ig	Immoglobulin
IS	Immunochromatographic strip
LCA	Life cycle assessment
LC-PCR	LightCycler real-time PCR
LFA	Lateral flow assay
LOD	Limit of detection
Man/MUA	Mannose/11-mercapto eleven acid
MH/Au	6-mercapto hexanol/gold
MMA	Methyl methacrylate
NMO	Nanostructured metal oxide
OVA	Ovalbumin
PB	Phosphate buffer
PBS	Phosphate buffer saline
PCR	Polymerase chain reaction
PDMS	Polydimethylsiloxane
PEI	Polyethylenimine

PMMA	Poly(methyl methacrylate)
PoC	Point-of-care
RBP	Receptor binding protein
RH	Relative humidity
rms	root mean squared
rpm	revolutions per minute
SARS-CoV-2	Severe acute respiratory syndrome coronavirus 2
SCF	Spontaneous capillary flow
SPR	Surface plasmon resonance
TBS-T	Tris buffered saline-Tween
TENTC	Tris EDTA NaCl Tween Casein
WEEE	Waste of electrical and electronic equipment
WHO	World Health Organization
μPAD	Microfluidic paper-based analytical device
μPED	Microfluidic paper-based electrical device

Contents

1 Introduction **7**

2 State of the art **9**
2.1 Interest for point-of-care (PoC) devices . . . 9
2.2 Classical bacteria detection . . . 9
2.3 Biosensors for PoC bacteria detection in a liquid media . . . 11
2.3.1 Bioreceptors . . . 12
2.3.1.1 Types of bioreceptors . . . 12
2.3.1.2 Irreversible immobilization techniques of the bioreceptor . 15
2.3.1.3 Reversible immobilization techniques of the bioreceptor . . 16
2.3.2 Transducers . . . 16
2.3.3 Microfluidics interest in PoC applications . . . 19
2.3.4 Support materials review . . . 20
2.4 Paper as a support for microfluidic biosensor . . . 28
2.4.1 Paper . . . 28
2.4.2 Nitrocellulose . . . 34
2.4.3 Porous media theory . . . 36
2.4.3.1 Porous media definition . . . 36
2.4.3.2 Volumetric distribution of pores . . . 36
2.4.3.3 Stop threshold of a porous media . . . 37
2.4.3.4 Pressure drop - Poiseuille equation . . . 37
2.4.3.5 Young-Laplace equation . . . 38
2.4.3.6 Capillarity . . . 39
2.4.3.7 Darcy equation . . . 42

3 Objectives **43**

4 Materials and methods **46**
4.1 Simulations and modelisations on COMSOL . . . 46
4.1.1 Water flow in the porous media . . . 46
4.1.2 Water flow at the pores scale . . . 49
4.2 Experiments . . . 53
4.2.1 Comparison of different papers by the absorption of one water drop 53
4.2.2 Effect of pores size and strip geometry on capillary flow . . . 54
4.2.3 Characterization porous structure . . . 55
4.2.4 Deposition of fluometric RBPs/CBDs . . . 55
4.2.5 Interaction bioreceptors-bacteria . . . 58

5 Results and discussion **59**
5.1 Nitrocellulose as a microfluidic platform for biosensing applications 59
5.1.1 Choice of the microfluidic and absorbent substrate 59
5.1.2 Porous structure characterization and modelization 62
5.1.2.1 Porous structure characterization 62
5.1.2.2 Porous structure modelization 63
5.1.3 Parameters influencing the capillary flow 65
5.1.3.1 Mean pore radius 68
5.1.3.2 Relative humidity 72
5.1.3.3 Strip geometry 74
5.1.3.4 Absorbent pad 82
5.2 Nitrocellulose as substrate for biological detection 84
5.2.1 Biofunctionalization of nitrocellulose membrane 84
5.2.2 Binding affinity 86

6 General technical discussion **87**
6.1 Microfluidics guidelines 87
6.1.1 Nitrocellulose membrane selection 87
6.1.2 Strip geometry 88
6.2 Biofunctionalization guidelines 88
6.2.1 Capture reagent solution 88
6.2.2 Application of bioreceptors to the membrane 89
6.2.3 Fixation of the bioreceptors 89
6.2.4 Non-specific detection and adsorption 90

7 Towards the design of a sustainable sensor **91**
7.1 Responsible design 91
7.1.1 Introduction 91
7.1.2 Emergence of systemic research questions 92
7.1.3 Methodologies to guide a multidimensional analysis 93
7.1.4 Introduction to LCA 94
7.2 Comparative Life Cycle Assessment 96
7.2.1 Introduction 96
7.2.2 Goal and scope definition 97
7.2.3 Data inventory 98
7.2.4 Results and discussion 104
7.2.4.1 Polyester backing 104
7.2.4.2 Comparison nitrocellulose and PDMS microfluidic devices 105
7.2.5 Conclusions 109

8 Conclusions and perspectives **110**

Bibliography **112**

Chapter 1

Introduction

The assessment and management of water quality contributes to access to safe and sufficient water in developed countries. Meanwhile, the lack of scientific and technical progress in developing countries leads to serious problems due to water pollution, as rigorous water quality analyses are not easily carried out.
The project that led to this master's thesis aims to produce a prototype point-of-care device adapted to developing countries. This affordable, portable and sensitive biosensor will consist of a disposable paper-based platform that allows the microfluidic displacement of a water sample and the electrical detection of the harmful *E. coli* bacteria found in it.

Although the primary targeted application is the detection of *E. coli* in water, this test could have other uses. One specific use has been identified with the appearance in 2019 of COVID-19 caused by SARS-CoV-2 infection. The most effective way to contain the spread of this virus is to trace its sources. However, many carriers may be asymptomatic, so the entire population living in infected countries must be tested, which implies mass screening. This is very difficult because it takes time but also because there are not enough testing technologies available. This is where the biosensor under study could be useful because it could, with appropriate receptors, be able to detect the SARS CoV-2 in the sewage of local areas and thus minimize the risk of spreading the pathogen by monitoring the corresponding population [1].

The research is based on the understanding of the parameters impacting the biosensor response. This involves understanding the microfluidics on the porous paper-based support and its design parameters, as well as understanding the biofunctionalization allowing the capture of bioelements of interest from the water sample and understanding the electrical platform allowing accurate quantitative detection of harmful bacteria. Environmental, socio-economic and health impact assessments will be integrated in the design phase in order to optimize the device and its applications and to evaluate a multidimensional analysis.

This work will specifically focus on providing guidelines for the design of the microfluidic device and initiating the biofunctionalization of this medium with innovative bioreceptors. The introduction being the first chapter, the second chapter will introduce important concepts for the contextualization and understanding of the following chapters. To this end, point-of-care devices as well as classical methods for bacterial detection will first

be presented. Then, the use of biosensors for the detection of bacteria will be explained and described. This section ends with a review of several biosensor support materials in order to get a general idea of what can be done and to compare these materials using technical and sustainable criteria. Finally, the last section of the state of the art will go into more detail on paper as a support material for microfluidic biosensors. The choice of the support platform is based on paper materials mainly because of its wicking capability and because, compared to other materials commonly used for biosensor applications, they are more environmentally friendly. However, the nitrocellulosic paper membrane will be used because of its higher wicking performance and bioaffinity, making it more attractive than cellulose paper for this application.
After introducing the objectives of the master thesis in the third chapter, the fourth chapter will describe the materials and methods and the fifth chapter will present the results obtained from them. The sixth chapter will draw conclusions towards general guidelines for microfluidic biosensor prototyping.
While technical performance will be the focus of the first part of the work, the last chapter will focus on the environmental issue with the aim of developing an effective integrated solution offering both technical and sustainable performance. To this end, the final chapter will provide guidance based on a comparative environmental study of the manufacture of two different microfluidic devices.

Chapter 2

State of the art

2.1 Interest for point-of-care (PoC) devices

While infectious diseases are not a problem in developed countries thanks to scientific and technical progress, they nevertheless pose many problems in developing countries, particularly because of bacterial pollution of water. There are various reliable methods for detecting bacteria in water samples, such as colony counting, polymerase chain reaction (PCR) and enzyme-linked immunosorbent assay (ELISA), which are briefly described in Section 2.2. However, developing countries lack the basic resources and well-equipped laboratory facilities needed for these diagnostic methods. In addition, these techniques are relatively expensive and are not suitable for such conditions.
This is where Point-of-Care devices (PoC) come in. Criteria for point-of-care detection devices suitable for these uses have been listed by the World Health Organization. This list is often known by the abbreviation "ASSURED": affordable, sensitive, specific, user-friendly, fast and robust, without equipment and delivered. In light of these guidelines and the critical area of water management, the Section 2.3 presents the biosensors that respond to these guidelines by offering the possibility of rapid and cost-effective bacterial detection at the point of use, particularly through the use of microfluidics.

2.2 Classical bacteria detection

The detection of pathogens is one of the most important keys to water treatment, alongside other typical water pollutants such as inorganic species and organic chemicals. The relevant legislation is strict because in certain circumstances the failure to detect critical pathogenic bacteria can lead to serious problems in the area of public health and safety. The main areas in which the detection of harmful bacteria is of great interest are, in order of importance, the food industry, the clinical field and the monitoring of water quality and the environment.
Of all the microorganisms detected, Salmonella and *E. coli* account for more than 50% of the distribution of the number of articles published in the literature .

Several methods have been implemented for the detection of bacteria. Among them, the most common are colony counting, polymerase chain reaction (PCR) and enzyme-linked

immunosorbent assay (ELISA) methods [2]. (see Table 2.1). Culture and colony counting methods do not require advanced equipment. They consist of a selective growth medium that detects specific bacteria, followed by direct counting by ocular inspection or other optical methods such as microscopic counts using a hemocytometer or counting chamber [3]. The PCR method is a technique based on different DNA amplification cycles (see Figure 2.1) [2] .

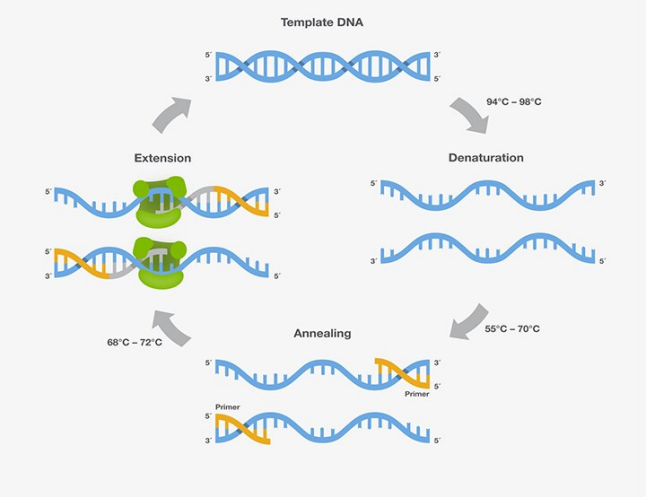


Figure 2.1: Illustration of the main steps in PCR: denaturation, annealing, extension to amplify target sequence from a template DNA [4].

The DNA sequence comprising the genetic material of the target bacterium is first denatured by heat. Then specific primers recognize the DNA strand and are added during the annealing step and finally the DNA strands are extended by polymerization. Then the amount of amplified sequence can be detected by gel electrophoresis. Among the different PCR methods, multiplex PCR allows the simultaneous detection of several organisms. The greatest disadvantage of PCR methods is that they do not differentiate between viable and non-viable cells.

The most common ELISA test is the sandwich ELISA [2]. It consists of four main steps: immobilisation of the antigen-specific antibody on a substrate ("capture antibody"), addition of the antigen (target bacteria), addition of the enzyme-labelled antibody ("detection antibody") and finally introduction of the enzyme substrate and appearance of the stained product (see Figure 2.2).

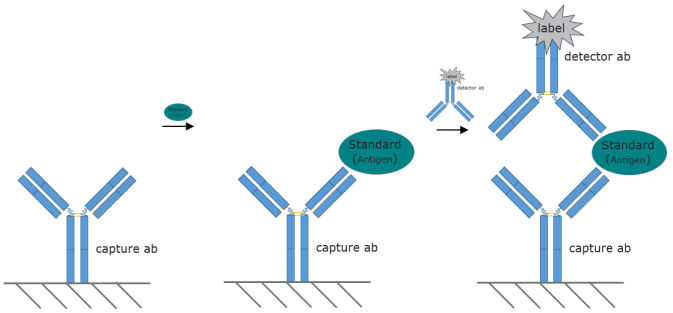


Figure 2.2: A representative image of the Sandwich format ELISA. The sandwich format is so named because the analyte is "sandwiched" between a capture and detection antibody [5].

These last two techniques can also be coupled with others giving other methods such as PCR-ELISA and LightCyber real-time PCR (LC-PCR) [2].

The Table 2.1 groups these three traditional detection techniques and their main parameters for *E. coli* detection. However, even these popular methods are sufficiently sensitive and are capable of detecting different bacteria depending on the detection technique used, they are time-consuming. This is the main reason why biosensors have become increasingly important in the field of pathogen detection in recent years.

Table 2.1: Traditional detection techniques for E. coli [2][6][7].

	Limit of detection [CFU mL^{-1}]	Response time	Cost
Culture and colony count	Low CFUs	Several days	Low
PCR	$\sim 10^3$	Approx. $>$ 2 h	High
ELISA	$\sim 10^3$	$\sim$ 1 day	Medium

2.3 Biosensors for PoC bacteria detection in a liquid media

Biosensors are powerful and innovative devices used to convert biological reactions into measurable signals to detect target analytes. The ELISA technique, briefly described in the Section 2.2, is the inspiration for many of them, so that the common principle of a biosensor is similar to that of its sandwich analysis. The block diagram of a biosensor is presented on Figure 2.3, it consists mainly of two parts, namely the sensory layer or bioreceptor layer and the transducer. The recognition element of a biosensor is generally referred to as the bioreceptor. Bioreceptors are usually enzymes or antibodies and are immobilised on support materials to use their ability to recognise the target compound

present in the so-called matrix. The transducer is then used to convert the signal resulting from this interaction into an observable signal [8].

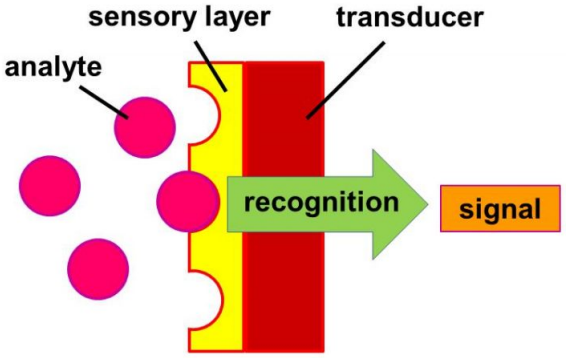


Figure 2.3: Block diagram of a biosensor [9].

Biosensors are used in various fields such as medicine, environment, industry, but much research is still being done. An important application is the detection of critical pathogens. For this purpose, several other methods have been implemented, such as colony counting, PCR and ELISA methods. These traditional techniques are discussed in Section 2.2. As already mentioned, biosensors have reached an important place in the field of pathogen detection because of their ability to solve the problem of the slowness of existing methods (discussed in Section 2.2), but they are also very promising for their sensitivity, selectivity and compactness [2].

2.3.1 Bioreceptors

The biological recognition element of a biosensor is generally referred to as a bioreceptor. Its role is to functionalize the support and catch the targeted molecule. It must therefore demonstrate a high selectivity for the specific analyte among other species that may be included in the sample matrix. Biosensors can use several mechanisms for biological signalling. These can be classified according to the group of recognition elements: enzymes, antibodies and antigens, nucleic acids (DNA), cell structures or whole cells and biomimetic receptors [2][10][11].

Bioreceptors can be attached to the substrate in different ways. The most commonly used immobilization techniques are covalent binding, cross-linking, trapping, adsorption and affinity binding.

2.3.1.1 Types of bioreceptors

Proteins

Phage proteins: Bacteriophages are viruses capable of infecting bacteria. They are usually able to infect a single bacterial species or a few strains. Phages produce a wide number of proteins with potential in biotechnology applications such as biosensors. The two most promising proteins are the Receptor Binding Protein (RBP) and the endolysins.

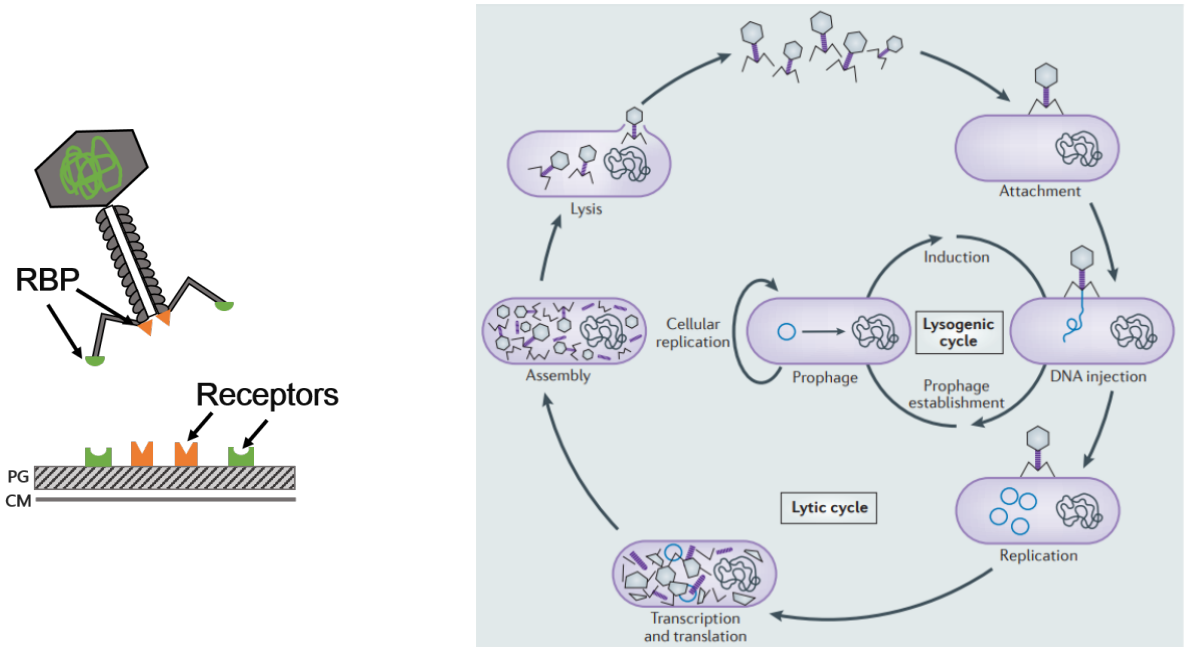


Figure 2.4: Left: Recognition bacteria by RBP [12]. Right: schematic representation of phage life cycles [13].

The life cycle of phages is represented on the right side of the Figure 2.4. The process of infection begins with the recognition of bacteria. This involves the irreversible binding of RBPs to specific bacterial receptors. This process takes place in several steps. First, random collisions occur between the phage and the host, then the phage reversibly binds to the bacterial surface and finally irreversibly binds to the bacterial receptors. Once this adsorption step is complete, phages can infect bacteria by injecting their genetic material into the host.
RBPs are proteins that allow infection of host cells through recognition of certain bacteria. Recognition is based on specific interactions between the phage RBP and host surface receptors (see the left side of Figure 2.4). RBPs can therefore be used as biosensors to detect bacteria by allowing specific immobilization.

This immobilization is governed by the specificity of the RBP but also by the host's receptors. The latter differ according to the type of bacteria, which can be Gram-positive or Gram-negative. These two bacteria can be distinguished by the difference in thickness, uniformity and lipid/lipoprotein content of their cell wall but their main difference is that Gram-negative bacteria have an external membrane while Gran-positive bacteria do not.

Endolysins are involved at the end of the phage cycle to lyse bacteria and liberate new produced virus. An endolysin is composed of two parts, the enzymatically active domain (EAD) having the lytic activity or the cell wall binding domain (CBD) responsible of the binding to the inner wall of the bacterium.
Endolysin is expressed only after a number of new virions are reached in the cell during the lytic cycle. Through degradation of the peptidoglycan layer, endolysins allow the release of new virions which then infect other bacterial cells (see the right side of Figure 2.4). The CBD then confers specificity to endolysins by recognizing and binding to ligands within the cell wall. Therefore, it is also an interesting candidate as a bioreceptor element [14].

Pathogen detection platforms typically use antibodies as bioreceptors. However, these offer biosensors with a lack of specificity, low separation efficiency and low sensitivity. In addition, their production is long, expensive and laborious and their activity may be lost due to changes in environmental conditions. Thanks to their properties described just before, tail proteins from bacteriophages may be an alternative. They have in fact been positively compared to antibodies and appear in various articles, cited in [15].

Antibodies and antigens: Antibodies (Ab) are Y-shaped proteins, also known as immoglobulins (Ig). They are produced primarily by plasma cells used by the immune system to neutralize pathogens. An antibody is specific by its variable part capable of binding to the corresponding pathogen through a single molecule called antigen [16][10]. The recognition step of this type of biosensor is therefore based on the specificity and high affinity between the antibody and the antigen.
The antibodies can be monoclonal, polyclonal or recombinant depending on their mode of synthesis and their selective properties [2]. For example, O157:H7 monoclonal antibodies are selective for *E. coli* [17].

Antibodies are widely used as recognition elements in biosensor applications, such as in the well-known lateral flow assay (LFA) where they can have two different functions. They can have a capture role and biofunctionalize the carrier to attach the target element to a specific capture line [18] and they can also be used as detection antibodies and be attached to colored nanoparticles (i.e. AuNP on Figure 2.5). This is the case with colorimetric tests where the molecules to be detected are made visible by being attached to the detection antibodies [19][20]. Both antibodies can naturally be present in the same GLA.

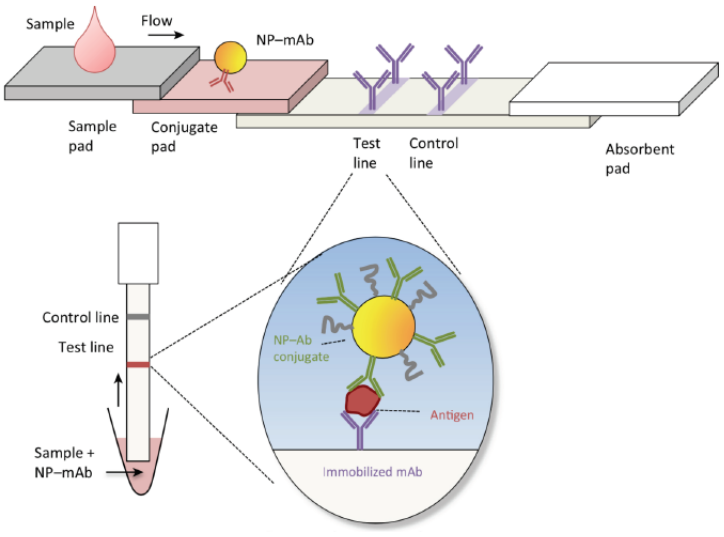


Figure 2.5: Both functions of antibodies (capture antibody in purple and detection antibody in green) used in a LFA [21].

Enzymes: Enzymes are defined as proteins that catalyze specific chemical reactions and are therefore very effective biocatalysts. They can be used by different mechanisms. In fact, this type of biosensor can recognize the analyte either by the conversion by the

enzyme of the target analyte into a product detectable by the sensor, or by the detection of an analyte acting as an enzyme activator or inhibitor, or by monitoring changes in the properties of the enzyme resulting from the interaction with the analyte [11]. However, enzymes tend to be used more often as markers than as recognition elements [2].

Nucleic acids
In the case of using the nucleic acid sequence as a bioreceptor, the recognition process is based on the highly specific affinity between complementary pairs of single strands of DNA (adenine:thymine or cytosine:guanine) [10][11]. Thus, if the target nucleic acid sequence is known, the corresponding sequence can be immobilized on the sensor.

Cells
Whole living cells or specific cell components (e.g. a non-catalytic receptor protein) can also be used as biorecognition elements because they are easily immobilized on the surface and are capable of detecting microenvironmental conditions or physiological parameters and can respond to several types of stimulants [11]. The main disadvantage of the cellular biosensor is that many conditions must be met in order for the cell to remain stable and alive [10].

Biomimetic receptors
The principle of this type of receiver is to artificially imitate a bioreceptor. For this purpose, receptors can be for example artificial membranes, aptamers or genetically modified molecules [11][10].

Others
Another detection surface tested is Man/MUA-MH/Au. This biologically active sable surface is prepared by immobilizing modified phenyl mannose molecules on the surface of the gold electrode, which has been modified by a self-assembled monolayer of 11-mercaptoalkanoic acid. and 6-mercapto hexanol. This method was specifically implemented for S. typhimurium because of its higher adsorption capacity for this surface [22].

2.3.1.2 Irreversible immobilization techniques of the bioreceptor

Covalent binding
The covalent bond between the support and the biomolecule is the most widely used and is generally irreversible due to the stable nature of the bonds. The covalent bond is made by functional groups in enzymes that are not essential for their catalytic activity. Usually the nucleophilic functional groups of the amino acid side chains, such as hydroxyl, amino, carboxylic and thiol groups, are used for the binding of antibodies or enzymes. By using surface active materials, such as dextran, gels or glass, the amino acid side chains can be covalently bound. Support materials have also been activated to allow covalent immobilization of a biomolecule using crosslinkers [8].

Crosslinking
Crosslinkers with reactive free ends are used to form covalent bonds that are strong and can anchor biomolecules to the substrate surface. When cross-linking is used, the bioreceptor must be bound without significantly affecting its conformation, as even slight modifications

can affect the binding of a ligand to a protein. The substrate material is not an absolute requirement in cross-linking (carrier-free technique) [8].

Entrapment
This method of physical immobilization uses a network of polymer gels prepared in a solution containing biomolecules. The structure is designed to retain the enzyme inside while allowing the substrate and products to pass through. Usually the enzyme is not attached to the support material in this method, unlike covalent bonding. Entrapment is primarily used when cells or cellular organelles are used. Passive trapping of cells in the pores of membranes made of cellulose or other synthetic materials is a well-known approach. Another common approach is to hold cells or enzymes in close proximity to the transducer surface using a dialysis membrane [8] .

2.3.1.3 Reversible immobilization techniques of the bioreceptor

Adsorption
This is the simplest method of immobilization, which involves bonding biomolecules to surfaces using hydrogen bonds, Van der Waal forces, multiple salt bonds and the formation of electron transition complexes. Many macromolecules such as cellulose, collodion, silica gel, glass, hydroxyapatite and collagen have the ability to adsorb enzymes. In addition to these macromolecules, synthetic polymers such as polyaniline, polyethyleneimine (PEI), polypyrrole and polystyrene can be used separately to glue biomolecules. Enzymes and antibodies are usually immobilized by adsorption prior to cross-linking [8].

Affinity binding
This method of immobilization involves non-covalent interactions that depend on the creation of affinity bonds between the activated support and a specific group of the protein sequence. The natural affinity relationship between biomolecules such as lectin and sugar and antibody and antigen can be used in the immobilization. The best known procedure in this method is the streptavidin-biotin interaction which leads to one of the strongest non-covalent formations. Another procedure is the formation of affinity interactions with a protein specific to the Fc regions of an antibody such as protein A or G [8].

2.3.2 Transducers

The transducer is the component of the biosensor that converts the bioreceptor-target molecule interaction into an output in the form of a measurable signal that must be proportional to the presence of the target analyte. The type of transduction method applied may, as a class of bioreceptor, categorise the biosensor. The three main types are optical, mechanical and electrochemical biosensors.

Optical
Optical biosensors are the most popular in bioanalysis because of their selectivity and sensitivity, but this type of signal also allows for quick and easy detection . However, its main disadvantage is that it is not very quantitative.
Fluorescence-based biosensors can be distinguished from those not labeled [23]. Fluorescence and surface plasmon resonance are respectively the most popular in these classes.

The detection method of the first class is based on the change in fluorescence of the substrate. Fluorescence is the excitation of a valence electron from its ground state to a singlet state excited by an external light source [2]. After excitation, the electron immediately returns to its initial position by emitting a lower energy photon which gives the fluorescent light. To observe this phenomenon, fluorescent markers must be added to the sample, which can be costly but also time-consuming because these compounds must be conjugated with the detection elements. Fluorescence can be integrated into fiber optic biosensors [10].

Surface plasmon resonance resonance (SPR) is a non-labelled optical method that detects changes in surface electromagnetic waves as the target molecule interacts with the biorecognition element. (see Figure 2.6). To do this, the system comprises a source of plane polarized light passing through a prism and the SPR transducer is included in the biorecognition element, so that when the interaction occurs, the refractive index at the sensor surface changes. This change induces a variation in the propagation of the surface plasmon wave which is measured by a spectrophotometer. Its sensitivity is generally low and it requires specialized personnel, but its main advantage is the ability to perform real-time measurements as it does not require any fluorescence or radioactivity [10][23].

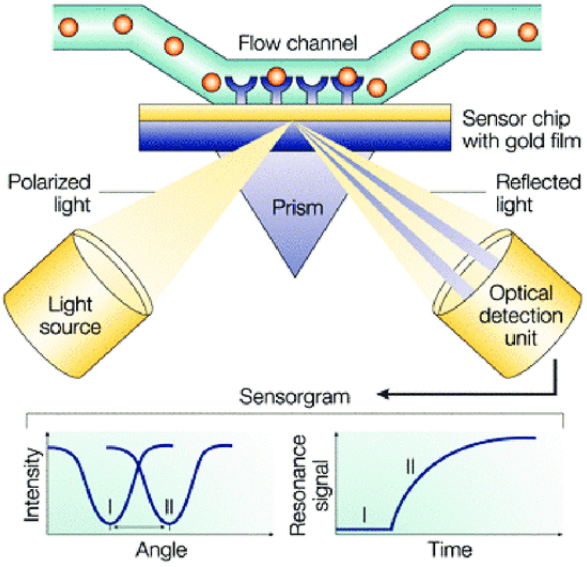


Figure 2.6: Surface plasmon resonance (SPR) [24].

Mechanical

The mechanical biosensors do not require sample processing or reagent addition, which allows fast processing [23]. Labelless piezoelectric biosensors and labelless microcantile biosensors are the two main categories.

The piezoelectric effect applied to biosensors works mainly on the principle that an oscillating crystal resonates at a natural resonant frequency [10].
The biosensing material is the transducer and consists of a piezoelectric material (usually quartz) vibrating at a natural frequency. The frequency is controlled by an external electrical signal producing a certain current. When the target analyte interacts with

the sensor surface, it changes the frequency, which changes the value of the current in proportion to the mass of the analyte.

Cantilevered sensors are also based on the change in frequency. In this case, the bioreceptor is a microcantilever oscillating at a certain resonant frequency and this frequency will change due to an increase in mass on the sensor surface [10].

Electrochemical

There are different types of electrochemical sensors such as potentiometric, amperometric and impedimetric sensors, but in all these cases, the transducer is an electrode and the current produced by the recognition of the analyte is proportional to its concentration [23]. This method has many advantages such as speed, simplicity, low cost and high sensitivity [10].

The **Potentiometric** biosensor uses ion-selective electrodes to measure the change in potential when the target molecule is recognized on the electrode surface and involves the enzyme-catalyzed reaction. This reaction either consumes or generates a substance detected by the electrode [2]. This method, with the exception of some innovative applications, is not able to provide specific signals for large analytes such as bacteria [23].

The **Amperometric** sensors measure the current generated by the oxidation-reduction of the species produced by the analyte-bioreceptor interaction.

Finally, **Electrical Impedance Spectroscopy** (EIS) was not often used in electrochemical detection, but it has become popular because it is cheaper than other methods, easily miniaturized, reagent-free and label-free unlike amperometry and potentiometry [10]. In addition, it allows the detection of bacteria from whole cells and is less destructive for biological and chemical analysis. These biosensors detect the change in impedance of the medium due to the binding of the analyte between the two electrodes. Its principle is schematized on Figure 2.7.

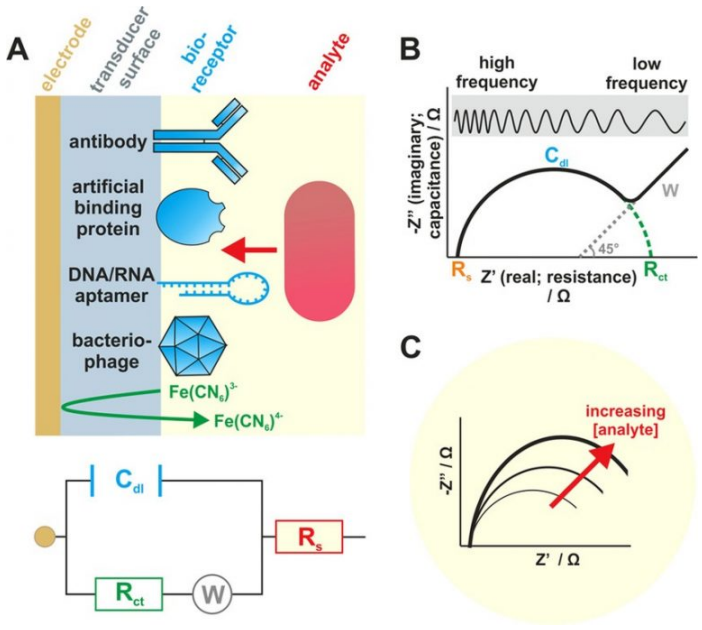


Figure 2.7: Electrochemical impedance spectroscopy principle [9]. At a specific frequency, the bacteria medium responds to the applied signal and an increase in the medium capacitance is observed. The magnitude of the capacitance change depends on the bacteria concentration.

2.3.3 Microfluidics interest in PoC applications

The market for microfluidics has been highly developed over the past decade but is not yet widely adopted, mainly due to the complexity and cost of these technologies. However, this market is expected to grow due to the multiple advantages of microfluidic devices, the growing interest in polymer uses and the increasing investments in the field that will lead to the increasing adoption of this technology in the years to come [25].

Microfluidics refers to the manipulation, control and behaviour of fluids contained in very small scale. In microfluidics devices, only small volumes are involved, typically femto to microliter, and the properties of the fluid are of great importance as they are not negligible compared to the small system. Today, many fields use this type of technology, such as engineering, physics, chemistry, biochemistry, nanotechnology and biotechnology. This is not surprising because its advantages are particularly relevant today. Its small size allows for a significant reduction in material and reagents and can therefore lead to lower costs and less environmental impact. Another positive point is the precision and selectivity of these devices, which can reach a high level. In addition, the time needed to obtain certain results or products can be reduced. Finally, microfluidics allow a high portability of the devices and therefore facilitate diagnosis and analysis in complex situations such as field actions or continuous monitoring of patient health. All these features make microfluidics of great interest in the field of PoC devices by meeting ASSURED criteria.

Microfluidics can be divided into different sub-domains according to the small-scale fluid behaviour. The three main ones are droplet microfluidics, flow microfluidics and open microfluidics.
Droplet microfluidics uses droplets in a filling medium. They are considered as an

independent sample where the reactions triggered remain encapsulated within it [26]. Figures 2.8 and 2.9 illustrate these two first sub-domains of microfluidics.

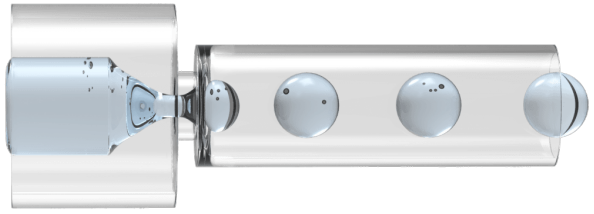


Figure 2.8: Generation of controlled size microfluidic droplets in a glass microfluidic chip by regulating the pressure rate and/or by regulating the flow rate [27].

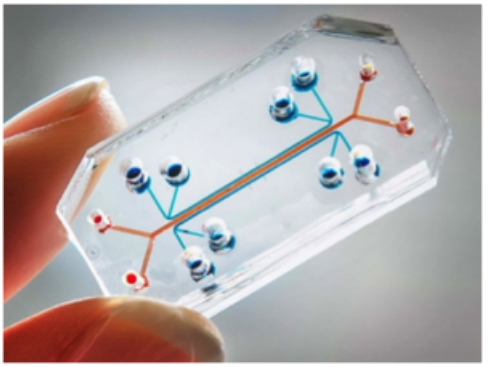


Figure 2.9: PDMS microfluidic device for microflow [28].

Open microfluidics is the field of interest of this master thesis because the flow of fluids in a porous medium with a capillary as the main small effect acting on the fluid will be studied (see illustration on Figure 2.10).

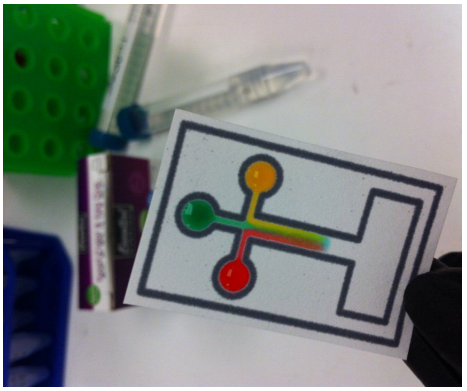


Figure 2.10: Paper-based microfluidic device [29].

The main methods of fluid transport in microfluidic channels are pressure flow, electrokinetic flow and fluid transport created by motor proteins [30]. Only when capillarity occurs is no additional micropump or electric field required.

2.3.4 Support materials review

The project aims to develop a PoC biosensor with good technical and durable performances. Different materials can be used to meet the needs of biosensors, namely biological materials for the immobilization of bioreceptors, electronic materials for the transduction method, in particular EIS, and microfluidic materials. In light of these criteria required for the specific application and in order to justify and identify the most attractive choice, this section reviews the different support materials.

In an electronic device, the substrate is used to support the other compounds. To fulfill this role, it usually has to be thicker and larger than the other functional components and therefore generates more waste. Because of the ultimate goal of this project, which is to create a single-use biosensor, its overall environmental impact as well as its price will be an important part of the project.

The biosensor aims to monitor water by capturing *E. coli* bacteria. To do this, the antigens must first be immobilized on the substrate before the focused bacteria can be fixed. The substrate should therefore be inert against the biomolecules used but biocompatible. The immobilization of biomolecules can be achieved using different techniques but in each of them they will bind to the functional groups of the support material, which should then contain easily modifiable groups [8].

The Tables 2.2, 2.3, 2.4 and 2.5 bring together information from the examination of the support materials according to several properties and factors for each of the main aspects, namely microfluidics, bioaffinity, electronic integration and environmental impact. These properties are listed and their role and importance are briefly described below.

- Microfluidics integration allows the flow of fluid into the biosensor.
  - Microfluidic manufacturing: by channels creation or by using the wicking ability of the material.
  - Optical properties: to make easy the monitoring (fluid imaging, fluorescence detection).
  - Mechanical properties: will impact the fabrication and the use of the biosensor.
  - Depth-to-width aspect ratio: important parameter to control design of flow channels and make them collapse-resistant after fabrication. A general rule is to stay above a low aspect ratio 1:10 (height:width) and a high aspect ratio below 4:1 [31].
  - Cost of material and manufacturing.
  - Young Modulus: high value means high rigidity.
  - Smallest channel dimension: characterizes what precision is possible to get.
  - Contact angle with water: characterizes the hydrophilicity.
- Bioaffinity allows the immobilization of biological elements for identification of the target molecule.
  - Biocompatibility of the material.
  - Specific area: influence the available surface for bioelements adsorption.
  - Pore diameter/porosity: percents of air present in the porous structure. Influence the movement and diffusion of biomolecules in the sensor.
  - Permeability to oxygen.
- Electronics integration.

  - Surface properties: important properties for printing.
  - Surface roughness rms: influence the printing resolution and easiness.
  - Compatibility with organic solvents.
  - Conductivity.
  - Dielectric constant: the ratio of permittivity of the substance to permittivity of the free space.
- Environmental impact.
  - Water consumption.
  - CO_2 footprint.
  - Biodegradability.
  - Recyclability: end of life strategies.
  - Embodied energy.
  - Ressources toxicity.
  - Scarcity.
  - Eutrophication/acidicification.

Table 2.2: Summary table for support materials - Microfluidics integration.

	Microfluidics integration							
Material	Microfluidic manufacturing	Optical properties	Mechanical properties	D/w aspect ratio	Cost material and manufacturing	Young Modulus [GPa]	Smallest channel dimension	Contact angle with water
Amorphous thermoplastics (ex: PMMA)	Simple thermoforming of channels: hot mold pressure, fast embossing or laser cutting [32] [33]	Excellent optical transmissivity in the visible range [34]	Rigid, high stiffness	Higher than PDMS, collapse-resistant channels [35]	Cheap material and manufacturing [32]	1.4-4.1 [36]	$\sim$ 100 nm [36]	Hydrophilic, $\sim$ 68° [37]
Thermosetting polymers (SU-8)	Patterning of channels by photolithography (time consuming) [35]	Very high optical transparency above 360 nm [38]	Rigid [35]	High shape factor [35]	Cheap material but not cheap microfabrication [32][35]	2.0-2.7 [36]	$<$ 100 nm [36]	Not highly hydrophilic, $\sim$ 79° [39]
Elastomers (PDMS)	Mainly casting (fast), possible hybrid structures, surface modif. needed if water [35][40][41][42]	Excellent optical transmissivity in the visible range, low fluorescence [30][34]	Elasticity [34][30]	Channels deformation issues [34][30]	Material $\sim$ 50 times more expensive than PMMA [34][30]	$\sim$ 0.0005 [36]	1 μm [36]	Hydrophobic, $\sim$ 110° [43][44][45]
Glass	Mostly bulk micromachining (complex and time consuming), possibility of sealing with other materials, hard integration of pumps/valves [35][32][41][46]	Optically transparent and low autofluorescence [47]	Rigid, brittle, thermal insulator [47][35]	High d/w ratio [32]	Expensive material and fabrication [32]	50-90 [36]	$<$100 nm [36]	Hydrophilic, $\sim 30-35°$ [48][49]
Silicon	Mostly bulk micromachining (complex), hard integration of pumps/valves [42][35][46]	Optically opaque [42]	Hardness (11.5 GPa), brittle, light [42][50][51]	High shape factors [32]	Expensive material and fabrication [32]	130-180 [36]	$<$100 nm [36]	5-96° [51]
Porous silicon	Channels creation or membrane fabrication (complex) [52]	Special opticophysical properties as luminescence [53]	Much lower hardness (0.2-10 GPa), slowly dissolvable in aqueous solution (fixed by oxidation process) [53][52][51]	High surface to volume ratio (pores) [53]	Quite inexpensive preparation from bulk silicon [53]	$\sim$ 1˘100 [54][51]	$\sim$ 100 nm [55]	Strongly dependent on pore sizes (smaller pore size lead to smaller contact angles), $\sim 20-140°$ [56]
Metals (ex: aluminium, NMOs)	Easy micromachining and cleaning of channels (Al) [57], nanoporous alumina by anodization[58]	Optically opaque	Excellent mech. prop., good thermal conductivity, resistant to organic solvents (Al) [57]	High surface to volume ratio (NMOs) [59]	Increases exponentially with design complexity	69 (Al) [60], different depending on NMO material [61]	Small	Hydrophilic, 35-45°(Al) [62]
Textile	Wicking ability, easy manufacturing [63][64]	Opacity depends on weaving	Flexible, wearability [47][63]	No need of patterned hydrophobic barriers [64]	Cheap manufacturing [64]	$\sim$ 3 [65]	/	Hydrophobic, $\sim$ 135° (coton) [66] [67]
Paper	Wicking ability, hydrophobic/hydrophilic channels creation [47][68][69][21]	Opacity depends on pulping process but low optical transparency [70] [36]	Flexible, light weight [47][68]	High surface to volume ratio [71]	Cheap[68]	0.0003-0.0025 [36]	$\sim$ 200 μm [36]	Strongly depends on time because of water affinity [72]
Nitrocellulose	Wicking ability, hydrophobic/hydrophilic channels creation (mostly by wax patterning), resolution 100 μm [73]	Idem than paper	Flexible, light weight [47][68]	High surface to volume ratio [71]	Inexpensive fabrication [73]	$\sim$ 0.00045 [74]	$\sim$ 60 μm [75]	Hydrophilic, $\sim$ 70° [76], strongly depends on time because of water affinity [72]

Table 2.3: Summary table for support materials - Bioaffinity.

	Bioaffinity			
Material	Biocompatibility	Specific area $[m^2/g]$	Pore diameter/Porosity	Permeability to oxygen [Barrer]
Amorphous thermoplastics (ex: PMMA)	For many biomolecules and cells [34][47]	Microchannels will define the allowed size of flowing molecules	No porous structure, microchannels will define the allowed size of flowing molecules	0.05-5 [46], 4.31-7.19 $(cm^3 \times mm)/(m^2 \times day \times atm)$ [EduPack]
Thermosetting polymers (SU-8)	Yes [77]	Idem	Idem	0.03-1 [46]
Elastomers (PDMS)	With many biomolecules [40][47]	Idem	Idem	∼500 [46]
Glass	With most biological samples but no long term adsorption [42][36]	Idem	Idem	<0.01 [46]
Silicon	Yes [50]	Idem	Idem	<0.01 [46]
Porous silicon	High biorecognition by surface modifications, high surface reactivity especially by adsorption [53]	100–800 [51]	2-50 nm / 20-95% [51]	
Metals (ex: aluminium)	Ability to bind biomolecules by physical adsorption or chemical binding (NMOs) [59]	Microchannels will define the allowed size of flowing molecules	No porous structure, microchannels will define the allowed size of flowing molecules	~ 0 (Al) [78]
Textile	Yes [64]	/	/	High
Paper	Yes [21] [68][79]	Very depending on refining [80]	15-70% [81][80], depending on refining	> 1 [46]
Nitrocellulose	Yes, very good bioimmobilization properties [73][82]	Idem, surface area ratio 50-200 [83]	70-80% [83]	High

Table 2.4: Summary table for support materials - Electronics integration.

	Electronics integration					
Material	Surface properties	Surface roughness rms [μm]	Compatibility with organic solvents	Conductivity [S/m]/ Resistivity [Ωm]	Dielectric constant [/]	Other
Amorphous thermoplastics (ex: PMMA)	Suitable for printed electronics [47], good surface properties, can bond well with adhesive [34]	$\sim 1.5 * 10^{-3}$ (untreated PMMA) [84]	Medium to high [36]	(pure PMMA) $10^{-18} S/m$, insulator [85], $> 2 \times 10^{15} \Omega cm$ [86]	3.2-3.4 [EduPack]	Deposed metal films can fractured easily because of its flexibility [35]
Thermosetting polymers (SU-8)	Suitable for printed electronics [47], good compatibility with electrodes integration [35][38][87]	$\sim$ 0.7 [88]	High [36]	$10^5 - 10^{14} \Omega cm$ [EduPack]	4-6 [EduPack]	/
Elastomers (PDMS)	Suitable for printed electronics [47], hybrid structure with glass can offer easy metal deposition possibility [40]	$\sim 5 * 10^{-3}$ [89]	Low [36]	Non-conducting material, $4 \times 10^{13} \Omega m$ [90]	2.3-2.8 [45]	Deposed metal films can fractured easily because of its flexibility [35]
Glass	Good compatibility with microelec. processes (easy metal deposition) [35][32][42]	$\sim 0.38 * 10^{-3}$ [91]	Very high [36]	$\sim 10^{14} \Omega m$ [92]	3.7-10 [93] [94]	/
Silicon	Good electronic integration (easy metal deposition) [42]	$\sim 0.18 * 10^{-3}$ [91]	Very high [36]	Semi-conductor, depends strongly on the presence of impurities [95]	11-12 [94] [96]	/
Porous silicon	Good adherence of printed materials thanks to porosity	$\sim 2 - 4 * 10^{-3}$ [97]	Idem	$10^3 - 10^{12}$ Ωcm [51]	1-12 depending on porosity [98]	/
Metals	/	1.32-2.26 (Al alloy) depending on cutting pattern [99]	Good to excellent [100]	Conductors, $\sim 10^{-8} - 10^{-7} \Omega m$ depending on metallic materials [101]	Infinite	/
Textile	Good adherence of printed materials thanks to textile fibers	/	Compatible with a wide range organic solvents (ex: cotton)	Low conductivity	/	/
Paper	Good adherence of printed materials thanks to porosity [102]	2 [21]	Medium [36]	$\sim 10^{10} - 10^{12} \Omega m$ [103]	$\sim$ 2 [94] [104]	/
Nitrocellulose	Good adherence of printed materials thanks to porosity, uniform porosity (more precise wax penetration), much more flat surface (uniform electrodes) [73][105]	0.5 [21]	Soluble in many organic solvents [106]	Very low conductivity	1.2-1.7 [107]	/

Table 2.5: Summary table for support materials - Environmental impact.

	Environmental impact						
Material	Water consumption [kg_w/kg]	GWP/carbon footprint [kg CO_2 eq/kg]	Biodegradability	End of life	Embodied energy [MJ/kg]	Scarcity	Acidification /Eutrophication potential [g_{SO_2} eq/kg]/ [$g_{PO_4^{3-}}$ eq/kg]
Amorphous thermoplastics (ex: PMMA)	614 [108]	4.77 [108]	No [EduPack]	Raw materials used can be recycled and reused (sulphuric acid, MMA), energy recovery or landfill [109][108] [EduPack]	Energy-consuming fabrication process, 131.5 (119 [MJ] of fossil fuels) [108]	$< 5\%_{wg}$ of critical elements [108][EduPack]	26.3/2.99 [108]
Thermosetting polymers (SU-8)	406 [110]	8.1 [110]	No [EduPack]	No recycling but energy recovery or landfill [EduPack]	Energy-consuming fabrication process, 137 (mostly fossil fuels)	$< 5\%_{wg}$ of critical elements [EduPack]	$< 0.1/ < 0.01$ [111]
Elastomers (PDMS)	190-571 [EduPack]	6.3 ± 1.3 [112]	Yes, harmless degradation by formation of silicon oxide, carbon dioxide and water [113] [114]	$> 97\%$ removed by adsorption in sewage sludge and then disposed with it (landfilled or incinerated) [114]	Energy-consuming fabrication process, 140 [EduPack]	$< 5\%_{wg}$ of critical elements [EduPack]	
Glass	1.44 [115][116]	1.23 [116]	No [117]	Fully recyclable [117]	9.1 [116]	Non-renewable raw material [115]	Acidification: SO_2 and NOx emissions ($\sim 1-3$) [115] [118]
Silicon	23.2-25.7 [EduPack]	4.78-5.27 [EduPack]	No [EduPack]	No recycling but landfill [EduPack]	116-128 [EduPack]	$> 5\%_{wg}$ of critical elements [EduPack]	
Porous silicon	Idem + electrochemical etching water consumption	Idem + electrochemical etching CO_2 emissions	Idem	Idem + electrochemical etching energy needs	Idem	Idem	
Metals (Al)	1140-1260 [EduPack]	12.5-13.8 [EduPack]	No [EduPack]	Recycling /reusability [57] [EduPack], landfill	190-209 [EduPack]	$> 5\%_{wg}$ of critical elements [EduPack]	131 [119] / 5.36 [120]
Textile (polyamide fibers)	176-194 [EduPack]	7.3-8.1 [EduPack]	No [EduPack]	Recycling, energy recovery, landfill [EduPack]	122-143 [EduPack]	$< 5\%_{wg}$ of critical elements [EduPack]	NOx formation [121]
Paper	1620-1790 [EduPack]	1.11-1.23 [EduPack]	Yes [32] [EduPack]	Recycling, energy recovery, landfill [EduPack]	49-54 [EduPack]	$< 5\%_{wg}$ of critical elements [EduPack]	
Nitrocellulose		~ 4	Yes [122]	Disposable or incineration	~ 65	$< 5\%_{wg}$ of critical elements [EduPack]	

As polydimethylsiloxane will be compared to nitrocellulose in a life cycle analysis in Chapter 7, the following section briefly describes its main properties and manufacturing techniques in parallel with the previous tables in order to have a sufficient knowledge of this material as a carrier for microfluidic biosensing applications.

PDMS is a silicon-based organic polymer and is the most widely used elastomer in biosensor applications. Its main advantages are its elasticity, optical transparency, low fluorescence, cost and speed of processing, but it can suffer from channel deformation and solvent swelling problems, which makes thermoplastics also interesting [34][30].

Microfluidics integration Micro-channels are mainly manufactured by casting where PDMS is poured directly into a mould before undergoing cross-linking. This mould is usually made with SU-8 [123]. The manufacture of multilayer PDMS devices or the integration of valves and pumps is possible thanks to its elastomeric nature which makes the layers easily conformable to each other [35]. The additional layer is bonded by a simple plasma treatment and can be another layer of PDMS but also a layer of another material. Another proposed hybrid structure is the bonding of PDMS to a PMMA layer where functional devices are integrated while PDMS provides support for microfluidics [41].

Due to its inherent hydrophobicity, it is not easy to work with aqueous solutions in the microchannels and hydrophobic compounds can be easily adsorbed but surface modifications can be implemented to solve this problem [41]. PDMS is gas permeable, which can be either an advantage (for cell culture for example) or a disadvantage depending on the application with regard to compatibility with organic solvents [32][46].

Bioaffinity Like thermoplastics, PDMS is biocompatible with many biomolecules [40]. In particular, PDMS has been used to study the growth of *E. coli* bacteria by fluorescence microscopy and is particularly suitable for cell culture due to its gas permeability [30].

Electronics integration The integration of metal deposition electrodes is a challenge because of its flexibility, which can easily lead to fracturing of the metal film [35].
To avoid this problem, a glass layer can be bonded to the PDMS so that PDMS multi-layer devices benefit from the possibilities of glass such as metal deposition and surface functionalization [40].

Environmental impact The base material for PDMS is silicon, which is found in nature in the form of SiO_2. Silicon metal powder is converted to methylchlorosilanes which are distilled and then hydrolyzed to methylsiloxanes. These are then used to produce PDMS by polymerization [112].
The GWP indicator is approximately $6.3 kg_{CO_2 eq}$ [112].
The degradation of PDMS has already been extensively studied and has shown that degradation is observed after only a few weeks of contact with the soil. The main degradation product is $(CH_3)_2Si(OH)_2$ which is then oxidized in the environment to form silica, carbon dioxide and water. No effects of these products on plant growth, seed germination or plant biomass have been observed [113].

2.4 Paper as a support for microfluidic biosensor

The first commercial biosensor was introduced in the mid-1970s for blood glucose monitoring, but it was not until 1987 that fully printed glucose biosensor strips (similar to those we know today) were introduced on the market. The success of this application for diabetes management, combined with advances in many other areas of technology such as microfabrication, microfluidics and electronics, marked the beginning of the exponential growth of the biosensor market.

The growing interest in biosensors has led to a considerable increase in the volume of electronic waste, and concerns about global warming and pollution worldwide are driving the search for environmentally friendly solutions. Due to its high recyclability, paper is emerging as an alternative to the traditional plastic biosensor. Miniaturized paper-based devices have been widely used in diagnostic biosensors because of their many other inherent advantages, including ease of fabrication, high portability, low cost and excellent capillarity [124].
The best known and most basic test is the colorimetric test used widely for private pools, which generally checks pH, chlorine, alkalinity and calcium hardness. The principle is based on changing the colour of paper pads by detecting a specific reagent. Although these tests are popular because of their ease of use and affordability, they are only qualitative and have a certain level of subjectivity. Biosensors solve this accuracy problem by using a quantitative transducer. Today, some paper-based biosensors have been developed by industries and have reached the market, such as the pregnancy test. However, they mainly provide qualitative or semi-quantitative yes/no answers, which limits their field of application.
In the meantime, research is underway to resolve these issues. Paper is now used as a substrate for printed electronic components, as do GREENSENS, IMPETUS or INNPAPER [124]. This improvement makes quantitative measurements possible.

2.4.1 Paper

Paper is an inexpensive cellulosic material characterized by a porous structure giving it a high surface/volume ratio [68][71]. These pores exist due to the binding of the paper fibres which is highly dependent on the papermaking process; further refining will reduce porosity and make the paper denser, but other steps such as surface sizing, coating, calendering and supercalendering will also play a role in porosity [70].

There are different papers: Whatman brand chromatographic paper, filter paper, bioactive paper and glossy paper to name just four. Each of them has specific properties due to their different manufacture, so it is important to know which type of paper is used to make the sensors [102]. Whatman filter paper is the most widely used because of its superior wicking capacity, relatively uniform thickness, and superior adsorption and retention of reagents compared to similar types of paper. Another important type of paper is the nitrocellulose membrane which has been used specifically for its ability to immobilize biomolecules through their chemical functional groups [71]. (see Section 2.4.2).

Microfluidics integration Its lightness, flexibility and especially its natural wicking ability make it an interesting material for biosensor applications [47][68]. Microfluidic

devices take full advantage of the latter property and the basis of the manufacturing methods is to create hydrophobic/hydrophilic channels [69]. These channels can be made by simple cutting or by cross-linking SU-8 resin, wax, PDMS or polystyrene [32].

The capillary action is highly dependent on the environment such as relative humidity and allows non-specific adsorption. To solve this problem, another manufacturing process was implemented in order to no longer use the fibrous matrix but to release channels made by hot embossing to allow spontaneous capillary flow. This flow can be generated thanks to a double-layer coating: the first coating makes the paper impermeable so that the liquid does not penetrate the pores and the second coating imparts hydrophilicity to the surface of the channels to obtain capillary forces. In this case, the spontaneous capillary flows must be studied in order to understand all the different factors that have an impact on them, and in particular the geometry of the channel [32].

Bioaffinity The paper devices are biocompatible and therefore able to detect biological substances [68]. The immobilization of biological molecules can be done by physical absorption, chemical coupling, deposition on a support or sol-gel treatment [79].
In many paper-based biosensors, the conjugation of biomolecules on the paper surface is crucial to increase the functionality of these devices. Most of the techniques used to immobilize biomolecules are based on physical adsorption between the biomolecule and reactive functional groups in the paper structure, mainly hydroxyl [125].
This binding to the paper fibers is direct but weak. Covalent bonding is one way to improve the functionalization of paper materials, but this technique must transform the hydroxyl groups, which are a compound of the paper, into other functional groups to allow the covalent immobilization of biomolecules by common bioconjugate techniques. To this end, various surface chemistries have been proposed to facilitate the covalent immobilization of biomolecules on paper, such as divinyl sulfone chemistry, diazonium chemistry or polymer chemistry [126][127]. However, it has been demonstrated in [126] that unmodified paper can be used for covalent conjugation of enzymes and serves as a tool for bioanalysis due to its low content of carboxyl groups facilitating covalent immobilization of biomolecules.

Electronics integration If electronic performance is to be incorporated into the device, the method generally involves printing on materials and photolithography, but techniques such as plasma processing, laser processing or wet etching may be other alternatives [69]. The porosity allows good adhesion of the printed materials [102]. To achieve good resolution, the paper must be treated to absorb ink but gives a wide contact angle [68]. Another way could be to incorporate conductive materials such as carbon and metallized fibers directly into the paper to make it conductive [102].

Screen printing was the first method used in electrochemical sensor applications and involves the spreading of ink on a designed pattern using a squeegee. Among other manufacturing methods for integrating electronic components such as electrodes onto a substrate, inkjet printing allows materials to be deposited onto paper in a controlled and economical manner. This method is well known because it is the one used in common printers and, in fact, these can be modified for use with conductive inks if moderate accuracy, control and speed are suitable for the application [68]. Wax printing is fast and inexpensive and consists of two main steps which are the printing of wax patterns and the melting of the wax to incorporate it into the porous substrate. Its significant

advantage, apart from its speed, is the fact that the whole process can be easily disposed of by incineration as it does not involve any organic solvent. However, the wax required is expensive [69].
Photolithography uses light through a mask to give the patterns the desired shape of the electrodes. It is fast, inexpensive and offers high resolution but requires organic solvents and expensive equipment [69].

Lateral flow strips Paper sensors based on the colorimetric method have been used extensively for various types of applications. The simple pH test is well known, but for several years more complex research has been carried out on the paper colorimetric technique, such as the detection of glucose or proteins [128].
Two major paper-based devices have already given good results: the analytical microfluidic paper-based device, μPAD, and the electrochemical microfluidic paper-based device, μPED.

The best known, the μPAD, is the lateral flow assay (LFA) which relies primarily on optical detection (colorimetric and fluorescence). This implies a lack of quantification and then a detection limit (LOD) too high for the detection of bacteria [21].
A μPED is a μPAD with electrochemical detection. It combines channel structuring with conductive ink printing [79]. It offers high sensitivity and selectivity of bioelectrochemical detection through the use of an electrical measurement method that allows a lower detection limit than the μPAD and quantitative tests [21].

In addition to optical and electrochemical methods, two other detection methods exist. The thermal detection method exploits the thermal response of tracing nanoparticles under external stimulation. The result is an increase in temperature that can be related to the amount of tracer particles. Similarly, the magnetic method exploits the magnetic response of magnetic nanoparticles under the application of an external magnetic field. The generated field can be detected by different methods [129]. These four different methods of LFA detection and their associated tracers are grouped on Figure 2.11.

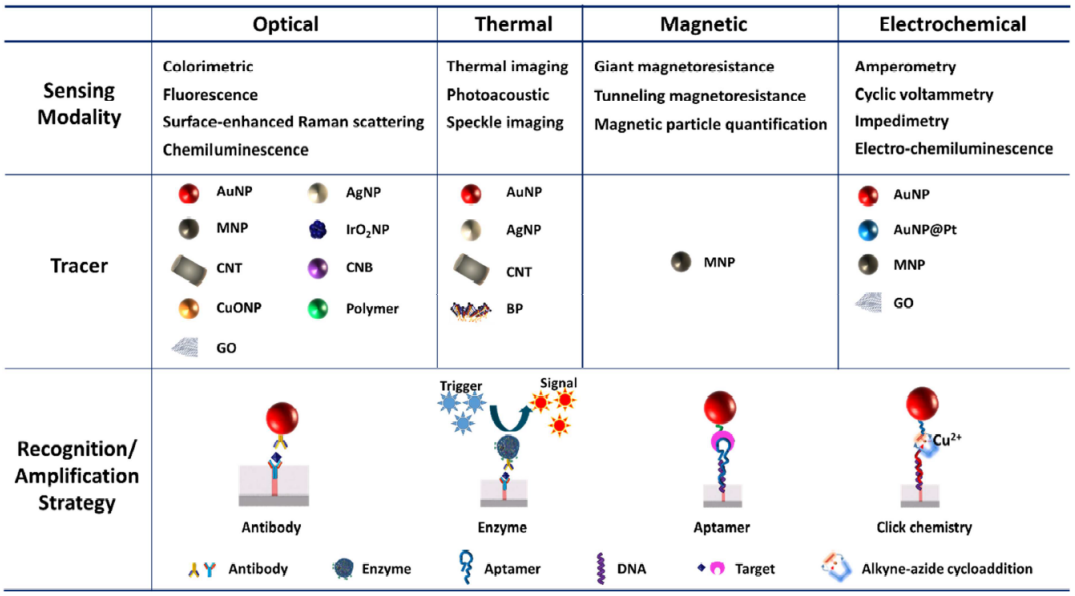


Figure 2.11: High-sensitivity LFA detection methods. The detection methods are categorized based on the sensing modalities that can operate with various tracers and recognition/amplification strategies. A binding method based on conventional immunochemistry is included for reference. AuNP, gold nanoparticle; AgNP, silver nanoparticle; CuONP, copper oxide nanoparticle; MNP, magnetic nanoparticle; IrO2NP, iridium oxide (IV) nanoparticle; GO, graphene oxide; CNT, carbon nanotube; CNB, cellulose nanobead; BP, black phosphor; Pt, platinum [129].

Although LFAs are inexpensive, portable, simple and fast, they have low sensitivity. This limits their applications for the detection of low-concentration targets. Chemical pre-treatments and physical methods such as hydrophobic barrier fabrication have been proposed to improve the performance of LFAs [130]. A further improvement to increase the detection sensitivity of these products is the incorporation of cotton yarn-based barriers into paper. This will reduce the sample throughput and thus increase the reaction time [131].

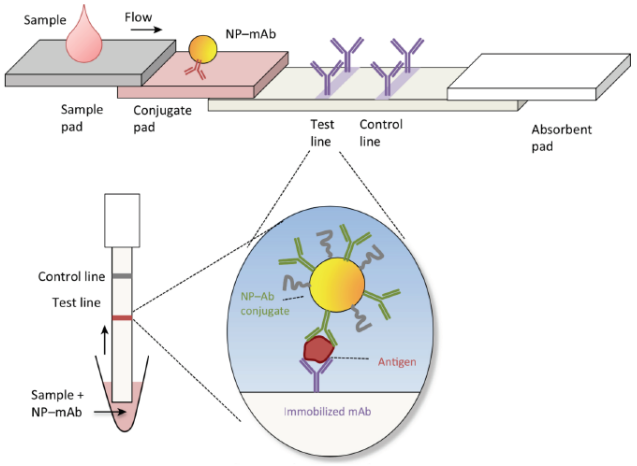


Figure 2.12: Lateral flow assay strip resulting in colored lines for positive test. The detection relies on the formation of a sandwich immunoassay when a targeted biomarker is present, which can be made visible because of the accumulation of gold nanoparticles (AuNP) - antibodies (Ab) conjugates at the test line [21].

Figure 2.12 schematizes an example of lateral flow assay. It consists of several pads.
The sample pad has different purposes. The primary objective is to ensure uniform and controlled distribution of the sample onto the conjugate pad. It can also be impregnated with different chemicals to perform different functions such as increasing the viscosity of the sample or changing the chemical nature of the sample to make it compatible with the test line. Usually this pad consists of a cellulose fiber filter or woven mesh. Cellulose filters are the most common because they are cheaper and have a larger bed volume, allowing sufficient loading of solutes.
The conjugate pad contains antibody-conjugated microspheres ($\leq 1/10$ the size of the membrane pores for optimal flow). When wetted with the sample, these detector reagents solubilize and if the bacteria are present in the sample, their antigenic sites bind to them. There exist two predominant approaches to the test, the first one is the non-competitive (or direct) reaction scheme and the second is the competitive reaction scheme. These two are best explained graphically on Figures 2.13 and 2.14 taken from [132].

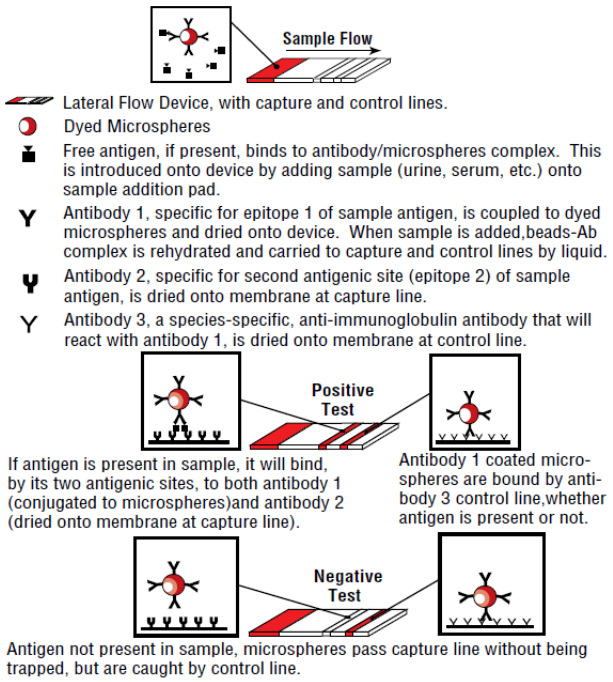


Figure 2.13: Direct reaction scheme [132].

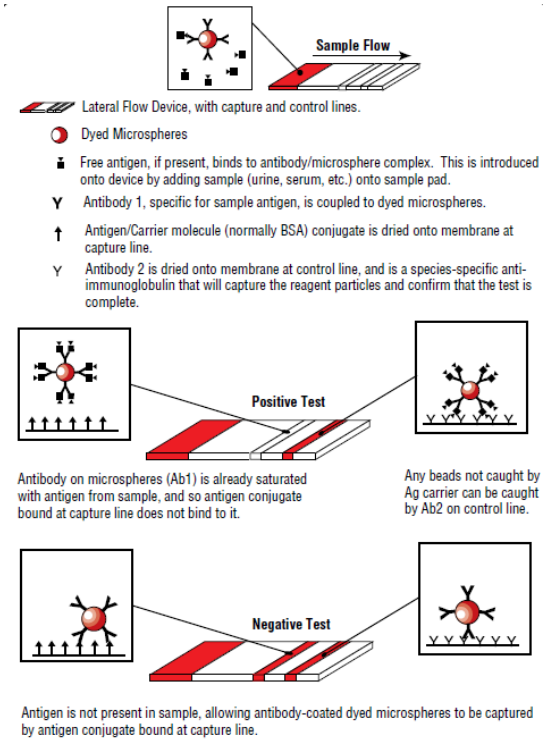


Figure 2.14: Competitive reaction scheme [132].

The conjugate pad must have weak non-specific binding so that the detector reagent and analyte are not made unavailable. Glass fiber filters, cellulose filters and surface-treated polyester (hydrophilic) or polypropylene filters are commonly used as a conjugate pad. The main function of the absorbent pad is to increase the volume of sample entering the strip. Most absorbent pads are made from cellulose filters [132].

These lateral flow test strips are already widely used in the biological field. Today, they are commercially available for ovulation monitoring, detection of infectious disease organisms, analysis of drugs of abuse and measurement of other analytes important for human physiology. Products have also been introduced for veterinary testing, agricultural applications, environmental testing and product quality assessment.
In the meantime, much research is still ongoing to develop new and increasingly technical LFAs. Many examples of paper-based electronic biosensor applications can therefore be found in the literature. Among others, the article "A paper electrode integrated lateral flow immunosensor for quantitative analysis of oxidative stress induced DNA damage" presents a device with electrodes printed on paper and taking advantage of the speed and low cost of the conventional strip test as well as the high reliability and accuracy of the electrochemical test [133]. Another, "Nanowire labelled direct-charge transfer biosensor for detecting *Bacillus* species", involves the manufacture of a biosensor using antibodies as the sensing element and a polyaniline nanowire as the molecular electrical transducer [134]. "Multiplexed electrochemical immunoassay using gold nanoparticle probes and immunochromatographic strips" describes a multiplexed electrochemical immunoassay based on the use of gold nanoparticle (Au-NP) probes and immunochromatographic

(IS) strips. The approach takes advantage of the speed and low cost of conventional IS assays and the high sensitivities of electrochemical immunoassays based on nanoparticles [135]. "Novel biosensor based on electrospun nanofibers and magnetic nanoparticles for the detection of *E. coli* O157:H7" features a lateral flow immunosensor with conductive magnetic nanoparticles bioconjugated with an antibody specific to *E. coli* O157:H7 to act as an immunomagnetic separator to extract and purify the target from the sample solution [136].

Environmental impact In addition to these technical considerations, the paper material is renewable because its raw material is wood, of natural origin. The wood cycle is even carbon dioxide neutral. Paper is biodegradable but it is also easily incinerated, which is advantageous for avoiding contamination and making them disposable devices [32].
Even though the paper comes from renewable sources, forests are disappearing due in part to harvesting for its production, which accounts for 42% of the world's total wood harvest. The world has already lost 80% of its forests and it is continuing at a rate of 375 km^2 per day [32].
One of its other drawbacks is its water consumption, which is huge because of the pulp washing stage; 1620 to 1790 liters of water per kilogram of paper [137][EuPack].
Depending on the pulping process, chemical or mechanical, the energy consumption is not the same. Chemical pulp mills are self-sufficient in terms of heat because the process produces more heat than is consumed, but this is not the case for mechanical pulping, which has about three times higher energy demand [137].
In addition, the paper industries have significant air emissions such as nitrogen oxides, sulphur oxides and carbon dioxide and use chemicals that create environmental problems and degradation.

2.4.2 Nitrocellulose

Different nitrocellulose materials exist according to the manufacturing process [73]. Nitrocellulose is a kind of paper substrate made of conventional cellulose treated with nitric acid or another nitrating agent in order to replace the hydroxyl groups in the cellulose with nitrate groups [82]. The manufacture of the membrane involves slow and controlled precipitation of the polymer from a solvent system and often includes the addition of a surfactant to render the inherent hydrophobic material hydrophilic [138]. One of its main advantages is that nitrocellulose is produced from wood, which is a natural renewable and biodegradable raw material [122].

Microfluidics integration The most widely used method of manufacturing nitrocellulose microchannels is wax modeling, which involves the formation of hydrophobic regions. This process comprises a printing step where the wax is deposited on the surface of the nitrocellulose and a baking step where the wax melts and penetrates through the nitrocellulose. These two steps can be completed in 10 minutes, which allows for easy and fast production, as well as low cost. In addition, it does not require any organic solvents [73].

The wax printing method can generate micro-channels up to a resolution of 100 million dollars, which is comparable to the photolithography method, which is much more complex because it includes many more steps: coating, pre-coating, exposure, post-coating,

development and curing [73]. The conditions of nitrocellulose must be carefully controlled because its flash point is about 200 degrees C and it is therefore highly flammable and explosive [73][105].

Another simple and inexpensive way of shaping the microchannels is laser cutting. To do this, the paper is first modified with a hydrophobic coating and then the carbon dioxide laser creates hydrophilic channels through the formation of carbonyl and hydroxyl groups. However, this required specialized equipment [71].

Another advantage of this type of membrane is that it prevents diffusion and leaching of the samples, which results in a higher degree of retention in the sensor [71]. Capillary effects also occur in this porous material and avoid the use and manufacture of pumps and valves needed to obtain fluid flow in the microchannels of the biosensor.

Bioaffinity Finally, nitrocellulose is used for its very good properties of immobilizing biomolecules. Due to the charge-charge interactions and the weak hydrogen bonds and van der Waals interactions, it allows easy electrostatic binding of proteins through the interaction of the strong dipole of nitrate esters with the strong dipoles of the peptide bonds within the protein [73][83] (see Figure 2.15).

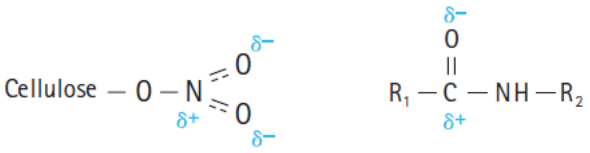


Figure 2.15: Structure of nitrocellulose ester and protein dipoles [83].

In addition, its porous structure makes this type of membrane ideal for adsorption [82]. Because of this, side-stream nitrocellulose assays often need to be pre-treated with a protein-based solution to avoid undesirable adsorption prior to the test line [82].
To achieve immobilization of the target particles, they must first be able to flow through the material and the two membrane parameters that affect this ability are pore size and flow rate. The pore size determines the size of the particles that can flow through and the flow rate gives the force required to push the particles through [138].

Cellulose acetate can also be used as a carrier material. It has about the same characteristics as nitrocellulose, but its ability to bind proteins is weak, which makes nitrocellulose more attractive.

Electronics integration Electrodes can be deposited on this material with a uniform thickness thanks to its much flatter surface than traditional cellulose paper [105]. Other electronic integration methods applied to paper materials can also be used in nitrocellulose.

Environmental impact As nitrocellulose is produced from a paper base. The environmental issues are similar to those of paper, but the stage of converting paper into nitrocellulose, including the production and integration of acids, must be added to the discussion.
The greatest risk in using nitrocellulose is its high flammability.

2.4.3 Porous media theory

Among all the materials examined, nitrocellulose will be the one used as a carrier for the studied application of bio-detection of molecules in a liquid medium.
Through the previous discussions and tables, some of the advantages highlighted for paper and nitrocellulose are their simplicity of manufacture, cost and flexibility. In addition, their carbon footprint is small compared to other materials.
Compared to paper, nitrocellulose is characterised by a very porous structure with flat surface, whereas cellulose paper has much larger fibres. The roughness of nitrocellulose is also lower than that of cellulose paper. These factors tend to shift towards nitrocellulose.

All the interest of the studied biosensor is to make it disposable because its use will be unique in order to avoid any contamination. Its impact on the environment is then of great importance. Durability has a significant importance in this thesis because if the nitrocellulose biosensor takes shape, it is not only the performance that is important but also the circularity of the object. These aspects will be discussed in more detail in Section 7.

The most important specificity of the nitrocellulose that will be used for the application is its porosity. The following section therefore focuses on the theory of porous media in order to provide sufficient context for the next chapters.

2.4.3.1 Porous media definition

A porous medium can be defined as a continuous solid phase in which a fluid phase is in intimate contact.
The solid phase can be considered as a "consolidated porous media" or from the "loose porous" family. The first denomination refers to materials having a precipitated continuity at the molecular level and behaving as a solid corpus even if heterogeneous. They may be derived from nature or artificially manufactured. If they are synthesised, consolidated porous supports are manufactured in such a way as to have a fairly homogeneous distribution of pores and pore size. The second case concerns materials consisting mainly of a disordered stacking of solid particles of different sizes and shapes. The solid phase is well continuous due to the contacts between the particles but is less rigid and more easily deformable.
In both cases, the fluid phase is present in free spaces, not occupied by the solid phase [139].

2.4.3.2 Volumetric distribution of pores

The porous media can be determined by the volumetric distribution of its pores.
If V_p is the total volume of pores in a sample of porous media, v is the volume of one pore of diameter x and $V_p(v)$ is the total volume of pores having a volume smaller than a certain volume v, the fraction of pores having a volume smaller than v can be defined by the function:

$$Z(v) = \frac{V_p(v)}{V_p}$$

This function $Z(v)$ is then varying between 0 and 1 and will look like the right Figure 2.16. This function can be derivated to give the volumetric distribution in the shape of a bell-shape curve more visual (left Figure 2.16) [139].

$$f(x) = F'(x)$$

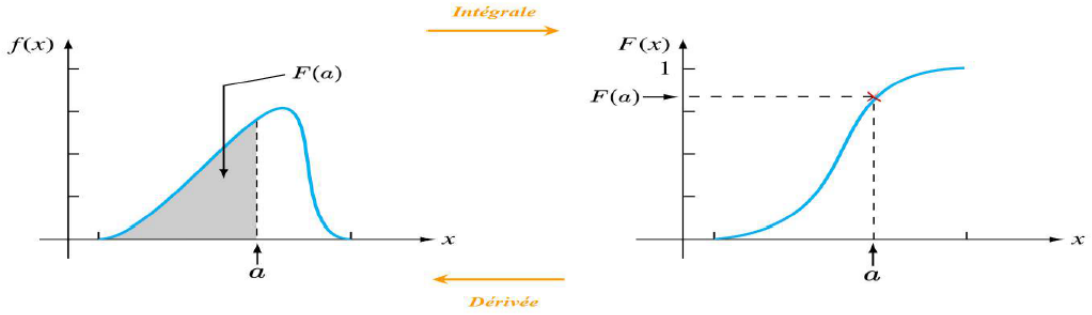


Figure 2.16: Fundamental theorem [140].

2.4.3.3 Stop threshold of a porous media

Solid particles transported by a fluid phase in a porous medium can be stopped in two ways.
The first way is sieving. Indeed, if the pores of the particle are larger than the surface pores of the solid phase, they will be stopped at the surface of the porous medium. In this case, the porous material will be completely free of particles.
The second way involves the obstruction of the porous medium. In fact, pores are also capable of stopping particles slightly smaller than the surface pores due to their progressive movement in the pore forest characterized by a variable cross-section of the channels. This clogging will be accelerated along the way as the stopped particles will reduce the internal diameter of the pores [139].

2.4.3.4 Pressure drop - Poiseuille equation

The equations for a Stoke flows in a 3D rectangular channel of dimensions $L \times W \times H$ (respectively in the x, y and z directions) are the continuity equation, $\frac{\partial}{\partial x}u + \frac{\partial}{\partial y}v + \frac{\partial}{\partial z}w = 0$, and:

$$\mu(\frac{\partial^2}{\partial x^2} + \frac{\partial^2}{\partial y^2} + \frac{\partial^2}{\partial z^2})u = \frac{\partial}{\partial x}p$$
$$\mu(\frac{\partial^2}{\partial x^2} + \frac{\partial^2}{\partial y^2} + \frac{\partial^2}{\partial z^2})v = \frac{\partial}{\partial y}p$$
$$\mu(\frac{\partial^2}{\partial x^2} + \frac{\partial^2}{\partial y^2} + \frac{\partial^2}{\partial z^2})w = \frac{\partial}{\partial z}p$$

If $H << W << L$, by analysing orders of magnitude of the continuity equation: $v \sim u\frac{W}{L} << u$ and $w \sim u\frac{H}{L} << u$. Consequently the flow is in the direction x as well as the pressure and the gradient is essentially along z. The differential equation is then:

$$\mu\frac{\partial^2 u}{\partial z^2} = \frac{\partial p}{\partial x} = -\frac{\Delta p}{L}$$

By a similar reasoning for a cylindrical of radius R:

$$\frac{\mu}{r}\frac{\partial}{\partial r}(r\frac{\partial u}{\partial r}) = -\frac{\Delta p}{L}$$

By resolving the equation for u and with $u_{r=R} = 0$ and $u_{r=0} = u_c$ as boundary conditions:

$$u = \frac{\Delta p}{4\mu L}(R^2 - r^2)$$

The flow rate Q is defined and calculated as:

$$Q = \int_S \mathbf{u} \cdot \mathbf{n} dS = \frac{\pi R^4 \Delta p}{8\mu L} = u_m \pi R^2$$

$$u_m = u_c/2$$

By rearrangement of these last equations, in laminar regime the pressure drop in a channel with a circular section of diameter D_h, a length L_h and travelled by a fluid of maximal velocity u_c and of a dynamic viscosity μ, is given by the Poiseuille equation:

$$\frac{\Delta P}{L_c} = \alpha \frac{32\mu u_c}{D_h^2} \tag{2.1}$$

with $\alpha = 1$ for a circular section of channel and $\alpha = 1 \pm 15\%$ to take into account the non-circularity. In a porous media the pressure drop can be calculated by applying this equation and its parameters to interstitial channels. To have an estimation of these factors simplified models can be used as the one of Kozeny which assumes the porous media as a stack of cylindrical channels having the same length and the same diameter and being independent from each other. In this model D_h is the hydraulic diameter and can be estimated as

$$D_h = \frac{4 \times surface\ area}{wet\ perimeter} = \frac{4 \times total\ volume\ of\ pores}{total\ wet\ surface}$$

and the length L_h can be estimated as

$$L_h = \tau L = \frac{1}{cos\theta} L$$

where θ is the average inclination angle of fluid trickles and L is the thickness of the stacking of trickles [141].

2.4.3.5 Young-Laplace equation

The Young-Laplace equation links pressure drop at an interface fluid-fluid to its geometry. This equation can be derivated by taking the simple case of a soap spherical bubble of radius R.
The total surface energy W of a soap spherical bubble of radius R is the superficial tension γ $[J/m^2]$ times the area of its 2 faces, $2 \times (4\pi R^2)$.

$$W = \gamma \times (8\pi R^2)$$

If the radius of the bubble is decreased by dR the surface energy is decreased of:

$$dW = d(\gamma \times 8\pi R^2) = 16\pi\gamma R dR$$

The decrease of the bubble volume dV is compensated by an internal pressure being higher of Δp than the external one. The work done for the decrease of dR is therefore:

$$\Delta p dV = \Delta p \times \left(\frac{4}{3} \times 3 \times \pi R^2 dR\right)$$

If the work is equaling to the variation of surface energy:

$$16\pi\gamma R dR = \Delta p \times (4\pi R^2 dR)$$

$$\Delta p = \frac{4\gamma}{R}$$

If the interface has only one side (for example a air bubble in a liquid) the equation becomes:

$$\Delta P = \frac{2\gamma}{R} \tag{2.2}$$

where γ is the tension at the interface and R the radius of the interface. This equation is known as the Young-Laplace formula.

2.4.3.6 Capillarity

Capillarity, or capillary action, describes the spontaneous flow of a liquid into a narrow tube or porous material. It occurs with water because this fluid is sticky which is a consequence of two types of intermolecular forces. The forces of cohesion involves that water molecules like to stay close together and the forces of adhesion makes that water molecules are attracted and stick to other substances. Capillary action occurs when the adhesion to the walls, or pores in the case of porous media, is stronger than the cohesive forces between the liquid molecules [142][143].

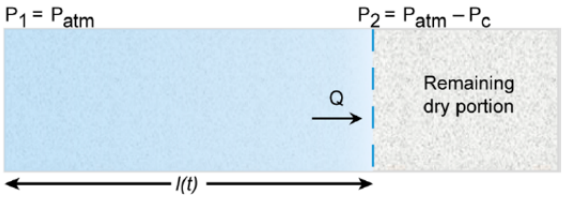


Figure 2.17: The wetted length, l(t), is directly proportional to the wicking time and a function of the fluid and material properties. P_{atm} is the atmospheric pressure, and P_c is the capillary pressure [144].

The capillary force reflects the energy gained by the replacement of a solid-gas interface by a solid-liquid interface. The capillary pressure, which is defined by the difference between the pressure of the non-wetting phase and the one of the wetting phase, is usually defined by the Equation 2.3 deduced from Equation 2.2.

$$P_{cap} = P_{atm} - P_c = \Delta P = \frac{2\gamma cos(\theta)}{R_c} \tag{2.3}$$

where γ is the superficial tension, θ the wetting angle of the liquid on the surface of the capillary, R_c the radius of the capillary ($cos(\theta) = R_c/R$) (see Figure 2.18) [145][146][32].

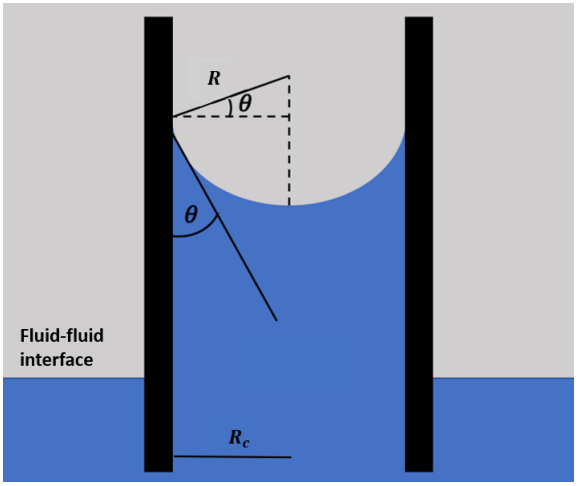


Figure 2.18: Scheme of capillary rise of a fluid. Adapted from [146].

The capillary pressure, dicted by the surface tension, is balanced by the gravity and by equaling both forces an upper height h_{max} can be found:

$$\frac{2\gamma cos\theta}{R_c} = gh_{max}(\rho - \rho_0)$$

$$h_{max} = \frac{2\gamma cos(\theta)}{\rho R_c g}$$

where ρ is the fluid density, ρ_0 is the gaseous fluid density and is then negligible compared to ρ and $g = 9.81\ [m^2/sec]$ is the gravitationnal acceleration [146][32].
Even if in the following equations the capillary speed will be shown to be decreasing with time, physically that is well the gravity that decreases the speed of the wicking water by decreasing the force resulting from the difference between the gravity force and the capillary force.

The Washburn's equation, extended to imbibition into porous materials, describes the passive wicking of fluids in dry porous media. This equation is obtained by putting the Young-Laplace equation (Equation 2.3) in the Poiseuille equation (Equation 2.1) where the length is here the height of penetration of the fluid in the porous media, also referenced as the liquid-front location L_{lf}:

$$\frac{4\gamma cos\theta}{D_c} = \frac{32\mu L_{lf}}{D_h^2}\frac{dL_{lf}}{dt}$$

$$L_{lf} = \sqrt{\frac{\gamma D_e cos\theta}{4\mu}t} \tag{2.4}$$

$$\frac{dL_{lf}}{dt} = \frac{\gamma D_e cos(\theta)}{8\mu L_{lf}}$$

D_e is the effective pore diameter, $D_e = \frac{D_h^2}{D_c}$. If the capillary diameter D_c and the hydraulic diameter D_h are equal, $D_e = D_h = D_c$. μ is the dynamic viscosity of the fluid.
This equation assumes a constant cross-section, uniform pores (typically far from reality),

no impurities, unlimited reservoir volume and no effect from hydrophobic channel walls. The wet-out rate $\frac{dL_{lf}}{dt}$ is then inversely proportional to fluid viscosity but proportional to pore diameter. The wettability can be improved by decrease the contact angle thanks to surfactant addition.
Once the material is fully wetted then the Darcy's equation (Equation 2.5) is the one to be applied.

The capillary flow rate is the speed at which a fluid front moves along a membrane strip when a liquid is introduced at one end. Most often the capillary flow time is measured instead of it because this rate decays exponentially as the liquid progresses along the membrane. The capillary flow time is defined as the time required for the liquid to completely fill a strip on a certain length and is usually expressed as cm/sec .
The assay sensitivity is proportional to the capillary flow time and therefore inversely proportional to the flow rate as an increase of flow rate decreases the length of time that the components of the reactive pair sample-receptors are close enough to bind to each other.
Another important consideration is the fact that the capillary flow rate decreases exponentially as the distance of the sample front from the origin increases as it will be shown in the experiences. That means the placement of the test line has a big impact on the sensitivity knowing the relation between the sensitivity and the flow rate [83].

Alternative models
The Lucas-Washburn model is the classical one. Originally it was developed to describe one-dimensional capillary flow in parallel bundle of cylindrical tubes, but as it has been shown in the previous section, it has been extended in order to link the wetted length to the wicking time in porous materials. However it does not take into account effects including evaporation, geometry and wetting characterisitics. Some alternative models have been developed to consider some of these.
Camplisson et al. developed a model to take into consideration the evaporation of the liquid [147]. Elizlde et al. developed one for non-uniforme cross-sections [148]. Finally Hong and Kim developed a modified form to account for contact angle variations due to hydrophobic barries such as wax [149].

Spontaneous capillary
A spontaneous capillary flow (SCF) occurs if the reservoir pressure P_{res} is higher than the pressure of the front of the fluid P_{cap}:

$$P_{res} > P_{cap}$$

These two pressures are located at one liquid-gas interface. P_{res} is considered as time independent and null compared to the atmospheric pressure so that finally P_{cap} has to be negative (compared to the atmospheric pressure) to satisfy the SCF condition [32].

2.4.3.7 Darcy equation

Fluid flow in wet, rigid and uniform porous media is described by the Darcy's law which is, for incompressible single-phase flow with negligible inertial and gravitational effects:

$$u_0 = \frac{Q}{S} = -\kappa \frac{\Delta P}{\mu L} \tag{2.5}$$

where u_0 is the average fluid velocity defined by the volumetric flow rate Q divided by the cross-sectional area of the flow S, ΔP is the fluid pressure difference, L is the length over which the pressure drop is taking place (the thickness of the bed), μ is the dynamic viscosity of the fluid and κ is the permeability coefficient of the substance. The porous structure influence is included in this last parameter. The negative sign comes from the fact that ΔP is negative as the fluid flows from a higher pressure to a lower pressure [150]. The assumptions of this equation are an infinite fluid source and a non-decreasing capillary pressure as the wicking pad becomes wetted [82][144].

Assuming a capillary model where the pores are modeled as a bundle of capillary tubes, an expression for the permeability κ of the porous media can be found by comparing two different equations for the liquid-front location L_{lf}.
The first one is the Washburn equation (Equation 2.4) and the second expression is the one found by Masoodi et al. from the Darcy's law and the Continuity equation :

$$L_{lf} = \sqrt{\frac{2\kappa P_c}{\epsilon \mu} t}$$

with $P_c = \frac{2\gamma cos\theta}{R_c}$ (Equation 2.3):

$$L_{lf} = \sqrt{\frac{4\kappa\gamma cos\theta}{\epsilon \mu R_c} t} \tag{2.6}$$

By comparing Equations 2.4 and 2.6 the following definition for κ is found:

$$\kappa = \frac{1}{8} \epsilon R_c^2 \tag{2.7}$$

where ϵ is the porosity of the media and R_c is the pore radius [151].

Chapter 3

Objectives

In this master thesis, the focus will be on the use of the nitrocellulose membrane as a biosensor substrate to detect *E. coli* bacteria from a water matrix. This takes place in the current context of drinking water shortage where current detection techniques are expensive, time consuming and require a well-equipped laboratory. Along with Salmonella, *E. coli* is the most pathogenic bacterium that is detected by a variety of methods. It is found in the environment, food and intestines and although some bacteria are harmless, *E. coli* can cause illness and infection [145][2].

The final device expected is shown on Figure 3.1. It consists of a strip of nitrocellulose to which a biological sample is added. The fluid then passes through the strip and the biomolecules within it are immobilized on the test line by proteins that functionnalize this specific area of the membrane. Due to the role of RBP and CBD in the human body, they are able to specifically recognize bacteria and therefore they can be used in another context as in this case as bioreceptors in biosensor applications.

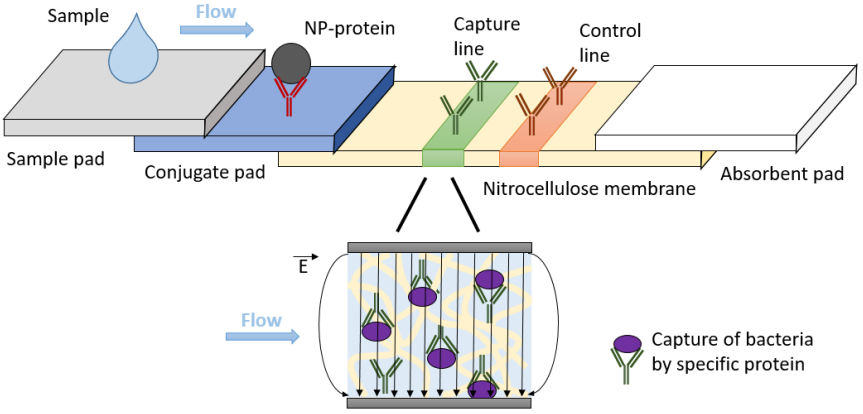


Figure 3.1: Scheme of the targeted final biosensor. A sample is added at the origin of the lateral flow assay. The fluid wicks through the strip through different pads. In the conjugate pad nano-particles NP are attached to targeted biomolecules present in the sample. In the nitrocellulose membrane the biomolecule is captured by specific proteins. At this place the change of impedance proportional to the concentration of immobilized biomolecules in all the thickness of the membrane is measured thanks to an impedance measurement. Inspired from [21].

The first existing tests presented qualitative results based on the coloration or not of a signal line made visible thanks to colored particles conjugated to the targeted biomolecule. However nowadays test design has progressed toward semiquantitative and quantitative assays thanks to the development of detection techniques. This important part of the development of the sensor is studied by Margo Hauwaert in her master thesis [107]. The idea is to use the EIS method in order to obtain a quantitative detection of bacteria. This is made possible by the fact that bacteria immobilized at the capture line will involve a change in the impedance, proportional to their concentration. More specifically Margo Hauwaert will use the impedance spectroscopy to observe changes in capacitance due to permittivity variations of the media in between the electrodes. As this change is small, nanoparticles could be conjugated to the targeted molecules, through the conjugate pad, similarly to colored particles for the qualitative tests, to amplify the detectable signal [83].

The goal of the following chapters is to obtain microfluidic and biologic guidelines for the design of the device. The microfluidic phenomenon present in the membrane is referenced as capillary. The capillary flow rate is then the important parameter to be hold. It is mainly influenced by the porous media characteristics and its conditions. The capillary flow rate is of high importance as it will affect the signal formation. In fact the chemical constituents are constantly moving in the porous media and in the meantime they have to react with the immobilized bioreceptors. The formation of complexes at the test line therefore depends on the finite time period that the components are sufficiently close to each other to bind to one another. The sensitivity of the biosensor will therefore be inversely proportional to the capillary flow rate. Another consideration is the decrease of the capillary flow rate with the increase of the sample front distance from the origin of the test strip. This also have to be taken into account for the implementation of the device. The volume of the sample is also of a point of interest as it is necessary to have enough fluid passing through the capture line and enough targeted molecules being immobilized there to be representative of the concentration in the tested media. This volume is often increased by an eventual absorbent pad.
The microfluidics research question has as goal to design a sensitive enough biosensor by playing with the influencing parameters of the strip and capture line geometries as well as with the sample volume. It can therefore be formulated as *"understand and characterise impacts of design parameters on biosensor response"* and it will be answered thanks to modelizations, simulations and experiments.

The biological guidelines are about the biofunctionalization of the nitrocellulose membrane by bioreceptors being specific to the targeted biomolecule. Proteins playing this role have to be adsorbed into the membrane. The adsorption should be stable so that proteins are keeping adsorbed to the nitrocellulose fibers for the needed time. Once the membrane biofunctionnalized, the bacteria flowing through the substrate have to be immobilized at the biofunctionalized line. At this time the important factors to be studied are then the interaction between these two biological components as well as the issue of the non-specific adsorption. In fact in practice the media is full of other molecules being eventually competing for the bioreceptor. Also an enough large concentration of bacteria should be captured at the test line in order to have a detection being comparable to the concentration in the tested liquid matrix. The research question is *"understand how RBP and CBD could be used as bioreceptors"*.

After that, the microfluidic and biological performances of the nitrocellulose membrane

would have been discussed and to support the choice of the support material of the sensor, a comparative life cycle assessment will be done in Chapter 7 in order to add to the discussion an eco-design view. This will or will not confirm the choice in term of substrate materials with the basis of a scientific method and environmental factors such as the embodied energy and the carbon footprint. To introduce this comparative study, tables in Section 2.3.4 gave an overview of different support materials and their parameters of interest.

Chapter 4

Materials and methods

4.1 Simulations and modelisations on COMSOL

4.1.1 Water flow in the porous media

The first simulation simulates the wicking of water in a nitrocellulose strip. This phenomenon occurs when a dry porous media is put into contact with a liquid and is due to capillary forces.

In this COMSOL simulation inspired from [152], the multiphysics interface Multiphase Flow in Porous Media is used, which couples the Darcy's Law and Phase Transport in Porous Media interfaces.

The model used for the Phase Transport in Porous Media interface calculates the average volume fractions s_i [/] of the non-wetting and wetting fluids based on the macroscopic mass conservation equations of each phase i:

$$\frac{\partial \epsilon_p \rho_i s_i}{\partial t} + \nabla \cdot (\rho_i \mathbf{u_i}) = Q_i \tag{4.1}$$

ϵ_p is the porosity [/], ρ_i is the density of the phase i $[kg/m^3]$ and Q_i is a mass source for phase i $[kg/(m^3 \cdot sec)]$.
It is assumed that the sum of the volume fractions of the phases equals 1 (volume constraint), so that N-1 phase volume fractions are independent and are possible to solve with the mass conservation equation and that one volume fraction s_{i_c} is expressed using the other volume fractions:

$$\sum_{i-1}^{N} s_i = 1$$

$$s_{i_c} = 1 - \left(\sum_{i=1, i \neq i_c}^{N} s_i \right)$$

The first term of Equation 4.1 is the mass change with time and the second is the convection at the superficial velocity (or the volumetric flux of phase i) $\mathbf{u_i}$ $[m_{fl}^3/(m^2 \cdot sec)]$ which is

determined by the extended Darcy's law:

$$\mathbf{u_i} = -\frac{\kappa_{r_i}}{\mu_i}\kappa(\nabla p_i - \rho_i \mathbf{g})$$

κ is the permeability $[m^2]$ of the porous media, $\mathbf{g}$ is the gravitational acceleration vector $[m^2/sec]$, μ_i is the dynamic viscosity $[kg/(m \cdot sec)]$ of the phase i, p_i is the pressure field [Pa], ρ_i is the density of the phase i and κ_{ri} is the relative permeability [/] of the phase i. The pressure of the phase computed from the volume constraint, p_{i_c}, is chosen independently and the other phase pressures are defined by the N-1 capillary pressure relations:

$$p_i = p_{i_c} + p_{c_i}(s_1, ..., s_N) \quad for\ i \neq i_c$$

The effects of the microscopic interfaces (pore scale) between the phase is taken into account via the capillary pressure functions p_{c_i} and the relative permeability κ_{r_i} which are calculated from the model of Brooks and Corey [153]. If the wetting phase is the same as the phase computed from the volume constraint, then:

$$p_i = p_{i_c} + p_c \quad for\ i \neq i_c$$

otherwise,

$$p_i = p_{i_c} - p_c \quad for\ i \neq i_c$$

The expression of the capillary pressure as a function of saturation follows the curve:

$$p_c = p_{ec}\frac{1}{\overline{s_w}^{1/\lambda_p}}$$

where λ_p is the pore distribution index and $\overline{s_w}$ denotes the effective saturation of the wetting phase. This equation means that the capillary pressure is maximal when the porous media is completly dry and equals 0 when the media is completely wet. The effective saturation of each phase is defined as:

$$\overline{s_i} = \frac{s_i - s_{ri}}{1 - \sum_{j=1}^{N} s_{rj}}$$

where s_{rj} denotes the residual saturation of phase j (usually called irreductible saturation in the petroleum litterature and representing the minimum possible water saturation). Here $s_{rj} = 0$.
The relative permeabilities are given by:

$$\kappa_{rs_w} = \overline{s_w}^{(3+2/\lambda_p)}$$

$$\kappa_{rs_n} = \overline{s_n}^2(1 - (1 - \overline{s_n})^{(1+2/\lambda_p)})$$

Initially the nitrocellulose strip is full of air with an relative humidity RH of 33% corresponding to an approximated initial water saturation of $s_{0,w} = 0.01$ [154].

Only the first 5 millimeters are referenced as completely wet (water saturation of 1) because they are the ones immersed in water.
No flux of air is assumed at the bottom boundary immersed and a mass flux for the air phase is defined with results from the pressure gradient given in the Darcy model.

The Darcy's law, together with the continuity equation and equation of state for the pore fluid provides a complete mathematical model suitable notably for porous media flows when the pressure gradient is the major driving force. The approach is to assume the porous and fluid media into a single medium. The Darcy's law interface computes the pressure field by combining the continuity equation and the Darcy's law [151]:

$$\frac{\partial}{\partial t}(\epsilon_p \rho) + \nabla \cdot (\rho \mathbf{u}) = Q_m$$

$$\mathbf{u} = -\frac{\kappa}{\mu}\nabla p$$

No water flow is assumed at the side boundaries of the nitrocellulose strip. The boundary conditions for the Darcy's law are the atmospheric pressure for water phase at the interface immersed in the water and the hydrostatic atmospheric pressure minus the capillary pressure at the top boundary. The capillary pressure is set to zero when the strip is totally soaked with water as no void volume is available anymore to pump more liquid by capillary action.

The height of the liquid front H_{lf} can also be calculated from the analytical expression of the Lucas-Washburn equation where the porous medium is assumed to be a bundle of aligned cylindrical tubes of the same radii [151]:

$$H_{lf} = \sqrt{\frac{\gamma R_c cos\theta}{2\mu_w} t}$$

The nitrocellulose material properties used are the ones of the CN140 membrane and are coming from experimental observations (see Figure 5.6) and porosity is assumed to be 0.75 [83]. The pore size distribution index is calculated with the index of distribution. These and properties of water and air are presented in Table 4.1.
The entry capillary pressure expression is deduced from the Young-Laplace equation (Equation 2.3) which assumes all pores having the same radius R_c. The expression for the permeability has been shown from the comparison between the Lucas-Washburn equation and the Darcy's law (see Equation 2.7) [151].

Table 4.1: Material properties for water, air and the CN140 membrane.

Material property	Symbol	Value	Unit
Density of water	ρ_w	1000	kg/m^3
Density of air	ρ_a	1	kg/m^3
Viscosity of water	μ_w	0.001	Pa$\times sec$
Viscosity of air	μ_a	1.76 $\times 10^{-5}$	Pa$\times sec$
Porosity	ϵ_p	0.75	/
Permeability	$\kappa = \epsilon_p \cdot R_c^2/8$	3.1568×10^{-13}	m^2
Mean pore radius	R_c	1.835×10^{-6}	m
Surface tension of water	γ	0.0723	N/m
Liquid-fiber contact angle	θ	1.4	rad
Entry capillary pressure	$p_{ec} = 2 \cdot \gamma \cdot cos(\theta)/R_c$	13394	Pa
Pore size distribution index	λ_p	1.5	/

4.1.2 Water flow at the pores scale

To study the flow of particles in the liquid in the pores themself the Creeping Flow module coupled with the Particles Tracing for Fluid Flow module are used.

The Creeping Flow interface is used for simulating fluid flows at very low Reynolds numbers for which the inertial term in the Navier-Stokes equations can be neglected. This is in fact the case here since the diameter of channels are at most $13\mu m$ (see Figure 5.6) and the maximum velocity is 1 mm/sec which makes the Reynolds number, $Re = \frac{VR\rho}{\mu}$, far away smaller than 1. Creeping flow, also referred to as Stokes flow, occurs in systems with high viscosity or small geometrical length scales as in microfluidics.

The general equations solved by the Creeping Flow interface are the continuity equation for conservation of mass and the Navier-Stokes equations for conservation of momentum:

$$\frac{\partial \rho}{\partial t} + \nabla \cdot (\rho \mathbf{u}) = 0$$

$$\rho \frac{\partial \mathbf{u}}{\partial t} + \rho(\mathbf{u} \cdot \nabla)\mathbf{u} = \nabla \cdot [-p\mathbf{I} + \tau] + \rho \mathbf{g}$$

where $\mathbf{I}$ is the identity matrix and τ is the viscous stress tensor [Pa]. For a viscous incompressible Newtonian fluid, τ is defined as:

$$\tau = 2\mu \mathbf{d}$$

$$\mathbf{d} = \frac{1}{2}(\nabla \mathbf{u} + (\nabla \mathbf{u})^T)$$

The Navier-Stokes equation becomes:

$$\rho\frac{\partial \mathbf{u}}{\partial t} + \rho(\mathbf{u}\cdot\nabla)\mathbf{u} = -\nabla p + \mu\nabla^2\mathbf{u} + \rho\mathbf{g} \tag{4.2}$$

The different terms can be associated to different contributions; the first left term is the local acceleration, the second left term is the convectional acceleration, the first right term is the pressure gradient, the second right term is the viscous shear and the last right term is the gravitational force. Two interesting non-dimensional number are the Reynolds number Re and the Womersley number α. Their respective order of magnitude can be estimated for a flow of characteristic size R, speed V, pressure P and timescale T, thanks to their definition:

$$Re = \frac{\text{convection acceleration}}{\text{viscous shear}} = \frac{VR\rho}{\mu}$$

$$\alpha = \sqrt{\frac{\text{local acceleration}}{\text{viscous shear}}} = \sqrt{\frac{\rho R^2}{\mu T}}$$

In the Stokes regime (creeping flow) $Re << 1$ and $\alpha << 1$ so that Equation 4.2 becomes:

$$\nabla p = \mu\nabla^2\mathbf{u} + \rho\mathbf{g}$$

The wall boundary condition assuming in this simulation is that there are no viscous effects at the slip wall and hence, no boundary layer develops. This is the slip condition and this constraint can be formulated as:

$$\mathbf{u}\cdot\mathbf{n} = 0$$

The parameters needed for the implementation of this simulation are presented in the Table 4.2. The particles properties are the ones of *E. coli*. Two different diameters are simulated in order to take into account the size of this bacteria which is $1\mu m \times 2\mu m$. The density of *E. coli* is 1 $pg/\mu m^3$, or equivalently 1000 kg/m^3.

Table 4.2: Material properties for water and particles.

Material property	Symbol	Value	Unit
Density of water	ρ_w	1000	kg/m^3
Density of particles	ρ_p	1000	kg/m^3
Viscosity of water	μ_w	0.001	Pa$\times sec$
Mean particles 1 diameter	d_{p_1}	1×10^{-6}	m
Mean particles 2 diameter	d_{p_2}	2×10^{-6}	m

The first idea of the following simulation was to use the particle tracing module of COMSOL in order to study the displacement of bacteria in the porous media. However this module does not take into account the particle diameter in the geometry constraints so that a diameter of particles larger than the pore diameter is going to enter and move through the

pore. Therefore it will not be possible to see if the bacteria will block the pores. As it was the main goal of the simulation, this last one was finally used in another goal: to find the geometry fitting the best the nitrocellulose membrane at the pores scale.

Three geometries of pores are going to be compared.
The first one simplifies the porous structure of the nitrocellulose membrane as a serie of layers of different diameters and that for each pore as shown on Figure 4.1. The properties of the porous media needed to draw the geometry such as the porosity and the mean pore diameter are the ones present in the Table 4.1 for the CN140 membrane.

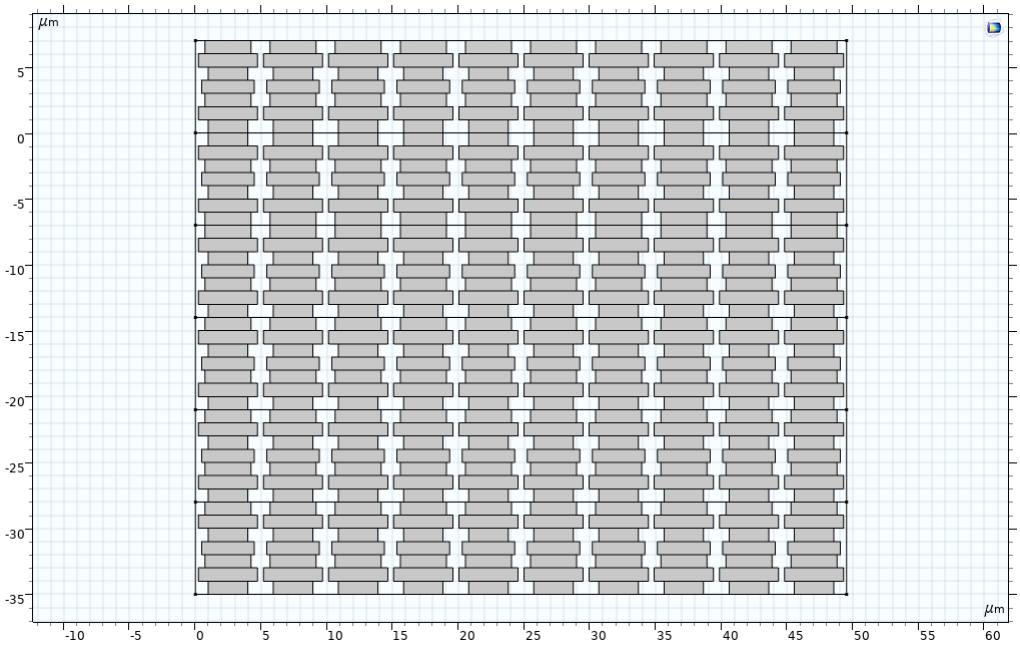


Figure 4.1: Geometry 1 for porous structure of the CN140 nitrocellulose membrane.

The second tested geometry (Figure 4.2) tries to include the interconnectivity between the pores of the nitrocellulose membrane. Again it is drawed by satisfying the properties of the porous media as a bed volume portion of 75% and a mean distance of pores of $4\mu m$. As it can be shown on the Figure 4.2 the porous structure is now simulated as small spherical holes representing a cut in the fibers. The water therefore flows in the space between holes representing the void volume. The horizontal distance between 2 holes is $3.8\mu m$ and the ones 45°-oriented is $4.2\mu m$ making the mean distance between nitrocellulose fibers equal $4\mu m$.
The assumptions and parameters needed for the creeping flow are the same than for the first geometry.

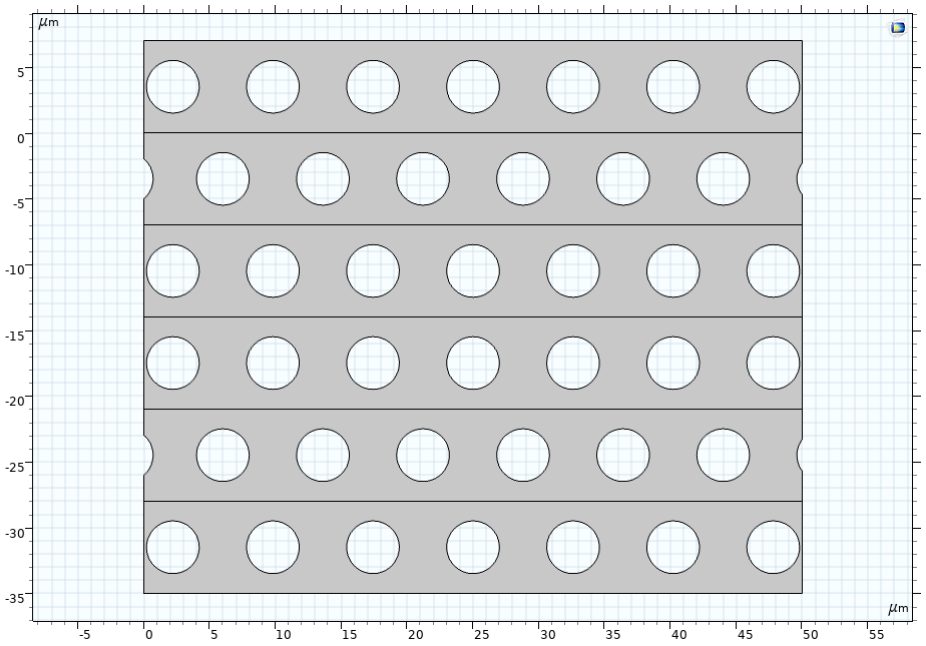


Figure 4.2: Geometry 2 for porous structure of the CN140 nitrocellulose membrane.

The last geometry shown on Figure 4.3 is inspired from the first geometry but also takes into account the interconnectivity between pores as does the second geometry.
Again the assumptions and parameters needed for the creeping flow are the same than for the first geometry.

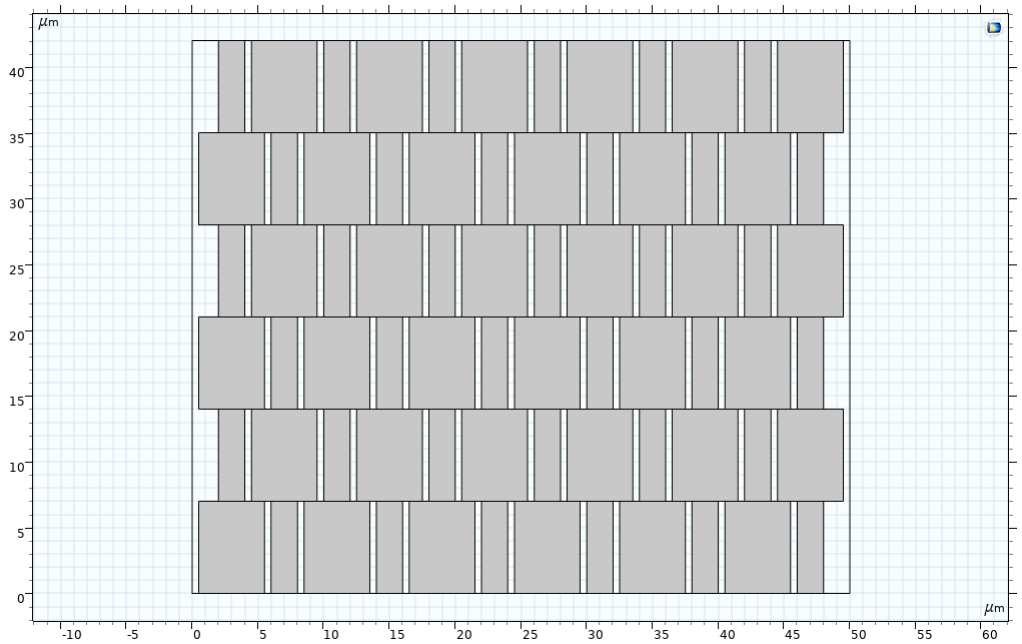


Figure 4.3: Geometry 3 for porous structure of the CN140 nitrocellulose membrane.

The pressure drop between the inlet and the outlet corresponds to the capillary pressure and is assumed to be only dependent on the length where the pressure is applied. It is

then calculated from the total pressure drop for the strip of 1cm x 5cm (p_{ec} in Table 4.1). The calculation is then for the three geometries:

$$1.39 \times 10^5 Pa \times \frac{42\mu m}{5cm} = 116.76\ Pa$$

4.2 Experiments

4.2.1 Comparison of different papers by the absorption of one water drop

Cellulose paper, Whatman paper, glazed paper and nitrocellulose paper will be compared depending on the absorption of one water drop. The water is colored with methyl blue in order to clearly see the absorption shape.

The parameters to be varied are the porosity by analysing the different papers and the deposited water volume (5, 10, 25, 50 and 100 μL).

The characteristics of the methyl blue are a molar mass of 319,85 g/mol, a solubility of 40 g/L and a shape of $17\text{Å} \times 7,6\text{Å} \times 3,3\text{Å}$. One Angström Å worth 0.1 nanometer so that it should easily go through all pores of the different papers.
The membrane made in cellulose nitrate is specified as *UniSart CN140 unbacked* and comes from the company SARTORIUS. The Whatman paper is a qualitative filter paper of grade 1. Its pore size is $11\mu m$, its porosity is 68% and its contact angle is 30° [155]. The thickness of the different studied papers have been measured with a micrometer and they are shown in the Table 4.3.

Table 4.3: Thickness of different papers used for the experience of a water drop absorption.

	Cellulose paper	CN140 unbacked	CN140 backed	Whatman	Glazed paper
Thickness [μm]	98	120-160	225-255 including backing of 100μm in polyester clear	194	196

The procedure followed is described hereafter:

1. Make the dilution 1/15 of methyl blue in pure water.
2. Cut the paper samples of 5cm x 5cm.
3. Depose orthogonally to the paper surface a volume of water with a pipette.
4. Wait 10 seconds.
5. Trace the shape formed by the water drop on both sides of the paper.
6. Do the same experience 3 times for the repeatability.

4.2.2 Effect of pores size and strip geometry on capillary flow

First of all different types of channels are feasible: non confined, confined on one side, completely confined. Once the method chosen, the main principle of microfluidic channels fabrication is to make hydrophobic the part of the support which is wanted to not be part of the channels [156]. However the simplest way is the cutting of a non-confined channel with the shape of a test strip. This is the one which will be studied in this thesis.

Different nitrocellulose membranes and geometries of strips will be compared by studying the flow of colored liquid. The relative humidity effect will also be studied on one specific membrane.

The procedure followed is described hereafter:

1. Cut the strip with the chosen geometry in the nitrocellulose membrane.
2. Put the membrane at equilibrium with a certain relative humidity (RH). To put a desiccator at the chosen RH a specific salt solution must be prepared. Each salt generates a specific RH at a fixed temperature [157].
   (a) Prepare the salt sursatured solution by putting $5-10\%_{wg}$ more than the needed salt mass for water saturation in heated water.
   (b) Make the solution get colder. The extra salt forms a layer at the bottom of the recipient.
   (c) Put the solution and the membrane in a closed enclosure for night at a given temperature.
3. Make the dilution 1/15 of methyl blue in pure water.
4. Quench 5mm of the strip in container filled with colored water **OR** put a drop of $100\mu L$ of colored liquid on the edge of a plastic container and quench the strip into it vertically **OR** put a drop of $100\mu L$ of colored liquid on the beginning of the strip laying vertically.
   In the first possibility the used containers have a radius of 8.5mm and then to have a quench of around 5mm the volume of liquid V to be filled is calculated as follows:
   $$V = \pi * (8.5)^2 * 5 = 1.13cm^3 \cong 1mL$$
5. Measure the length of the front of water on the strip after a certain amount of time.
6. Do the experience 3 times for the repeatability.

The nitrocellulose membranes studied are the *UniSart* ones coming from the company SARTORIUS. Their specifications and characteristics provided by SARTORIUS are shown in the Table 4.4.

Table 4.4: Specifications and characteristics of used SARTORIUS UniSart membranes of cellulose nitrate.

	CN95 backed	CN140 unbacked	CN140 backed	CN180 backed
Backing	100 μm polyester	none	100 μm polyester	100 μm polyester
Thickness [μm]	240-270	120-160	225-255	225-255
Capillary speed down web, purified water [sec/4mm]	65-115	90-150	95-155	135-175

4.2.3 Characterization porous structure

Thanks to the confocal microscopy used to observe the deposition of proteins on the nitrocellulose membrane (see Section 5.2.1) scans of high resolution have been obtaining. These highlight the porous structure of the CN140 unbacked membrane thanks to the fluorescence of the deposed GFP and therefore allow to study pores size, pores size distribution, percentage of available pores for bacteria in surface and in different cuts by an image treatment.

4.2.4 Deposition of fluometric RBPs/CBDs

Using tagged antibodies and by means of fluorescence imaging of the substrate cross-section, the adsorption of the antibodies in the nitrocellulose substrate was found by Grégoire Lebrun to be complete and homogeneous on the whole membrane thickness [21][158]. The goal of this experiment is to make a similar observation with other bioreceptors. As discussed on Section 2.3.1.1 bioreceptors of interest are phage proteins such as RBPs and CBDs.

To have fluorescence imaging, proteins must be made fluorescent by fused its C- or N-terminal to respectively the N- or C-terminal of the Green Fluorescent Protein (GFP). GFP is a versatile biological marker for among others visualizing protein localization. It is a protein composed of amino acid residues that exhibits bright green fluorescence when exposed to light in blue to ultraviolet range [159].

Once proteins tagged with GFP, the protocole of deposition is the same than for antibodies and is described hereafter:

1. Put the CN140 unbacked membrane at equilibrium at a certain relative humidity (RH).
   (a) Prepare the salt sursatured solution by putting $5-10\%_{wg}$ more than the needed salt mass for water saturation in heated water.
   (b) Make the solution get colder. The extra salt forms a layer at the bottom of the recipient.

(c) Put the solution and the membrane in a closed enclosure for night at a certain temperature in function of the wanted RH.

2. Cut a square of 1cm x 1cm in the membrane.
3. Prepare the 0.1 mg/mL solution of proteins by dilution with ultra pure water and put in in the centrifuge at 1 rpm for 10 seconds. Keep the solution in the dark by covering it with aluminium foil.
4. Apply 40-50 μL of solution on the membrane by covering all the piece of membrane. Keep the membrane with proteins in the dark by covering it with aluminium foil. It is advised to apply the solution to the side which was in contact with belt during the manufacture of the membrane (shinier one) as it rarely presents physical irregularities.
5. Wait at least 10 min.
6. Wipe the excess solution.
7. Make holes in the aluminium foil and dry the membrane at 37°C during 1h to take out the water excess in the membrane.
8. Keep the membrane in the desiccator (< 30°C) for at least 30 min to fix proteins.
9. Rinse the membrane with distilled water (2 baths of 2 minutes).
10. Wipe the excess solution.
11. Dry the membrane 30 min at 30°C in the desiccator.
12. Stock in the fridge and in the dark to keep the fluorescence of proteins.

The drying steps is of high importance as the proteins retain its structural integrity while completely dried. Thanks to that and while waiting to be used, the sensor may be stored at ambient temperature (in dry conditions). By rehydrating the proteins by the sample they should be instantly reactive.

The different bioreceptors deposed as well as the concentration of their initial solution and the wavelength at which these fluorescent proteins are excited and emitted are shown in the Table 4.5. The purity of the solutions of proteins was verified by Audrey Leprince thanks to protein electrophoresis. This method gives the electrophoresis gel shown on the Figure 4.4.

Table 4.5: Characteristics of used GFP. One amino acid of a protein represents about 100 Da and its size can be approximated as 3.5Å or 0.35 nm.

	gp221_CBD deep-blue	gp32_CBD deep-purple	gp185 deep-blue RBP
Initial solution concentration [mg/mL]	0,96	1,44	0,22
Size [kDa]	50	40	56
Excitation GFP [nm]	460-500	460-500	460-500
Emission GFP [nm]	512-542	512-542	512-542

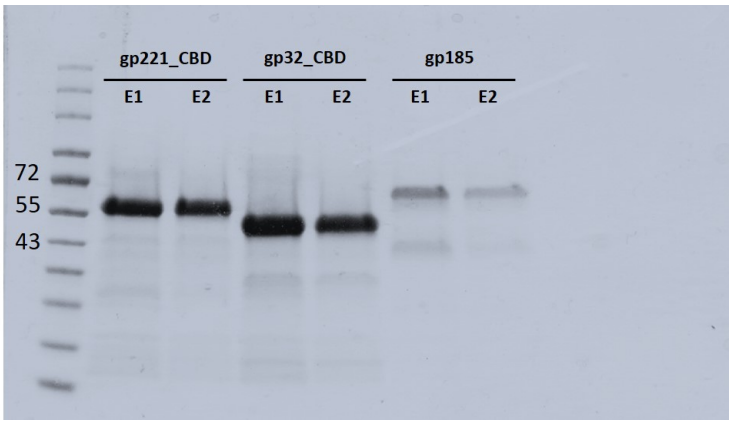


Figure 4.4: Electrophoresis of gp221_CBD, gp32_CBD and gp185 (blue RBP).

To observe the deposition of the proteins in the nitrocellulose membrane epifluorescence and confocal microscopes will be used.
The epifluorescence microscopy uses a light source illuminating the sample to analyze with a certain wavelength selected by the excitation filter. In the case of GFP the wavelength is the one of the green color. Once the light reaches the sample, the fluorescence emitted by it is focused to the detector (see Figure 4.5).

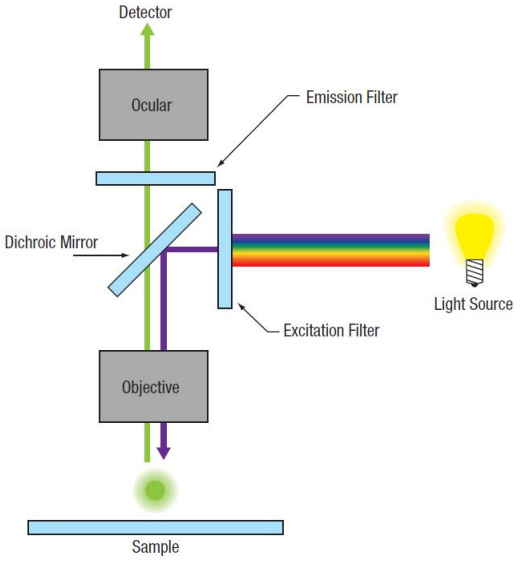


Figure 4.5: Working principle of epifluorescence microscope [160].

The confocal laser scanning microscopy is another optical method but its resolution is higher and it allows to obtain 3D images of the surface texture of the sample by capturing 2D images at different depths. A light source is sent to the object and is then returning on the detector like for conventional microscope but in a confocal microscope only a smaller beam of light at one narrow depth level at a time penetrates into the specimen. Thanks to a rotating aperture disk with holes the whole surface of the object is detected. To get 3D scanning the distance of the lens from the object can be adjusted (see Figure 4.6).

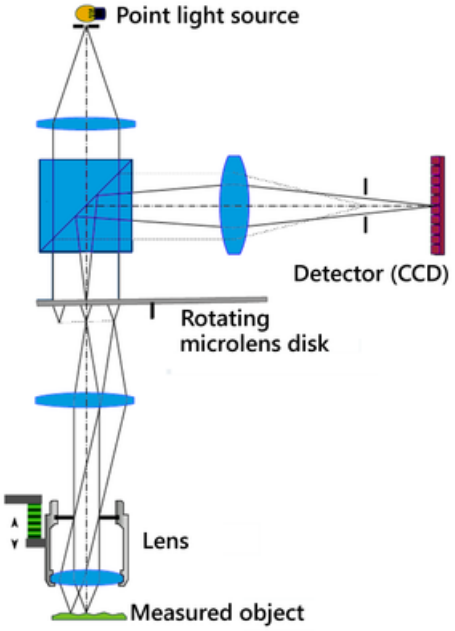


Figure 4.6: Working principle of confocal microscope [161].

4.2.5 Interaction bioreceptors-bacteria

A first experiment was conducted by Audrey Leprince and studies the interaction between one strain of the *Bacillus* thuringiensis (GBJ001) and GFP fused CBDs (gp221).
The protocole followed is described hereafter:

1. The bacteria was incubated overnight in LB medium at 30°C with an agitation of 120 rpm.
2. The overnight culture was diluted in fresh LB medium (1:100) and further incubated (30°C - 120 rpm) until the bacteria reach the exponential phase. At this stage, the bacteria are more sensitive to the attachment of the CBD as the peptidoglycan is less cross-linked.
3. Centrifuge the culture (10 000g - 5 min) in order to collect the bacterial pellet which is then washed 2 times with PBS and resuspend in 100 μL of PBS.
4. Add 10 μg of fluorescent proteins to the bacterial suspension and incubate it at 28°C during 15 min with agitation.
5. Centrifuge 2 minutes at 4°C and 10 000g and the supernantant. Wash the bacterial pellet at least two times with cold PBS to removed unadsorbed proteins.
6. Finally, resuspend the bacterial pellet in 100 μL of PBS and observe the bacteria under the fluorescent microscope (zoom 100x).

Chapter 5

Results and discussion

5.1 Nitrocellulose as a microfluidic platform for biosensing applications

5.1.1 Choice of the microfluidic and absorbent substrate

Thanks to the observation of the absorption of one water drop on different support materials, different papers such as an glazed paper, a cellulosic paper, a nitrocellulosic paper and a Whatman paper have been compared.

The cellulosic paper as well as the glazed paper do not allow the water to be absorbed and that for several minutes. The water is then forming a curved drop on the surface as it can be seen on Figures 5.1 and 5.2. Both sides of the glossy paper, i.e. the glossy side and the matt side, have been studied and show the same results for the adsorption of different volumes of water drops as shown in the Table 5.1 giving the characteristics of the different deposits.

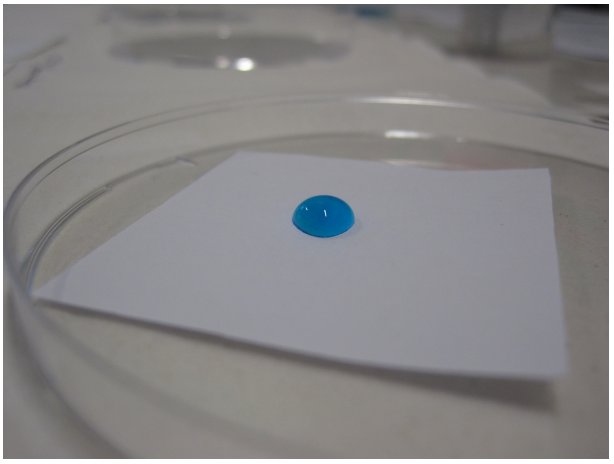


Figure 5.1: Shape taken by one water drop of $100\mu L$ on a cellulosic paper.

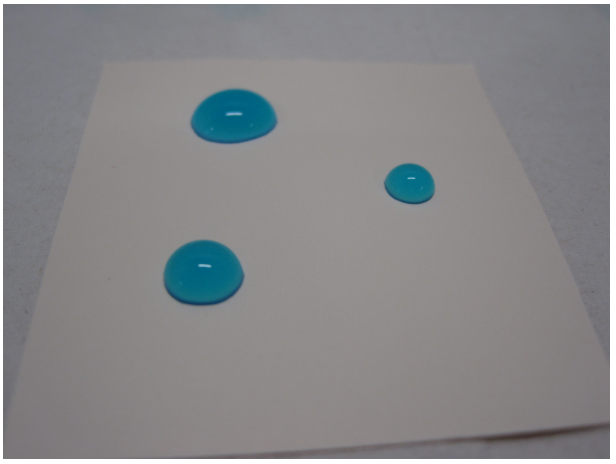


Figure 5.2: Shape taken by water drops on the mat side of a glazed paper.

Table 5.1: Diameters of water drops of different volumes deposed on different papers of hydrophobic appearance.

$V_i[\mu L]$	Cellulose paper [cm]	Glazed paper, glazed side [cm]	Glazed paper, mat side [cm]
5	0.3	0.25	0.25
10	0.35	0.3	0.3
25	0.4	0.4	0.45
50	0.5	0.6	0.55
100	0.7	0.8	0.8

For the other papers materials the volume of the water deposed V_i on the support is linked to the final volume occupied by the water drop into it V_f which is calculated as follows:

$$V_f = A_f \times e$$

with A_f is the measured surface of the water shape on the support material and e is the thickness of the paper.

The results have been plotted into a graph shown on Figure 5.3. This graph shows that Whatman paper is much more absorbent than the nitrocellulose membrane as the same volume of water deposed on the Whatman support takes a volume into it around 6 times larger than in the nitrocellulose membrane. Also there is no significant difference between the nitrocellulose membranes backed and unbacked. The Whatman paper may therefore be used as absorbent pad in the biosensor strip.

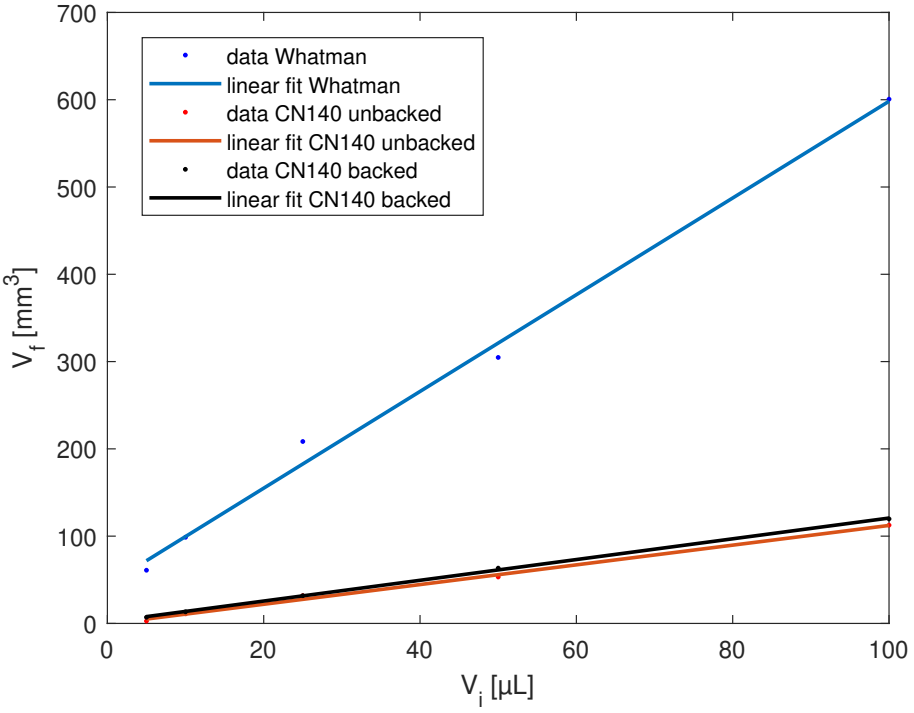


Figure 5.3: Volume final V_f occupied in different papers by one water drop of initial volume V_i.

Another remarkable fact is the observation of a pattern left on the support after the evaporation of the water. This effect is known as the coffee ring effect and is especially noticeable within the nitrocellulose membranes as it can be seen on Figure 5.4.

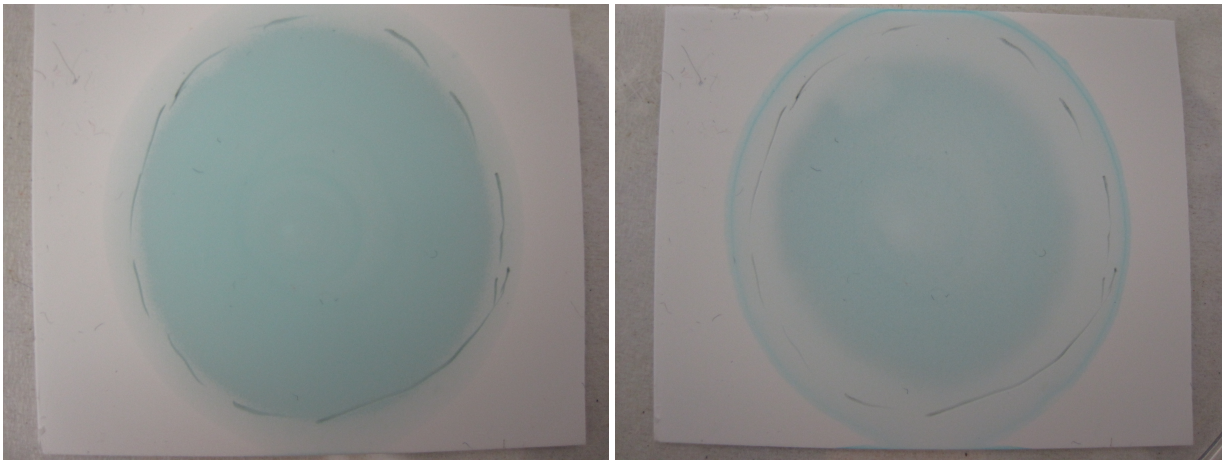


Figure 5.4: Shape and front of one colored water drop of $100\mu L$ on CN140 backed membrane after 20 seconds (left) and 10 minutes (right).

The coffee ring effect is described as the phenomenon concentrating solid and spherical particles on the ring of the perimeter of a liquid drop containing initially uniformly dispersed particles. This is due to the capillary flow induced by the differential evaporation rate.

Indeed the liquid evaporated at the edge of the drop is replenished by the internal liquid thanks to capillarity [162]. That effect is even accentuated at the end of the evaporation process [163]. That is actually what it is observed as on the left Figure 5.4 the drop is not dried yet.

This capillary flow with a direction from interior to exterior of the drop is balanced by the Marangoni flow induced by the evaporation and having an opposite direction. Consequently to observe the coffee stain effect this last flow has to be weak, which is the case for pure water. This Marangoni flow is due to a gradient of surface tension and therefore surfactants can be added to lower it by reducing the liquid's surface tension [164].
These rings are forming because of spherical particles agglomerating. One way to suppress this effect is actually to add elongated particles as cellulose fibers to the spherical ones [163]. Even the blue methyl molecules used in this experience are not spherical they may be approximated as such compared to cellulose fibers.

The coffee ring effect can be disruptive when uniform dried deposit is required. This effect is then not expected to impact the bacteria flow but could well affect the biofunctionnalization of the test line by bioreceptors deposition.

5.1.2 Porous structure characterization and modelization

The porosity characterizing the paper material is on high interest in particular for its influence on capillary and for its ability to immobilize a large amount of biomolecules. Actually the porous structure of nitrocellulose membrane makes it ideal for adsorption as it will be discussed in Section 5.2.

5.1.2.1 Porous structure characterization

Cellulose and nitrocellulose substrate were characterized by optical and SEM microscopies and profilometry by Grégoire Le Brun. Nitrocellulose was shown to provide a highly porous structure with flat surface, while cellulose paper has much larger fibres. A mean surface roughness of about 2 μm and 0.5 μm were found for cellulose and nitrocellulose sheets respectively [21].

By selecting two different places on the layer at a depth of 10.19 μm of one 3D scan of the confocal microscope (see Figure 5.5) showing fluorescent of RBPs into the structure of CN140 unbacked, the mean pore size of the membrane as well as its pore distribution and the percentage of available pores for bacteria have been collecting.
The mean pore diameter is 3.55 μm. *E. coli* having a size about $1\mu m \times 2\mu m$ and regarding the pore size distribution presented on Figure 5.6, the percentage of available pores for bacteria diffusion in the liquid media into the nitrocellulose membrane CN140 unbacked, namely the percentage of pores having a diameter larger than $2\mu m$ is 73.12%.

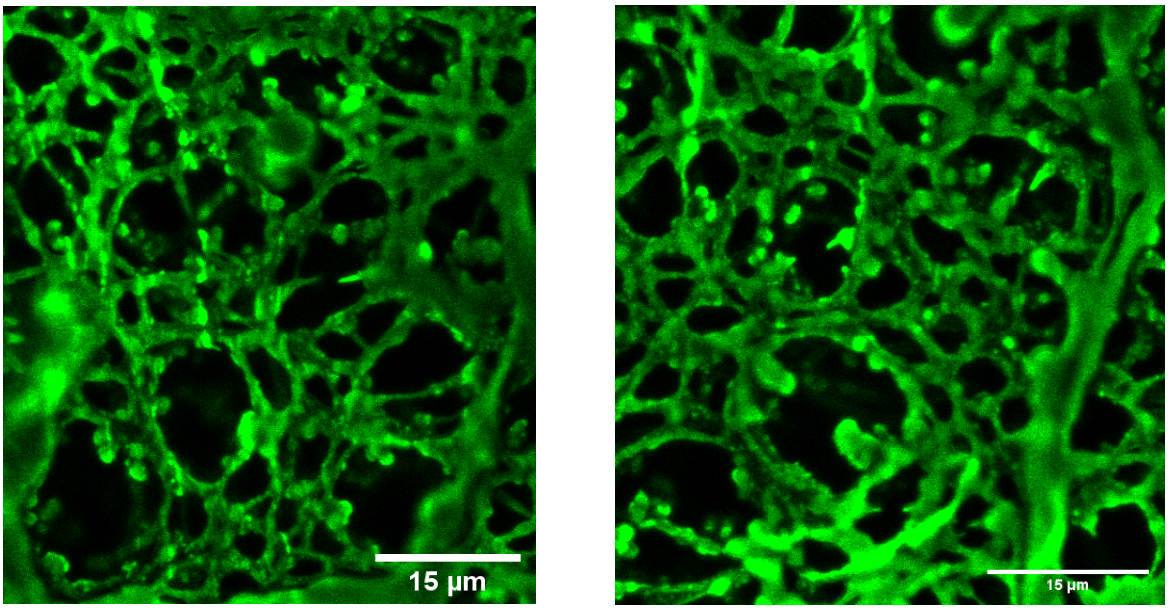


Figure 5.5: Confocal images of CN140 unbacked membrane biofunctionnalized with fluorescent RBPs a depth of 10.19 μm.

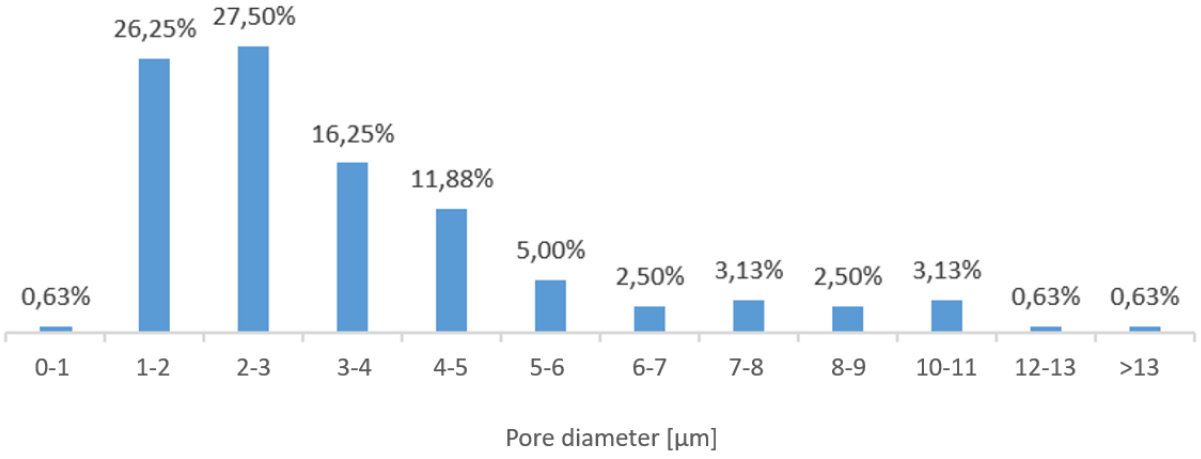


Figure 5.6: Pore size distribution of CN140 unbacked membrane, based on Figure 5.5.

5.1.2.2 Porous structure modelization

Figures 5.7, 5.8 and 5.9 show the velocity field due to capillary pressure in three different pore structure geometries. From experiments it is known that the capillary speed in the first seconds (when the gravity has a negligible effect) and in a strip of 1cm x 5cm is about 1 mm/sec (see Figure 5.17). This value is therefore the one to be approached as average velocity in the tested geometries.

The geometry presented on Figure 5.7 is too simple, it does not take into account the connectivity between pores and the resulting average velocity (2.1 mm/sec) is too high.

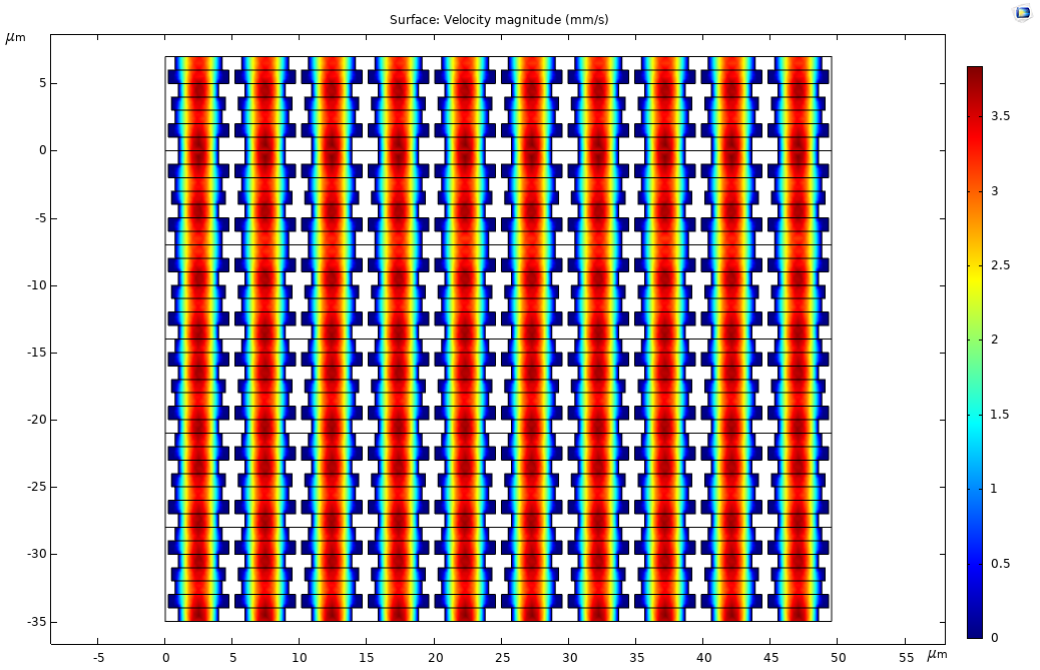


Figure 5.7: Velocity field in the first pore structure geometry when pressure drop is 116.76 Pa.

The average velocity that can be observed on Figure 5.8 is too high as well (3.1 mm/sec), meaning that this second geometry is too simple as well to modelize the porous structure.

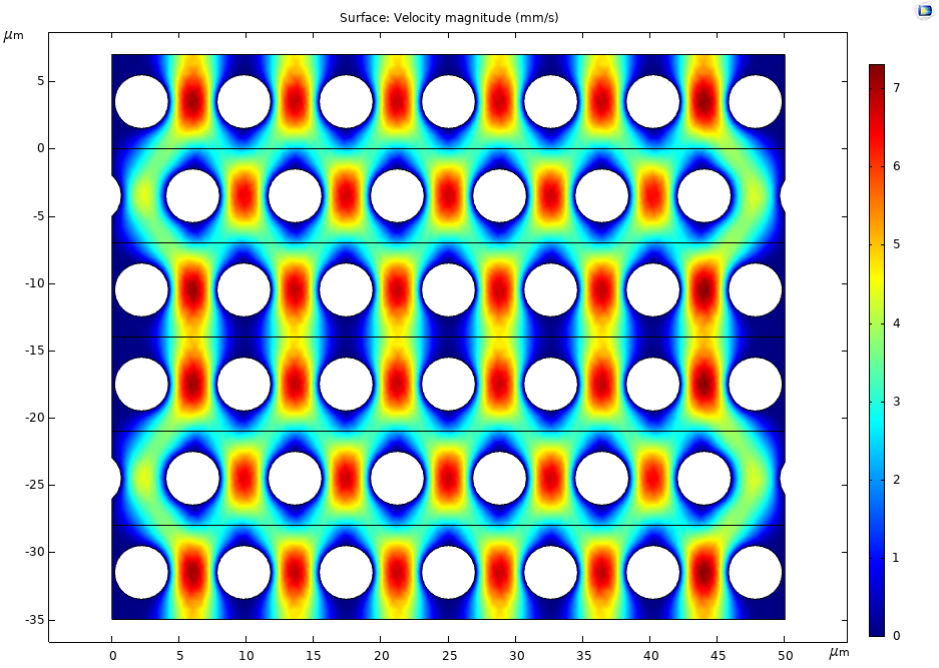


Figure 5.8: Velocity field in the second pore structure geometry when pressure drop is 116.76 Pa.

Finally the last geometry presents an average velocity (1.3 mm/sec) that jibe more with the reality of experiments. The velocity field is quite complex as it is seen on Figure 5.9.

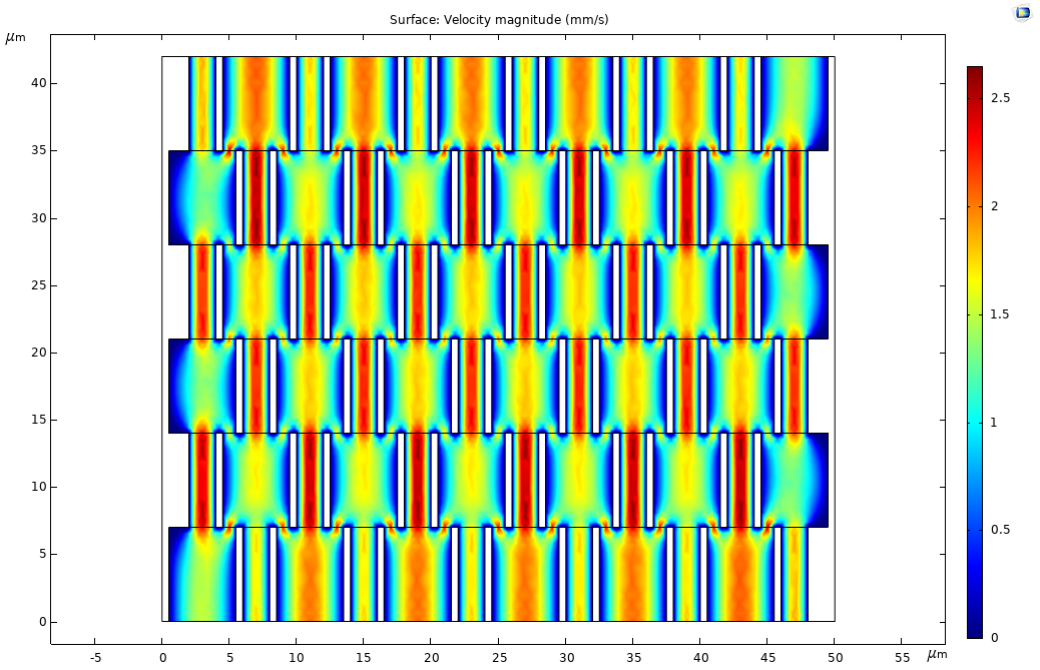


Figure 5.9: Velocity field in the third pores structure geometry when pressure drop is 116.76 Pa.

5.1.3 Parameters influencing the capillary flow

Figure 5.10 shows the simulation of the wicking of water in a CN140 strip of a geometry of 1cm x 5cm. It represents the water saturation in the length of the strip and for different times.

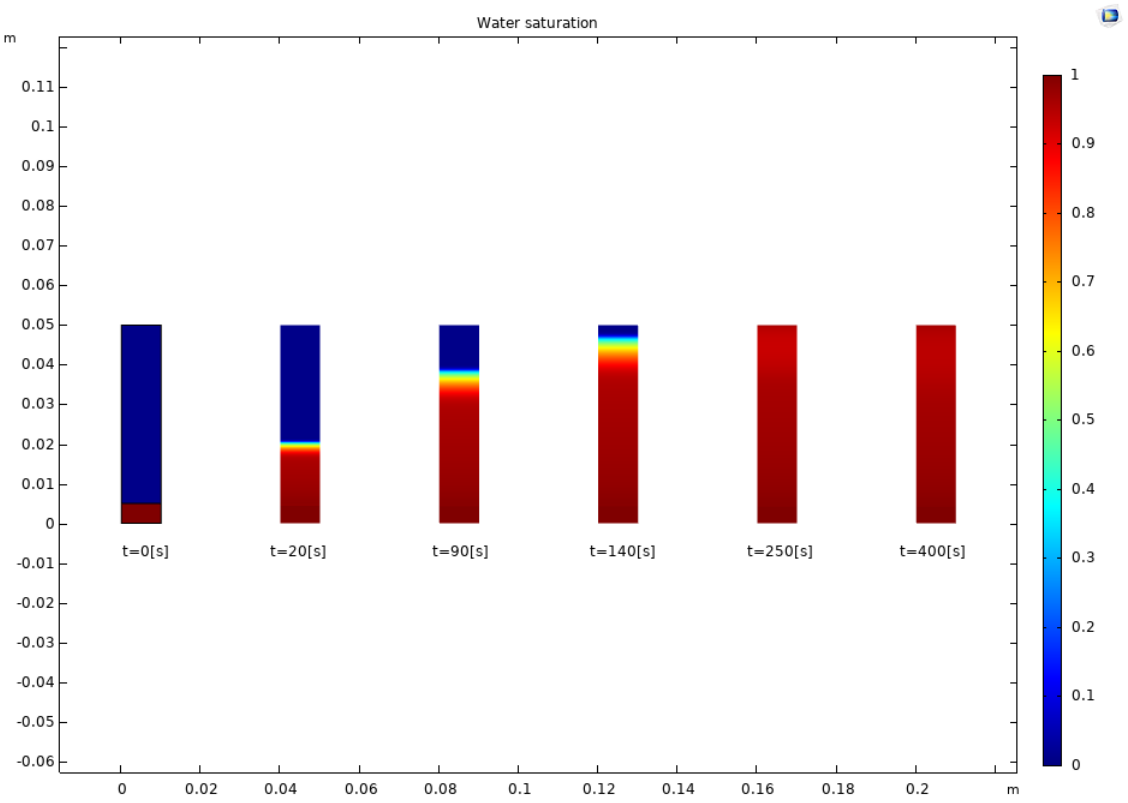


Figure 5.10: Water Saturation in the nitrocellulose CN140 strip 1x5 cm^2 after 20, 90, 140, 250 and 400 seconds.

The observation of capillary flow were also done by the mean of experiment with colored water in different cellulose nitrate membranes. Vertical and horizontal flows have been studied. As shown on Figure 5.11 two distinct fronts (referenced as 1 and 2) are in almost each case observed. The first one is the front of the saturated zone and the zone in between the first and the second front is the unsaturated zone.

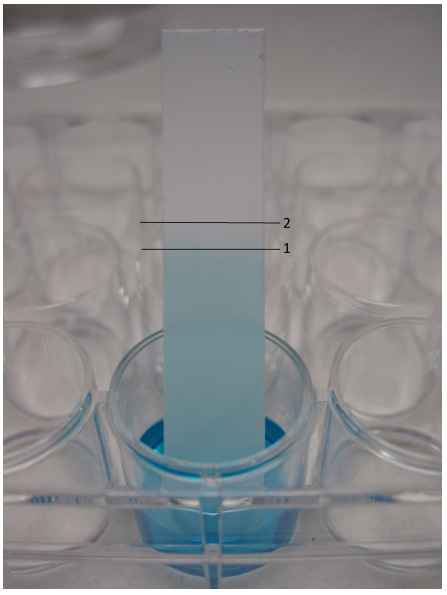


Figure 5.11: Observation of the 2 different fronts in vertical capillary flow in CN180 backed.

The evolution of the liquid front is represented on a graph (see Figure 5.12) where the simulation values (blue solid line) are compared with those calculated from the analytical expression given by the Lucas-Washburn equation (see Equation 2.4) (dashed line) and with the experiment (green solid line). The plateau means that after around 3.5 minutes the strip is completely soaked.
The differences between the model and the simulation can be due to the fact that the Lucas-Washburn equation does not take into account the non-uniformity of pore sizes but only a mean pore radius.

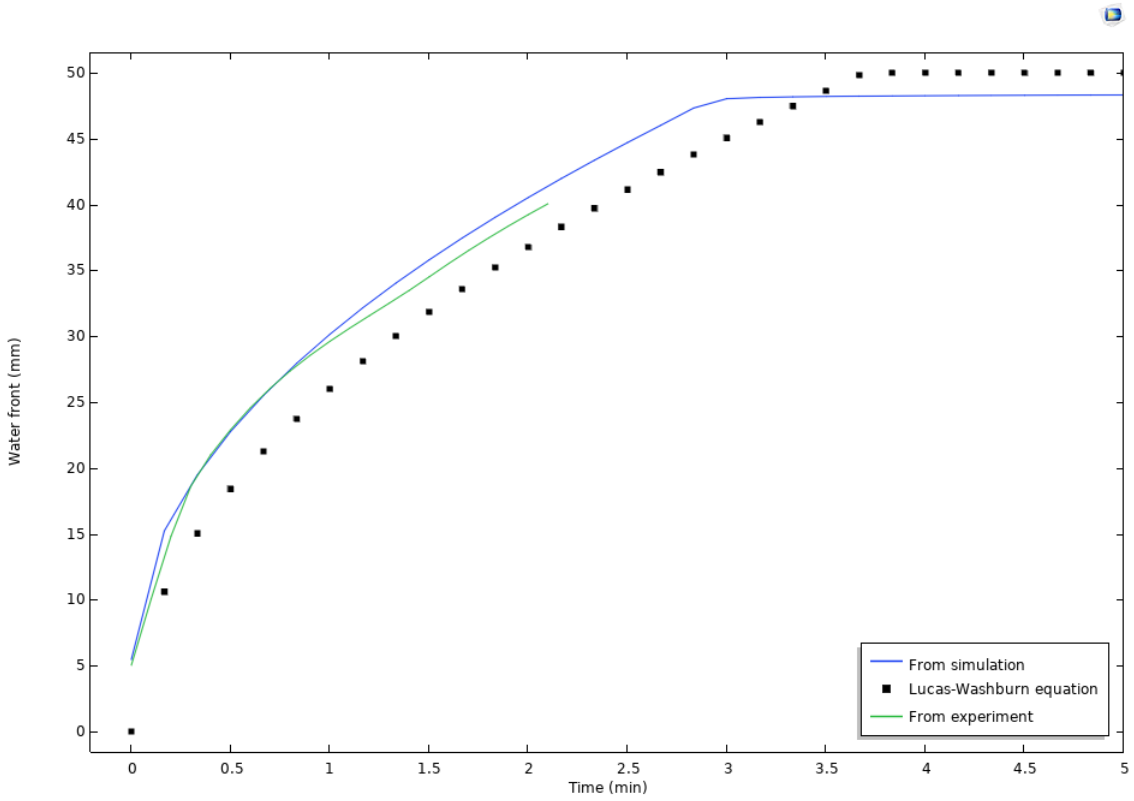


Figure 5.12: Water front versus time. Solid blue line: numerical solution. Dashed line: analytical expression given by the Lucas-Washburn equation. Solid green line: experimental curve.

The value of the contact angle θ between the nitrocellulose fibers and the water is found through trial and error in this wicking simulation. It is the one fitting the best the experimental values with the simulation.

The influence of different parameters as the porosity, the mean pore radius, the pore size distribution index and the geometry of the strip will be studied through simulations and experiments.
The porosity was shown to not play a major role. Actually the difference in simulated water saturation fronts between a porosity of 0.9 and one of 0.4 is imperceptible.

5.1.3.1 Mean pore radius

The mean pore radius has a large influence on the capillary speed. Figure 5.13 shows the water saturation for different times in a nitrocellulose strip of a geometry of 1cm x 5cm and having a mean radius of pores twice the one of the CN140 membrane.
It is observed that by increasing the mean radius of pores the capillary speed increases as well. Actually that is in adequacy with the Lucas-Washburn equation (Equation 2.4) in which it can be seen that the capillary speed is directly proportional to the square of the mean pore radius: $\frac{\partial H_{lf}}{\partial t} \propto \sqrt{R_c}$.

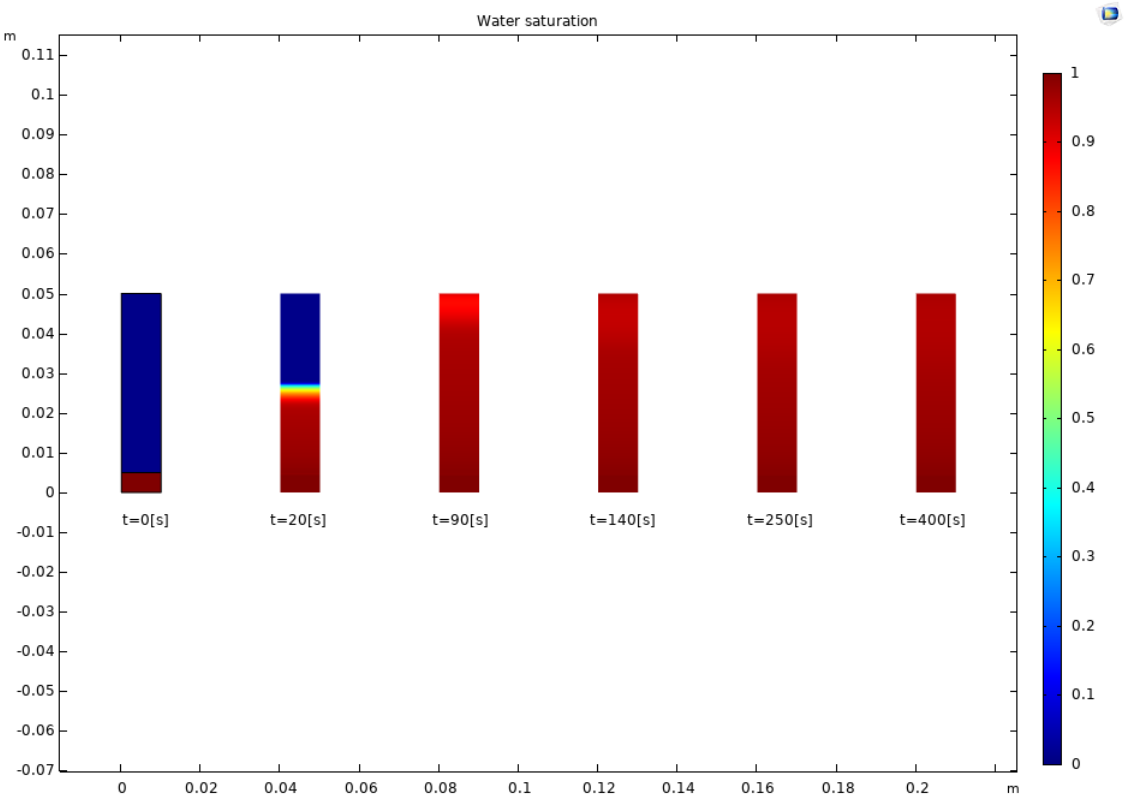


Figure 5.13: Water Saturation in the nitrocellulose strip 1x5 cm^2 after 20, 90, 140, 250 and 400 seconds. The porous material has a mean radius of pores twice the one of the CN140.

This parameter explains the major difference between the different nitrocellulosic membranes tested in experiments (see Figure 5.17). In fact thanks to SARTORIUS SEM's pictures it is known that CN95 is the membrane having the largest mean pore radius and the CN180 the one having the smallest one.
The results of vertical capillary flow experiment comparing membranes having different mean pore radius but the same geometry, namely 1cm x 5cm, are recorded in Table 5.2.

Table 5.2: Data from vertical capillary flow experiment on different CN membranes with a geometry of 1cm x 5cm.

	CN95 backed		CN140 backed		CN180 backed	
RH [%]	33%		33%		33%	
Front	1	2	1	2	1	2
Distance [cm] after 90 sec	3.9	4.15	3.3	3.6	2.9	3.4
Time [sec] for 2 cm	14.3	14.3	20	22.3	25.7	34
Time [sec] for 4 cm	82.3	91.3	115.7	135.3	148.7	173

The values presented in the Table 5.2 are an average from 3 repeats for each experiment. The average standard deviation for the CN140 backed's data is 1.66, for the CN95 backed's data is 1.80 and for CN180 backed's data is 0.53.

Figures 5.14, 5.15 and 5.16 show how the fronts of vertical flow with the strip's geometry 1cm x 5cm are. The fronts of the CN95 backed membranes are less homogeneous as well as its repeatability.

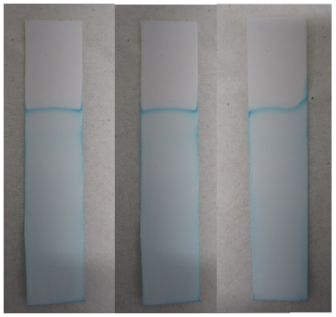


Figure 5.14: Fronts CN140 backed 1cm x 5cm at 33%RH.

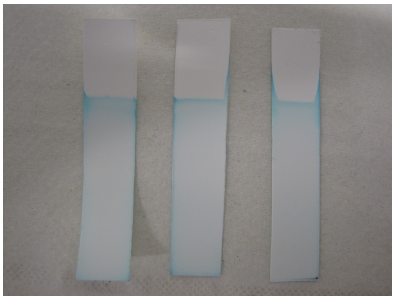


Figure 5.15: Fronts CN180 backed 1cm x 5cm at 33%RH.

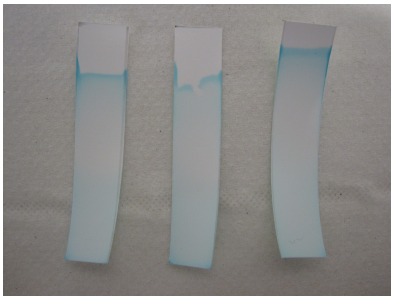


Figure 5.16: Fronts CN95 backed 1cm x 5cm at 33%RH.

If an average between the two distinct fronts is taken, the capillary speed graph for the relative humidity rate of 33% can be obtained to compare the CN95 backed, the CN140 backed and the CN180 backed membrane. This is presented on Figure 5.17.

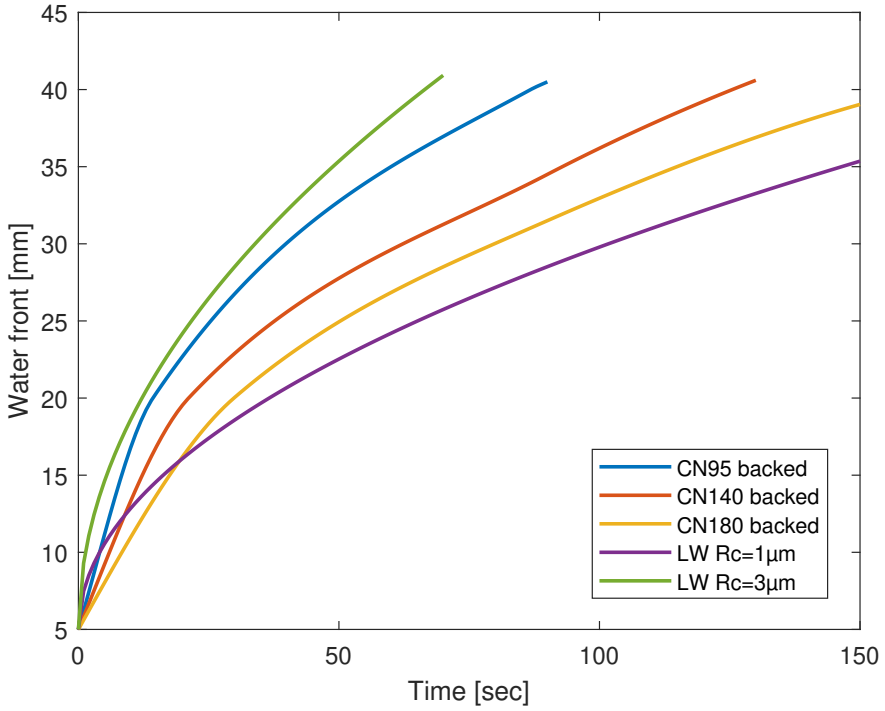


Figure 5.17: Capillary speed graph of CN membranes of 1cm x 5cm at 33% RH.

Two Lucas-Washburn equations are also plotted on Figure 5.17. They have been plotted through trial and error in order to enclose the capillary speed curves of the CN membranes and have an estimation of the mean pore radius range of these membranes.

Compared to the values given by SARTORIUS, even if the values obtained are not the same, though similar, the order of magnitude is the same as the smaller capillary flow time is the one of the CN95 backed and the higher one is the one of the CN180 backed. From SARTORIUS it is known that there is no significant difference in the void volume (or equivalently in the porosity) between CN95 and CN180. That even confirms that the differences are due to other properties of the porous structure of the different CN membranes, such as the pore size and the pore distribution.

The graph on Figure 5.17 shows that the capillary speed decays exponentially as the liquid progresses along the membrane. Approximately it takes five times as long from the flow to move from 20 to 40 mm as it takes from 0 to 20 mm. This can be explained by the fact that the difference between the capillary force and the gravitational one is decreasing with the increase of the height of the liquid front.
The capillary flow rate has consequently an effect on the detectability of the signal at the test line. Actually the chemical compounds are constantly moving through the porous media and therefore the formation of complexes at the test line depends on the finite time period during which the components are sufficiently close at the molecular level to bind to one another. The flow rate determines the length of this time period.
This impacts largely the placement of the test line as further it is from the origin, lower is the flow rate passing through it and therefore higher is the sensitivity of the sensor. Also the CN180 membrane allows a better sensitivity than the two other ones.

The capillary flow speed values in mm/sec can be converted in μL/sec knowing the void volume of the membrane:

$$y\ [\mu L/sec] = x\ [cm/sec] \times width\ [cm] \times thickness\ [cm] \times porosity\ [/] \times 10^3\ [\mu L/cm^3]$$

If we assume a porosity of 75%, Figure 5.18 is obtained.

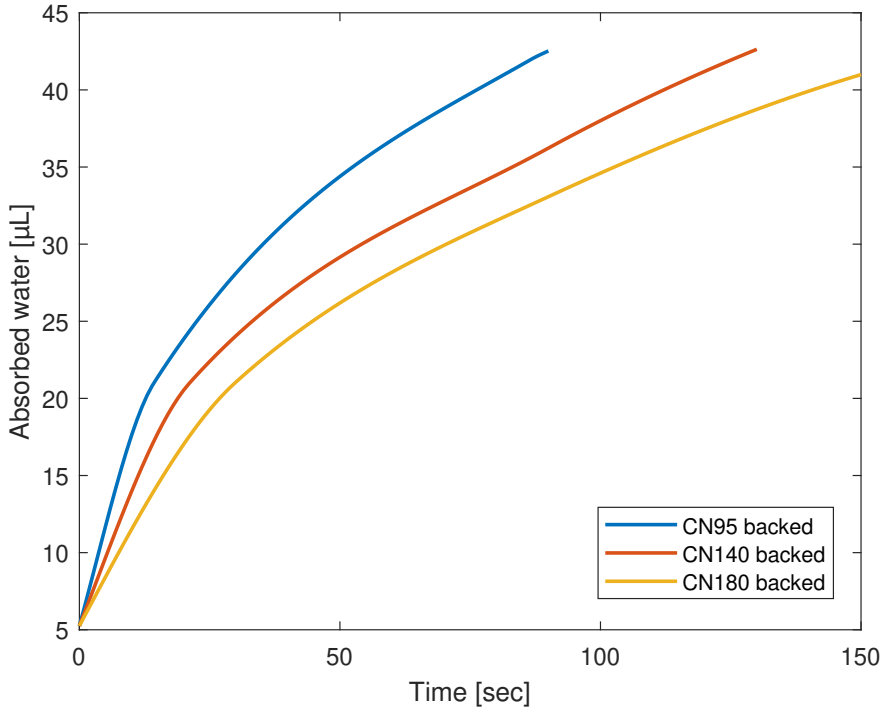


Figure 5.18: Amount of water absorbed as a function of the time for different CN membranes of 1cm x 5cm.

On Figure 5.19 it has been found that the mean pore radius fitting the best the experimental curve through the Lucas-Washburn equation was $1.6\mu m$, which is close of the value determined thanks to Figure 5.6.

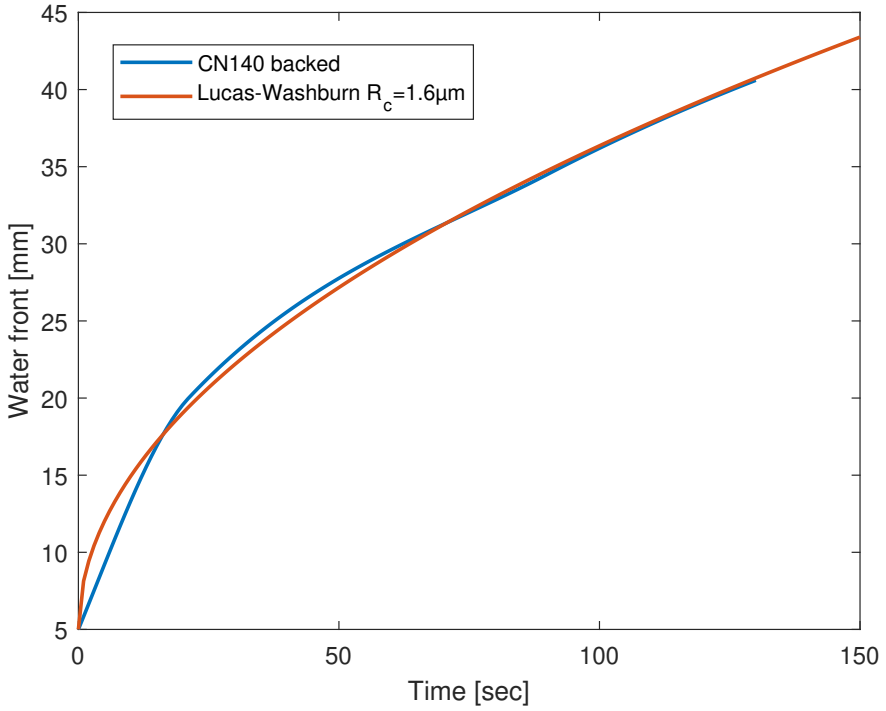


Figure 5.19: Capillary speed CN140 membrane of 1cm x 5cm at 33% RH.

5.1.3.2 Relative humidity

As clearly observable on Figure 5.20, if the water saturation (or relative humidity) is increasing, the capillary speed is increasing as well. The strip is soaked well faster when the water saturation is 0.5 than when is is 0.01.

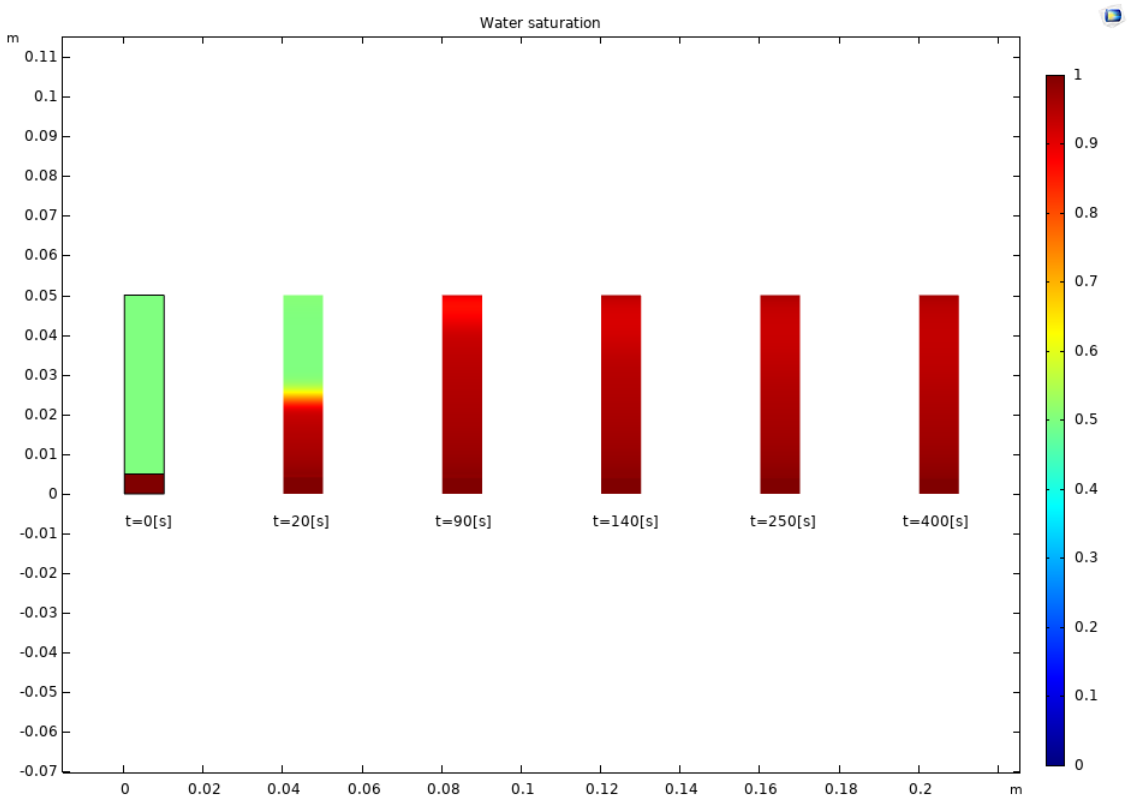


Figure 5.20: Water Saturation in the nitrocellulose strip 1x5 cm^2 after 20, 90, 140, 250 and 400 seconds. The initial air saturation of the strip is 0.5 (instead of 0.99).

A high relative humidity of 95% corresponds to an initial water saturation of the strip of about 0.08 and a relative humidity of 76% to an initial water saturation of the strip of about 0.04. In practice and depending on the exterior environment the difference in capillary flow rate will be consequently light unless the membrane is exposed to a condensing atmosphere.
Figure 5.21 shows the capillary speed curve for CN140 backed at two different relative humidity's namely 33% and 76%. A small difference is observable. However to draw conclusions on the effect of RH on capillary, more value of RH should have been experimented. Actually Walji and MacDonald conclude in their article [165] that paper strip with varying humidity levels can yield consistent flow behaviour regardless of fluctuating levels of humidity. However this article is based on pure cellulose chromatography paper strips so that the difference observed on Figure 5.21 reflects either a different behavior for nitrocellulose or is due to experimental error. The last case may be explained by the storage of the membrane at a high level of humidity during more than two months that may have affected membrane properties and chemicals as that is not the recommended storage conditions. In any case, further experiments have to be carried out to be able to conclude to one of these possibilities.
Figure 5.23 and the associated discussion tends to confirm the tendency of an increase in capillary speed with a decrease in relative humidity.

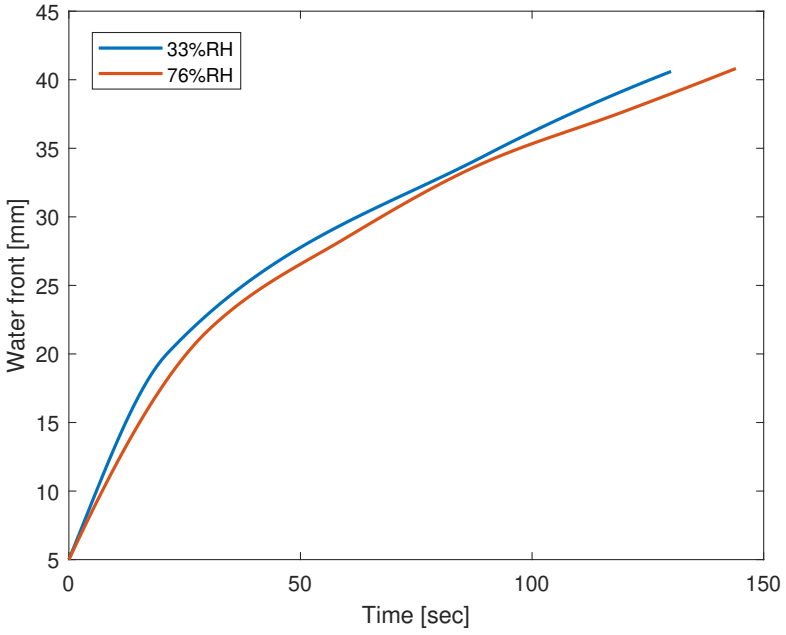


Figure 5.21: Capillary speed in CN140 backed 1cm x 5cm at 33% RH and 76% RH.

5.1.3.3 Strip geometry

The last parameter to study is the geometry.
By simulating a strip of 1x7 cm^2, one of 1x10 cm^2 and one of 0.5x5 cm^2 the simulation values do not significantly differ.

This observation is also done in experiments and in the article [166]. On Figure 5.22 it is seen that the different geometries, having the same area ($5cm^2$) and therefore the same void volume, do not induces significant differences. The length and the width of the strip do not influence the flow velocity. The width would have been an influencing parameter if a capillary tube was studied because it will directly affect the amount of water in the tube. Consequently the gravitational force applied on it will be higher and will compensate more the capillary force. In comparison, a porous media may be seen as plenty of small capillary tubes being characteristic of the pores, so that a increase of width does not increase the geometry of the pores, only the one of the global porous media.
Bohm et al. [167] observed slower flow in channels with smaller widths for paper strips with hydrophobic barriers and widths of 1 to 5 mm, and found that the dependence on width diminished above 4 mm. This behaviour was attributed to the large number of pores that were “terminated” at the channel walls (dead-end pores) where the hydrophobic barrier was located, thus interrupting flow and resulting in slower fluid flow (longer time to fill a given volume of space). Hong and Kim [168] investigated small channel widths of 1, 2, and 4 mm and concluded that the effects of hydrophobic channel boundaries are significant with a width on the order of 1 mm. The slower flow in channels with smaller widths was attributed to the surface tension forces at the hydrophobic boundaries that oppose the flow, and therefore they expect no variation for paper strips with cut edges.
The slight differences that can be observed on Figure 5.22 can not be explained but from experimental errors.

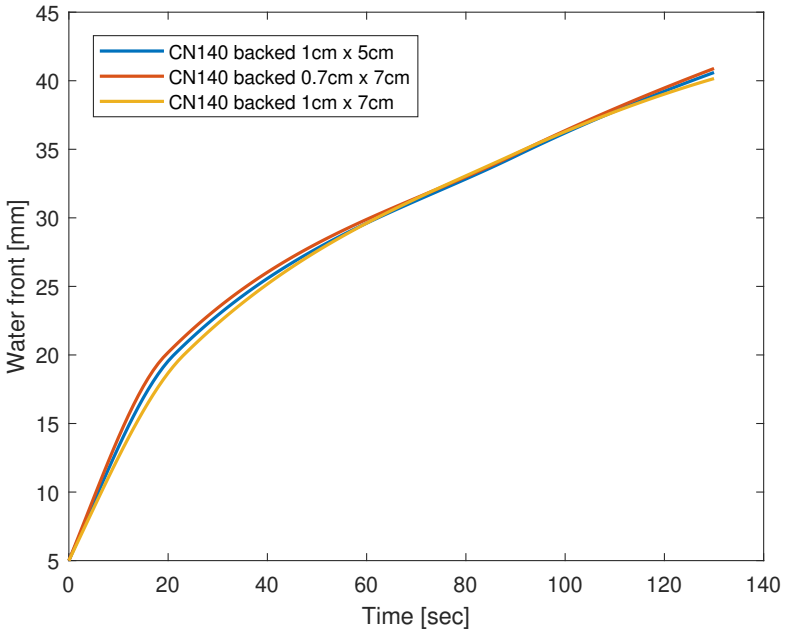


Figure 5.22: Capillary speed graph at 33% RH for three different strip's geometries. Two of them have the same length and two others have the same width.

Figure 5.23 also presents the capillary speed graph for the three same different strip's geometries than on Figure 5.22 but in this case the nitrocellulose membranes have been put at a relative humidity of 76%. The capillary velocity is observed to be increasing with the length of the strip and to be decreasing with the width. However none previous work have shown a dependence with the length. Some previous work have observed a dependence on width but that one is inverse to the one observed here [165][167][168]. One explanation may be the waiting time in between the experiments during which the nitrocellulose strips were not in a 76% RH environment anymore but in ambient conditions. The experiments have consequently been conducted during the time where the strips were in between two different relative humidity's and temperatures. This explanation may therefore confirm the behavior observed on Figure 5.21 as the first tested strip was the 1cm x 7cm one and the last one was the 0.7cm x 7cm one. There would not have any length and width dependence but well an increase in velocity with a decrease in relative humidity.

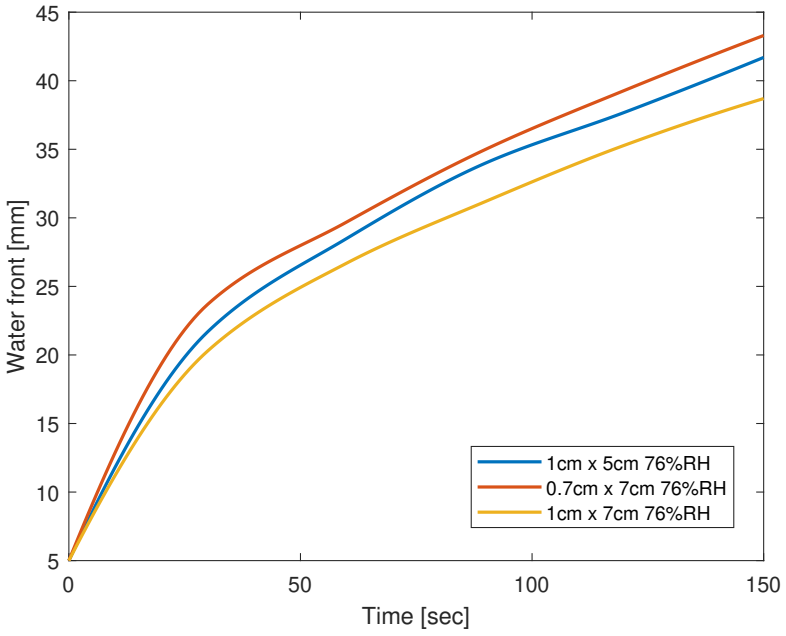


Figure 5.23: Capillary speed graph at 76% RH for three different strip's geometries. Two of them have the same length and two others have the same width.

What is going to change more with the geometry in strip with cut edges is the assay sensitivity as for longer strip, more sample will pass over the capture line (if assumed to be located at the same position in all geometries) as more bed volume are available downstream the capture line for acting as absorbent material for the capillarity. This concept is represented on Figure 5.24. Generally in lateral flow assay an absorbent pad is present at the end of the membrane strip. In this case the consideration of the bed volume of the strip is unimportant as it becomes naturally negligible compared to the one of the absorbing pad.
Comparing two strip having the same length, the flux of reagent delivered will be directly proportional to the width and inversely.

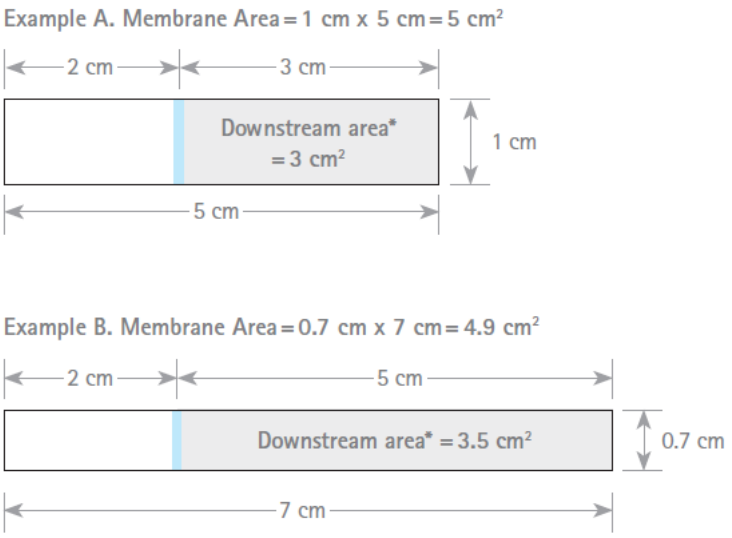


Figure 5.24: Effect of membrane dimensions on volume of sample analyzed [83].

Because gravity may have an non-negligible impact on the vertical flow, horizontal flow experiments have been conducted. This can start by putting the strip on the water drop or by putting the drop on the strip. The problem in the first case is that another capillary flow occurs in parallel between the plastic support and the backing of the nitrocellulose membrane as it can be observed on Figure 5.25. The same phenomenon occurs when the nitrocellulose strip is reversed. That distorts the results and influences a lot the repeatability as catching the membrane at the end of the experience with a clamp can make contacting the water layer with the unbacked part of the nitrocellulose. The problem in the second case is that a flow is induced because of the pressure at which the drop of water is deposited with the pipette. Repeatability is in this case not guaranteed either.
Since it is not feasible to keep the unbacked strip vertically, horizontal data could not have been compared with vertical ones.
These results could have therefore not be gathered to draw conclusions.

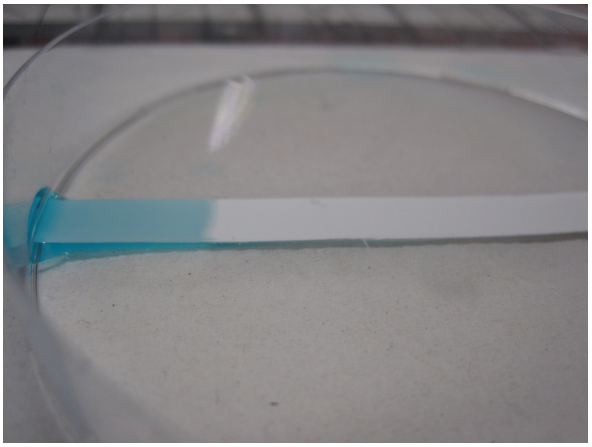


Figure 5.25: Layer of water in between the backing of 0.7cm x 7cm CN140 backed and the plastic support.

A particularity can be observed on Figure 5.26 presenting the experiment of one CN140 unbacked strip deposition on a water drop of 100 μL. This phenomenon is called the Saffman-Taylor instability or the viscous fingering instability and is the formation of patterns in a morphologically unstable interface between two fluids in a porous medium. Horizontally it occurs when a more viscous fluid is deplaced by a less viscous fluid. In the case on Figure 5.26, the more viscous fluid is the water without methyl blue, having its interface a little bit above the one of the less viscous fluid being the water colored with methyl blue. That would mean that the blue methyl solution is less viscous than the pure water.

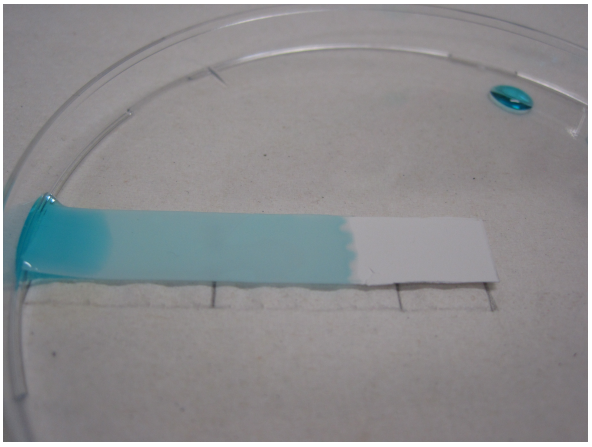


Figure 5.26: Viscous fingering instability on CN140 unbacked strip, with deposition of the strip on one colored water drop of 100 μL.

It has been seen that a change of width does not affect the capillary speed, but a sudden change of width in the geometry does as it will be shown in this part of the discussion about the strip geometry.
In the case of an sudden expansion, the assumptions of the Lucas-Washburn equation of a non-limiting source of liquid and of a constant cross-sectional area are violated. Figure 5.27 shows that the capillary speed decreases because of the width expansion. This can be explained instinctively by the fact that a longer time is required for the fluid to fill a volume element having a certain length and a larger width than a volume element having the same length and a smaller width.

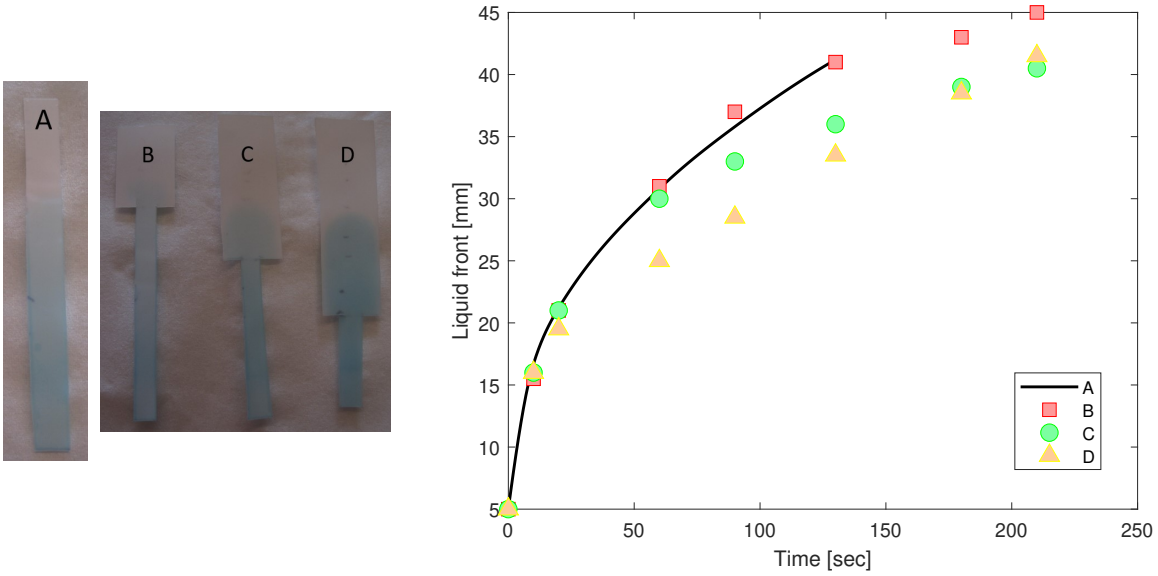


Figure 5.27: Impact of a sudden-expansion in the strip geometries of the capillary speed. The smaller width is 4mm and the larger one is 1cm for each geometry. The total length of each strip is 5cm. The strip B has its expansion at 3.5cm, the strip C has its expansion at 2.5cm and the strip D has its expansion at 1.5cm. The curve A corresponds to a strip of 0.5cm x 5cm.

When there is a sudden contraction in the geometry the assumption of Lucas-Washburn equation of the constant cross-sectional area is violated but on the contrary on an expansion, the assumption of a non-limiting source of liquid is correct. Figure 5.28 shows the impact of a contraction on the capillary speed.

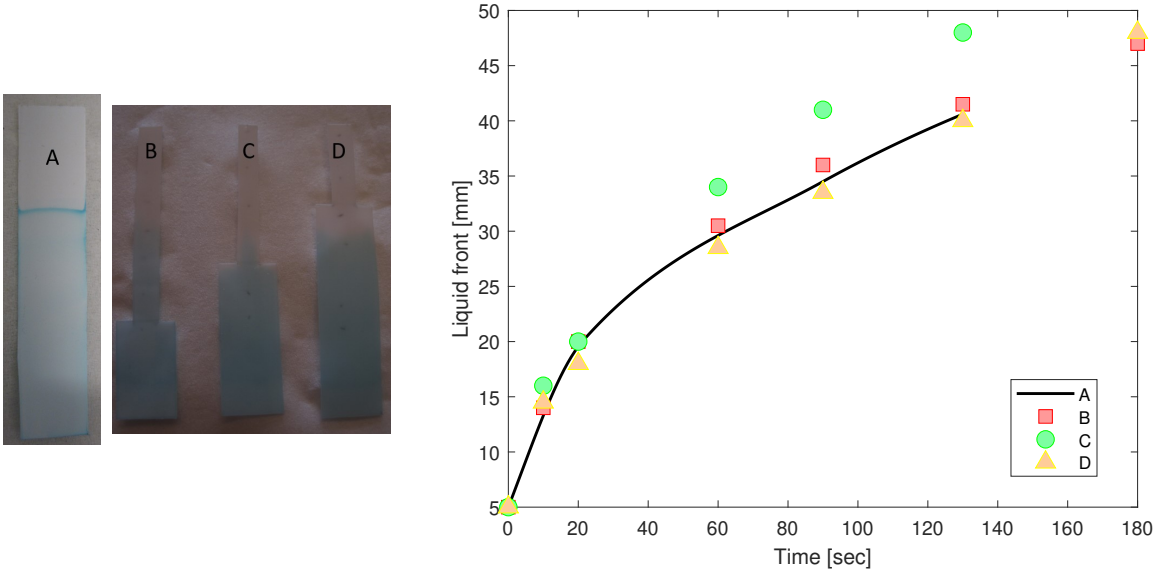


Figure 5.28: Impact of a sudden-contraction in the strip geometries of the capillary speed. The smaller width is 4mm and the larger one is 1cm for each geometry. The total length of each strip is 5cm. The strip B has its contraction at 1.5cm, the strip C has its contraction at 2.5cm and the strip D has its contraction at 3.5cm.

Once the second width reached, the front follows the Washburn equation as in the first segment but with a relative time $t - t_1$ where t_1 is the time required to the fluid to reach the end of the first segment of the strip.
On Figure 5.28 it can be clearly seen that the strip minimizing the capillary time needed to reach a certain height of the front is the strip C having both segments of equal length. This can be explained by the following development.
From Equation 2.4 the velocity equations for the segment before the contraction and for the segment after it can be simplified respectively as (from [166], with τ is the amount of time needed to reach the behavior described by the Lucas-Wahsburn equation):

$$v_1(t) = \frac{v_{01}\sqrt{\tau}}{\sqrt{\tau + t}} \tag{5.1}$$

$$v_2(t) = \frac{v_{02}\sqrt{\tau}}{\sqrt{\tau + t - t_1}} \tag{5.2}$$

Assuming that the Lucas-Washburn equation applies at all times is equivalent to assuming that the inertia of the fluid is negligible, and that the fluid instantaneously adapts its velocity to satisfy a balance between viscous friction forces and capillary forces. This equilibrium implies that, at the interface between the segments of different width, the flow evolves without discontinuity (because both the driving capillary pressure and the total hydraulic resistance evolve continuously). The boundary condition consequently leads to a relation between v_{01} and v_{02}:

$$v_2(t_1)W_2 = v_{02}W_2 = v_1(t_1)W_1 = \frac{v_{01}W_1\sqrt{\tau}}{\sqrt{\tau + t_1}} \tag{5.3}$$

The equations for the liquid front distance can be obtained by integration of equations 5.1 and 5.2 (with the initial conditions $d_1(0) = 0$ and $d_2(t_1) = d_1(t_1)$):

$$d_1(t) = 2v_{01}\sqrt{\tau}(\sqrt{\tau + t} - \sqrt{\tau})$$

$$d_2(t) = d_1(t_1) + 2v_{02}\sqrt{\tau}(\sqrt{\tau + t - t_1} - \sqrt{\tau})$$

If t_T is defined as the total required time to reach a distance d_T:

$$t_T = t_1 - \tau + \left(\frac{d_T - d_1(t_1)}{2v_{02}\sqrt{\tau}} + \sqrt{\tau}\right)^2$$

By assuming $t_1 >> \sqrt{\tau}$ and by using Equation 5.3, the solution that minimizes t_T is found to be $d_1 = \frac{d_T}{2}$ whatever the ratio W_1/W_2, which corresponds to the observation done on Figure 5.28. It is important to mention that this result does not take into account the presence of "dead zones" in the corners of the widest channel during the section contraction. This means that the cross-sectional area useful for the passage of the flow is smaller than the total width of the channel. These areas are likely to have a characteristic length in the order of the difference of widths.

When fully wetted the Darcy's law is the one to be applied. The sudden change in the geometry of the strip will also affect the flow of water once the porous media wetted. Actually by a simple calculation, it will be found the same condition saying that to have the greatest transport time the length of both segments have to be equal [166].
If Equation 2.5 is generalized to the case of a strip with different segments of different width:

$$Q = -\frac{\Delta P}{\frac{\mu}{\kappa}\sum_{i=1}^{N}\frac{L_i}{W_i H_i}}$$

The equation for the time t required to fill a volume V of strip is defined as $t = \frac{V}{Q}$ with $V = L_1 W_1 H + L_2 W_2 H$ in the case of two different widths. Then it can be written:

$$t = -\frac{\mu}{\Delta P \kappa}(L_1 W_1 + L_2 W_2) H \left(\frac{L_1}{W_1} + \frac{L_2}{W_2}\right) = -\frac{\mu}{\Delta P \kappa} H \delta$$

If $\gamma = \frac{L_2}{L_1}$ and $\beta = \frac{W_2}{W_1}$:

$$\delta = L_1 L_2 \left(1 + \frac{1}{\beta\gamma}\right)(\beta + \gamma)$$

By derivating this by γ and by equaling the derivation to 0 a value for γ minimizing the required time is found:

$$\gamma = 1$$

That means that for any non-equal W_1 and W_2 the greatest transport time can be obtained for $L_1 = L_2 = L$ (same conclusion than for non-fully wet strip).
With this condition and if $\beta >> 1$, $\delta = L^2(\beta + 1)$, so that β has to be increased if longer time t is wanted. Figure 5.29 shows that this conclusion is also verified in non-fully wet strips.

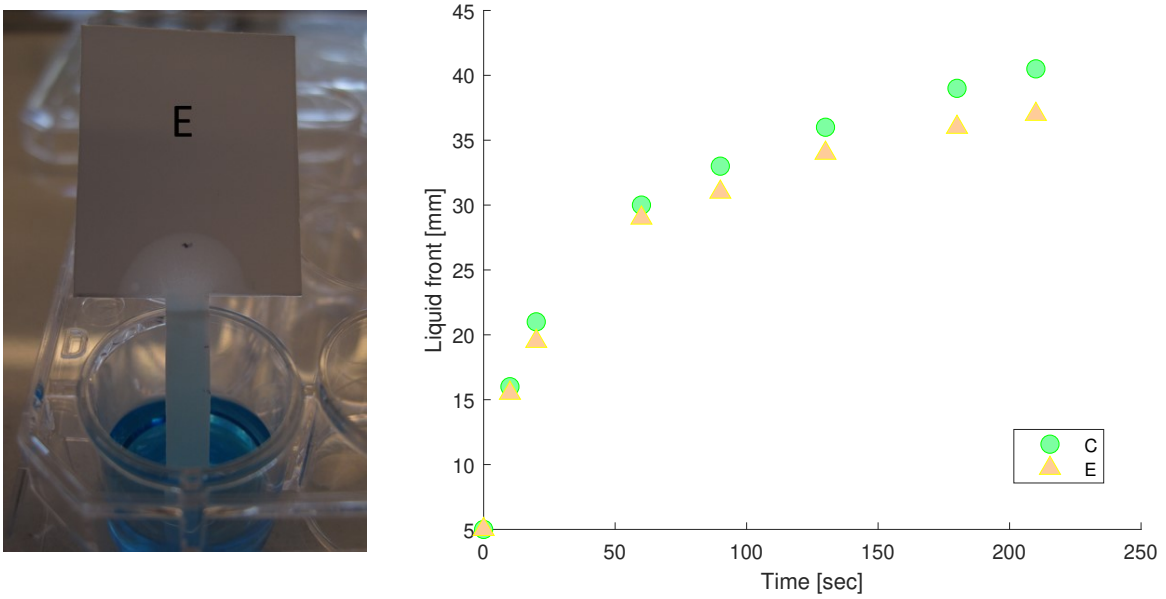


Figure 5.29: Effect of β increase in a non-fully wet strip. The smaller width is 4mm, the total length is 5cm and the expansion is located at 3.5cm for each geometry. The beta parameter of strip E has a value of 5 while the beta parameter of strip A has a value of 2.5.

This results have been compared and are in accordance with the scientific article [166].

5.1.3.4 Absorbent pad

Generally the pore radius of an absorbent pad are bigger and its contact angle with water as well so that the capillary speed in that media would be higher than in the nitrocellulose strip. However its main function is to increase the volume of sample that can be analyzed thanks to its high void volume and its addition at the top of the biosensor.
Figure 5.30 compares the Lucas-Washburn equation for the CN membrane and for the Whatman paper. It can be observed that the graph looks like the one on Figure 5.3.
Figure 5.31 shows the results of the experiment of capillary flow in the Whatman paper compared to the ones obtained in the CN140 membrane. The difference with Figure 5.30 must have to do with the fact that the experiment is done vertically because when the strip is placed horizontally as done for Figure 5.3, this sudden slow down in capillary flow is not observed. That could be due to the fact that the Whatman paper becomes very weak once wet and the strip is therefore kept vertical by manual means during experiments.

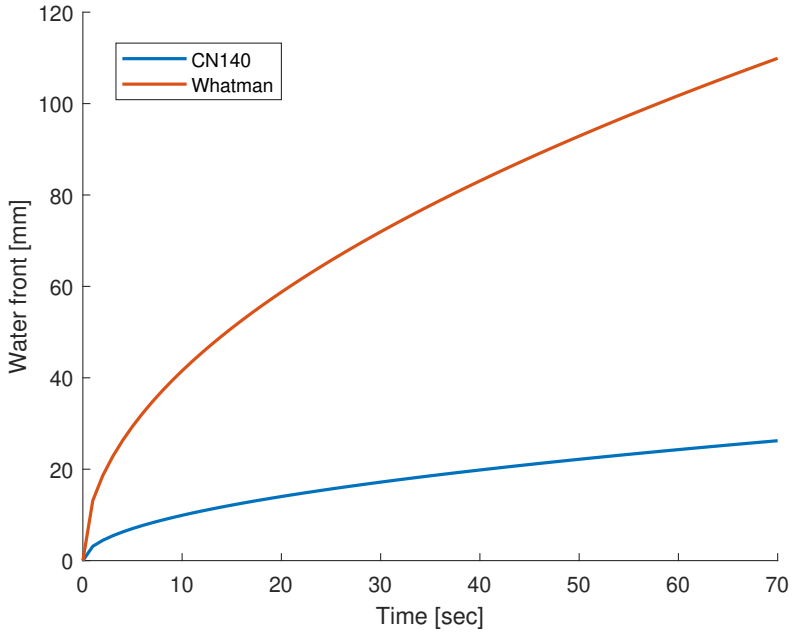


Figure 5.30: Lucas-Washburn equation for the CN membrane and for the Whatman paper of grade 1. This type of Whatman paper as a thickness of 194 μm, a pore size of 11 μm, a porosity of 68% and a contact angle of 30° [155].

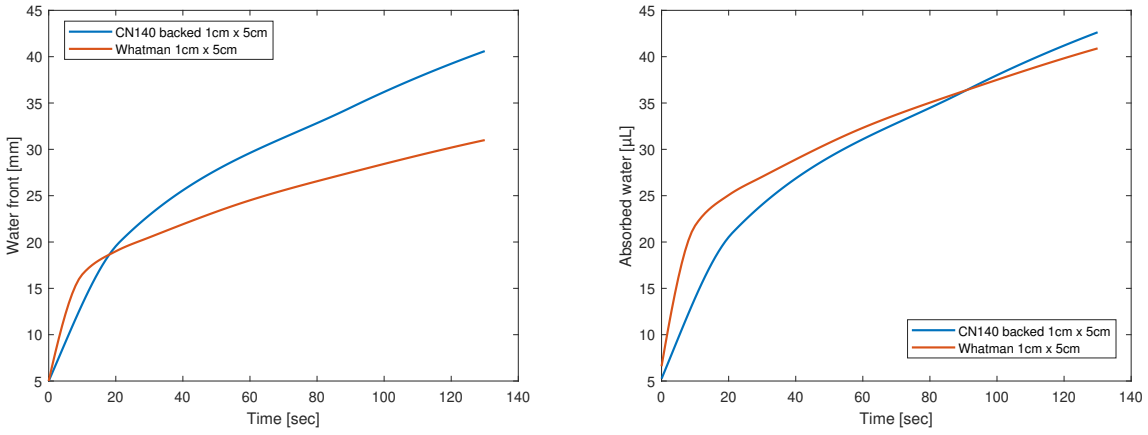


Figure 5.31: Comparison of water front and absorbed water as a function of time in CN140 backed and Whatman filter paper of grade 1.

In the case where an absorbent pad is added at the end of the biosensing strop, the water is going to start flowing through it when all the strip becomes wet. At this time the capillary flow rate in the strip should shown a variation as the absorbent pad will then play the role of "absorbent" and increase the flow rate in the strip.
Another possible use of an absorbent pad is to consider it as a flow delay. In fact if this kind of pad is put at a certain place on the strip the capillary flow will be delayed because more volume must be wetted because of this additional pad having a high void volume [144].

5.2 Nitrocellulose as substrate for biological detection

5.2.1 Biofunctionalization of nitrocellulose membrane

For lateral flow test strips, the nitrocellulose membrane must irreversibly bind the bioreceptors at the test lines. This binding capacity is determined by the surface area available for the immobilization. This area depends mainly on pore size, porosity and thickness of the membrane. The loading capacity of a protein acting as receptor depends on its structure and its effective diameter. For example the loading capacity of the antibody IgG is $1\mu g/cm^2$. To have a value for the binding capacity of the nitrocellulose membrane, the loading capacity has to be multiplied by the surface area ratio which is typically found in the range 50-200. Then assuming a test line of 1x0.1 cm^2, the amount of capture reagent is 5-20 μg which is greater than required for most assays [83].

The opacity of the nitrocellulose make the observation of the particles inside the membrane difficult. Indeed any reagent bound deeper then $\sim 10\mu m$ from the surface becomes invisible to the user. Then the percent of visible signal is related to the membrane's thickness [83].

The first adsorption of GFP RBPs on CN140 unbacked membrane was made by deposition on one side of 5 drops of $5\mu L$ each in order to wet all the surface of the membrane piece. After the observation of the proteins' fluorescence with Epifluo (see Figure 5.32) and confocal microscopes (see Figure 5.33), it has been seen that the deposition was not uniform and that no RBPs were observed on both sides of the membrane. This is especially observable on Epifluo images where the shape of the deposed drop in clearly visible (coffee ring effect) and on Confocal image where the maximal depth of captured fluorescent is $17.32\mu m$.
This issue should be solved by putting an larger drop of bioreceptors' solution. Knowing the void volume of the membrane (70-80%) and the volume of the membrane into which the drop is applied ($\sim$2cm x 2cm x $140\mu m$), $40\mu L$ should be appropriated.

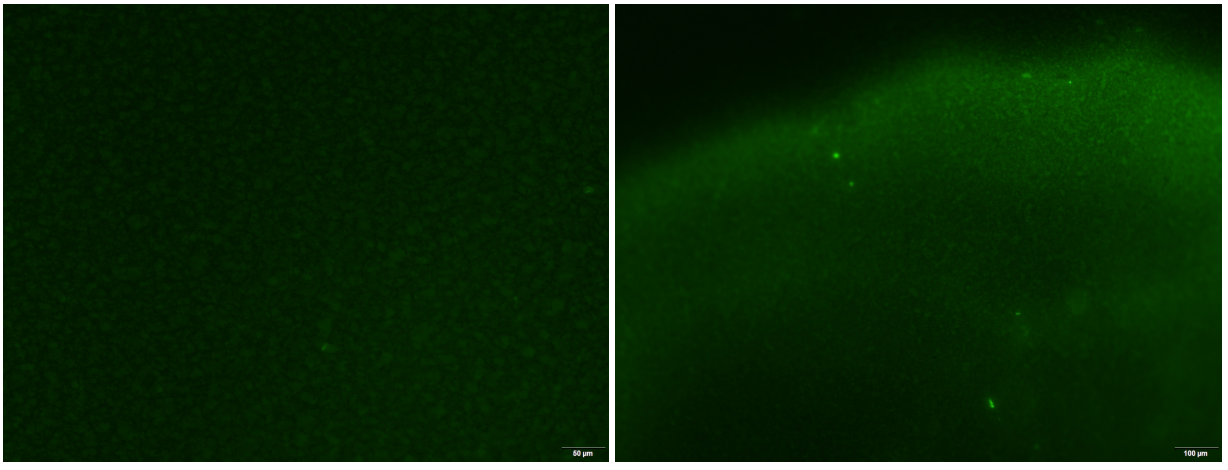


Figure 5.32: Epifluo microscope images of CN140 unbacked biofunctionnalized with RBPs.

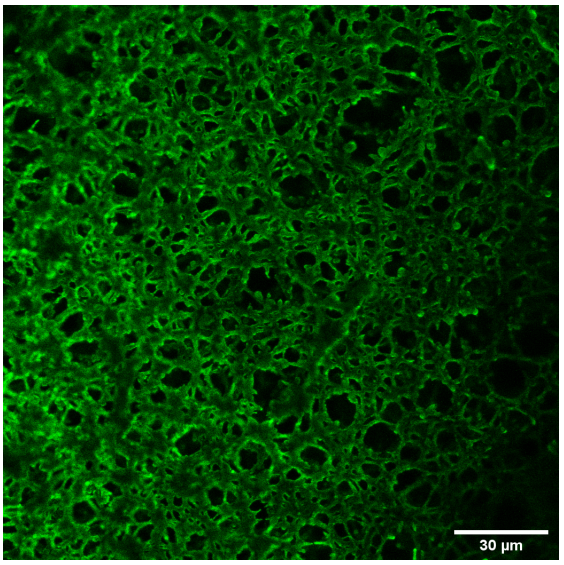


Figure 5.33: Confocal microscope image of CN140 unbacked biofunctionnalized with RBPs. 2D scans from 0 to 17.32 μm depth.

During the manufacturing of the test strip, detergents or surfactants are added to the naturally hydrophobic membrane in order to make it wettable. Figure 5.34 shows qualitative influences of the detergent concentration.

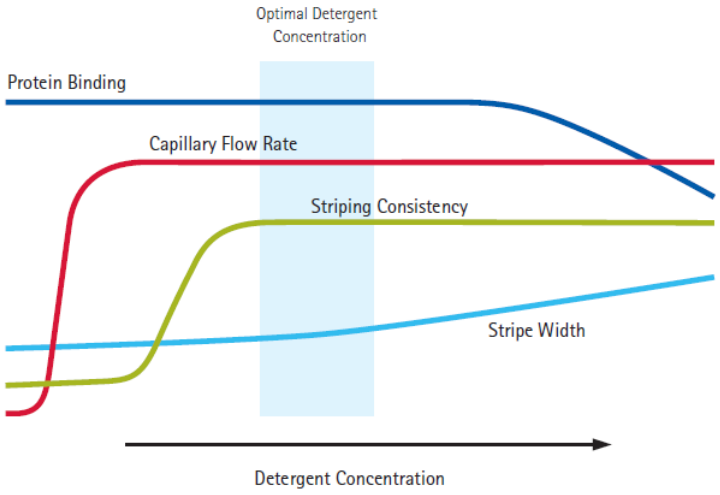


Figure 5.34: Effect of detergent or surfactant concentration on various membrane performance characteristics [83].

As seen on Figure 5.34, this addition may decrease the protein binding ability of the membrane by masking the nitrocellulose and broader the test band width which could lead to a decrease in sensitivity [83]. For these reasons, the concentration of surfactant should be hold at the minimum needed to make the membrane wettable.

5.2.2 Binding affinity

Figures 5.35 and 5.36 shows that respectively gp221_CBD and gp185 (blue RBP) specifically recognize strains GBJ001 from *Bacillus* cereus group. These strains have a length about $10\mu m$ with a much smaller width. Their move in the porous media of the nitrocellulose should not be an issue if the membrane with larger pores is selected, namely the CN95 (see Figure 5.17).

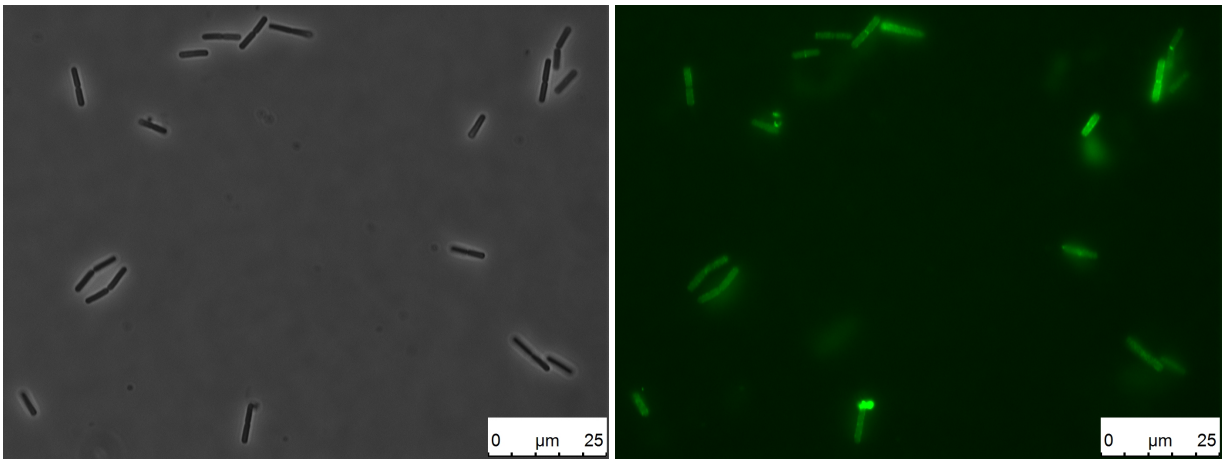


Figure 5.35: Strains GBJ001 from *Bacillus* cereus group recognized by fluorescent gp221_CBD.

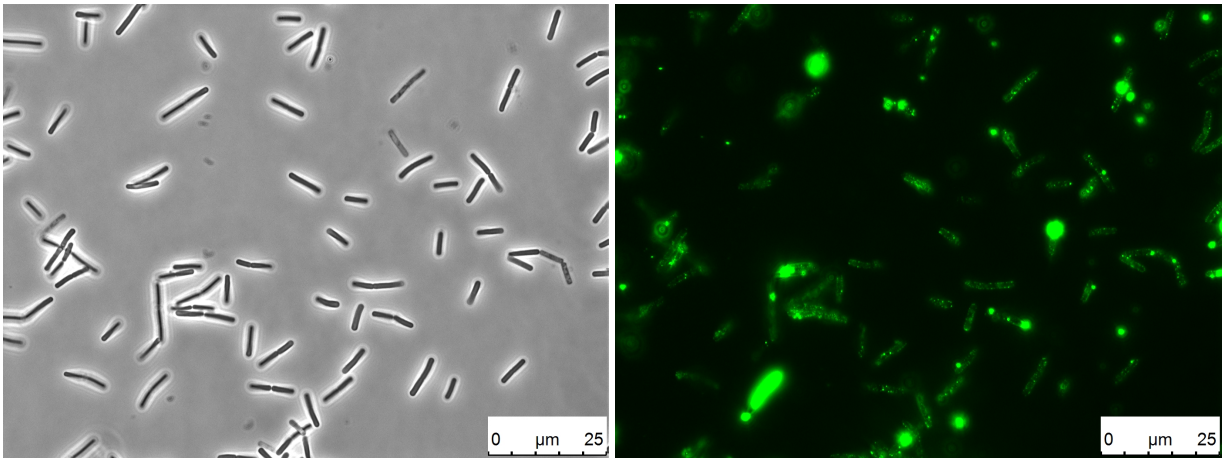


Figure 5.36: Strains GBJ001 from *Bacillus* cereus group recognized by fluorescent gp185 (blue RBP).

Chapter 6

General technical discussion

6.1 Microfluidics guidelines

6.1.1 Nitrocellulose membrane selection

For the selection of the membrane two main parameters must be taken into account.

The first one is pore size through the mean pore size and the distribution of the pores sizes. It has to be adapted to the size of the molecules present in the sample in order to avoid inopportune clogging of the pores and allow the displacement of most particles in the sample. Not only targeted molecules (*E. coli* is approximated as a cylindrical of $1\mu m$ of diameter and $2\mu m$ of height) are of importance as other bigger molecules in the complex sampling media could clog the ways and cause the non-detection of bacteria of interest at the test line. For this purpose membrane with the highest mean pore radius is the best choice.

The second parameter influenced by the choice of the membrane is the test sensitivity. Actually it has been shown that membranes with larger pores are characterized by a larger capillary flow. In the meantime the formation of complexes at the test line depends on the finite time period during which the components are sufficiently close at the molecular level to bind to one another. Consequently the capillary flow rate, even if it gives the force needed to push the particles, affects the detectability of the signal at the test line by affecting this finite time period that allows the binding between the target bacteria (Ag) and the bioreceptors (P). The effective concentration of analyte has even been linked to the capillary flow rate in [83] and is found to be inversely proportional to the square of the change in flow rate. The following equations illustrates the influence of the capillary flow rate on the amount of formed complexes R by the "effective" change in concentration of P and Ag. In the case of a flow rate of $1X$: $R = k[P][Ag]$ while in the case of a flow rate of $2X$: $R = k[0.25P][0.25Ag]$.

However it has also been observed in this master thesis that a sudden change in the strip width influences the capillary flow rate and could therefore be used to adjust the sensitivity. Another enhancement to improve the detection sensitivity involves the integration of cotton thread-based barriers into paper. It has been shown in the article [131] that it decreases the flow rate of sample and extends the reaction time. The article [130] described the

development of novel device integrating dialysis-based concentration method into LFAs with the aim to increase the sensitivity.
That leads to the conclusion that the membrane with a large enough mean pore size is recommended to ensure a sufficient displacement of the particles in the strip as the sensitivity issue can be fixed by other means.

6.1.2 Strip geometry

The strip geometry influences the sensitivity of the biosensor by the volume of sample that will flow through the test line and by the capillary speed of the sample at the test line.

The void volume downstream the test line represents the volume of sample that will pass through this line and of which the target biomolecules will have the possibility to be bound to the bioreceptors. An increase of area downstream the capture line leads therefore to an increase of sensitivity of the sensor.
The volume of sample needed is the volume of sample that will enable enough bacteria to be captured at the test line. This is constraint in an electrical one as it is linked to the minimal amount of bacteria needed to the transducer to allow an optimal detection. This point is discussed by Margo Hauwaert in her master thesis [107]. Once the needed amount of bacteria would be known or approximated, it will be possible to determine the volume of sample that has to be analyzed as well as the width of the test line needed to have the corresponding needed amount of bioreceptors. This last parameter should not be limiting as the bionfunctionalization is done with a high concentration in bioreceptors which are well smaller than bacteria (see Table 4.5). The volume of sample that will flow through the capture line should taken into account to be able to determine the real concentration of the target molecule in the media where the sample is taken.

Thanks to the sudden width expansion in the strip geometry, the capillary speed is decreasing. As already mentioned, the sensitivity is inversely proportional to the square of the capillary flow rate so that a sudden expansion before the test line will increase the sensitivity.
The proper capillary speed at the capture line location will be consequently influenced by the characteristics of the interaction between the bacteria and the RBP or CBD. Tests should be done to determined the capillary flow rate allowing the optimal detection of the bacteria. This flow rate should then be kept in mind for the choice of the location of the sudden width change as well as for the choice of the widths ratio of this change.

6.2 Biofunctionalization guidelines

The following guidelines are mostly inspired from the document [83] written by EMD Millipore.

6.2.1 Capture reagent solution

Different parameters have to be taken into account when preparing the solution of capture reagents that will biofunctionalize the test line. The main ones are the the pH, the ionic strength, the use of alcohol and detergents and the concentration of reagent.

If the solubility of proteins increases, their tendency to partition onto the membrane increases. The solubility of protein is minimal when it has no net charge, namely at the isoelectric point. To reach minimal solubility, the pH has then to be adjusted to be close to the isoelectric point of the proteins of interest.

The ionic strength of the buffer should be as small as possible because ions can interfere with electrostatic interactions occuring between the membrane and the capture reagents.

The addition of small amount of alcohol such as methanol, ethanol or isopropanol in the capture reagent solution may have very positive effects. The first one is that it will lower the viscosity of the solution and its surface tension. Then it will decrease the solubility of the proteins and enhance the adsorption of the bioreceptors onto the nitrocellulose membrane. Finally it will improve the drying and the protein fixation.

If the test line addition displaces the surfactant present in the membrane, this line will wet more slowly than other parts of the membrane and the front of the flow will become deformed. To avoid this a small amount of detergent/surfactant can be added to the reagent solution.

By decreasing the surface tension, the add of alcohol and/or surfactant lowers the Marangoni flow responsible for the coffee ring effect. This effect mentioned in Section 5.1.1 could occur during the drying of the capture line and be disruptive by resulting in a non-uniform dried deposit, as observable on Figure 5.32.

Last but not least the concentration of bioreceptor elements in the capture reagent solution will play an important role in the amount of immobilized protein along the capture line and therefore also in the possible captured biomolecules. As already said this amount of molecules fixed at the test line is an electrical constraint as it depends on how many bacteria should be present at this line to be able to have a sufficient detection by the transducer.

6.2.2 Application of bioreceptors to the membrane

For detection purposes, it is important to properly apply the capture reagent solution into the membrane at the test line location. The parameters to take into account are mainly the humidity of the membrane and the side of the membrane in case of unbacked one.

It is said in [83] that under conditions of low humidity, nitrocellulose membranes develop a significant static charge. Water droplets being naturally electronegative, the droplets could be repelled by static charge. The consequence would be a strong variation in the width of the reagent line. A relative humidity about 50% at ambient temperature offers optimal results according to this article.

It is advised to apply the solution to the side which was in contact with belt during the manufacture of the membrane (shinier one) as it rarely presents physical irregularities. The deposition will be therefore more uniform.

6.2.3 Fixation of the bioreceptors

Once applied, the solution of RBPs and CBDs has to be dried so that these proteins retain their structural integrity waiting to be rehydrated. Because of this characteristic, the

biosensor must be stored in dry conditions to prevent rehydratation of the bioreceptors. The article [83] cites a relative humidity that has to be kept below 15% and a temperature comprises in the range 4-20°C.

6.2.4 Non-specific detection and adsorption

The question of non-specific adsorption may be discussed through two different points. The first one is the adsorption of unwanted compound at the test line. This is of high importance as in the case of water monitoring goal, the sample will come from a complex water media plenty of other molecules than the one wanted to be detected. The second one is the non-specific adsorption of the target bacteria to the nitrocellulose out of the capture line.

Before discussing different blocking agents that could be added to the sample or to the membrane, a first important step should be to rinse the biosensor strip before doing the electrical measurement at the test line. This rinsing will permit to clear the biosensor from most non-adsorbed species. The wash buffer solution has to be optimized so that the bindings between the bioreceptors and the target bacteria are uncompromised. PBS and low pH PB rinses have been shown in to increase the LOD of the sensor [169].

To emphasize the detection of target molecules, nanoparticles could be added to them through the conjugate pad. This in addition to the rinsing should strongly decrease the influence of non-specific adsorption at the detection line.
To be able to detect the specific compounds and to not take into account the change of impedance associated to unwanted particles, an extra electric measurement should be done out of the test line location. This value must be then subtracted from the one that will be obtained at the test line.

Usually and according to [83], proteins present in the initial sample or blocking agents added to the sample are sufficient to avoid non-specific adsorption to the nitrocellulose membrane. Both TBS-T, TENTC or again BSA and OVA are commonly used as blocking reagents in immunoassays [170][171]. However in some cases the blocking of the membrane is required. It consists of immersing the entire membrane into the blocking solution after having applied and dried the capture reagents. The choice of the blocking agents and its concentration have to be determined depending on the application. The excess blocking agent must be removed thanks to a washing in a weak buffer solution to avoid clogging of pores (ex: PBS buffer) [171].

Chapter 7

Towards the design of a sustainable sensor

7.1 Responsible design

7.1.1 Introduction

Technologies are not neural. Several critical aspects may condition the manufacturing of the technology in the long term, such as the availability, access and extraction of raw materials, the impacts of typical elements for biosensor developments (materials and energy-consuming processes) and its impacts on the environment (*e.g.* toxicity). Along with the raw material impact assessments, societal implications of technologies must be collectively managed towards socially robust decisions on their development and implementation.

Our team conducted innovative researches with the aim to develop appropriate, alternative, sustainable biosensors for affordable water quality assessments. Such disruptive ways of electronics design require multidisciplinary impact assessment studies about how and how much these alternative products could be more appropriate than the current counterparts. Specifically, there is a critical need to integrate holistic impact assessments (performances, environment, socio-economic) at the technology design level to anticipate new technology-related consequences hidden at first sight, and to activate the adequate levers to promote their sustainable development and diligent dissemination.

Implementation of multidimensional evaluation prior to the deployment of such technological innovations, *i.e.* right from the early stages of researches, should aim at guiding the design towards most appropriate technologies. From the scientist/technology designer point of view, this implies to be driven by the desire to bring the right technology to the right application/basic need and by mitigating technology-related consequences. In our case, the objective of this study is to guide the design of water quality sensors to offer the complete specification of a sustainable solution in all the relevant dimensions and an efficient integrated solution (device, information system and assessment methodology), most appropriate for the assessment of water quality in resource-poor settings.

Altogether, bringing ethics into science and technology-based innovation through multidimensional analysis allows us to question the preconceptions and hypotheses behind

researches currently carried out and raise guidelines in order to become actor of its own research path. Therefore, findings from this multidisciplinary study will also showcase how to support the crisis medical diagnostic research field accommodating with sustainable development goals and social accountability.

7.1.2 Emergence of systemic research questions

Before setting out the research questions that guide our systemic analysis, we emphasise, as researchers in the applied science field, on considering the limits of our skills and techniques in solving societal problems. We therefore insist on the necessity to be surrounded by experienced mentors in the explored fields when conducting such an evaluation.

Technology assessments request for systemic methodologies, applied on the whole technology value chain. Life Cycle Thinking (LCT) is the basic concept referring to the need for assessing the burden of products adopting a holistic perspective following a Cradle-to-Grave approach, from raw material extraction to end-of-life.

The Life Cycle Thinking approach recognizes that a balance is necessary across the three pillars of sustainable development: environmental, social and economic. In order to integrate all the possible dimensions in a holistic methodology, we question the technology considered at the system level (*i.e.* integrated solution: production, device and information system in a societal ecosystem). Going along the wheel on Figure 7.1, we showed the emergence of research questions based on these three pillars all along the value-chain and the life-cycle stages of the products.

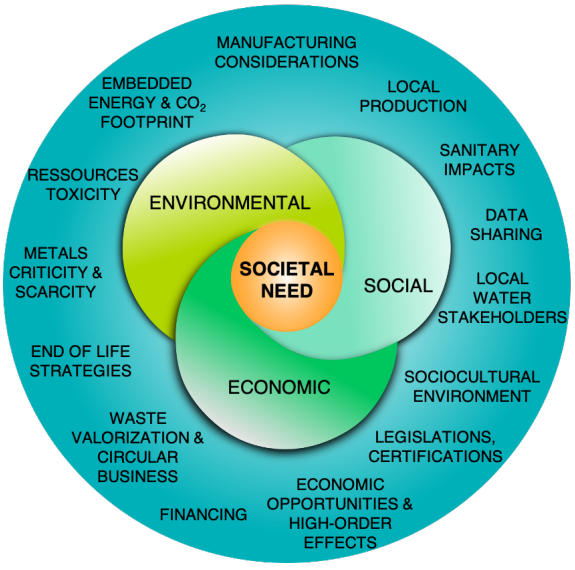


Figure 7.1: Emergence of research questions for the multidimensional analysis of affordable water quality sensors. Life cycle thinking applied to the three sustainability pillars shows the emergence of questions all along the technology value chain, and from Cradle-to-Grave.

In our case, the research questions focus on reducing the overall effect of the biosensor product on the environment and by studying the efficiency of the solution from a socio-economic perspective (affordability, implementation). The answers to these questions will be integrated to raise guidelines for the designer point of view.

From this objective, the following questions are emerging.

- Are the considered materials (support, metals, nanomaterials) better than other materials in term of environmental impact (resource depletion, energy consumption and CO_2 footprint at the extraction and processing of raw materials), human health treath (toxicity) as well as economic perspectives (price, criticality) ?
- Is it interesting for single-use sensors to be paper-based, especially in terms of production and end-of-life management? What are the main levers and barriers for the recycling or re-manufacturing of such sensors ?
- What are the possible end-of-life strategies of the bio-contaminated and electronic sensor? Which one is the best adapted to its usage?
- What are the most appropriated manufacturing techniques to reach the project objectives (including performance, low-cost, affordability, reproducibility, improved environmental impact,...)?
- What are the risks of production faults according to the production methods? To what extend will this bias the measurement?
- Who are the major stakeholders to be included in the design of a solution answering such a basic need (accessibility to information on drinkable water)?
- What impact can a widespread use of this sensor have on a community in terms of water management?
- Can the sensor measurement result be made accessible to users without any scientific background?
- Can the production of this sensor be upscaled? If so, what is the impact of this upscaling process on the final sensor quality and -price?
- Is this sensor relevant compared to other existing technologies? If so, in what context? What is the market to be targeted?
- How could production and distribution of the sensors be aligned and implemented and with the purpose of the project (giving accessibility to water quality in crisis situations)?
- How could the sensor design be adapted to accommodate with regulations (diagnostic performances in terms of detection limit and time, electronic wastes) and with certification procedures ?
- In what extend would it be possible to generate economical value from the integration of circular economy principles in the product design (related to end-of-life management - waste valorization)? What are the main requirements to set up a circular business model from single-use paper-based sensing solutions?

7.1.3 Methodologies to guide a multidimensional analysis

Eco-Design refers to an approach to innovative design of a product or service that take into consideration the entire life cycle. The challenge is to design a circular system around the product or service in order to increase its value for customers, decrease its environmental

and societal impact and maximise its business impact all along its life cycle.
From more than 30 years now, methodologies are developed in an attempt to answer the various and tailored-needs raised by the sustainability sciences. These tools and methods help to ecodesigning by providing information to answer the different emerged research questions [1].

The life cycle assessment (LCA) is a support and a tool for systematic evaluation of the environmental aspects of a product or service system through all stages of its life cycle. LCA studies are carried out in conformity with the ISO 14040 series. This is now accepted as effective approach to provide an adequate instrument for environmental decision support by analysing scientifically energy consumption and environmental impact associated with a product or service.

Use2Use design comprises creating opportunities to enable and facilitate the circulation of products from one user to another. Two major possibilities exist. First, design for exchange, which implies either designing circular service offers or by designing products that directly facilitate exchanges. Second, design for Multiple Use-Cycles, which ensures a satisfying user experience not only for the first user, but also for the second, the tenth or even the hundredth user.

In 2019-2020, two parallel assesments were made.

O. Crahay carried out a LCA comparing nitrocellulosic paper to PDMS as material supporting the microfluidics of the sensor. Two environmental indicators have been selected to be studied in this first simplified assessment: the embodied energy and the CO_2 footprint. Both materials and manufacturing processes are playing a role in these factors. The choice of raw materials can be crucial because of the often significant embodied energy and CO_2 footprint associated with their extraction and/or production. Manufacturing processes and especially microfabrications can also be energy-consuming and have a high CO_2 impact.

Alongside production process and materials, a usage-oriented assessment was made by M. Hauwaert [107]. Indeed, an accessible and cheap sensor might become widely spread, thus adding a lot of information in community structures. However, this information can be biased in many ways: due to a fault in sensor design, due to wrong sensor handling, due to misreading or even intentional information manipulation. From a usage perspective, this sensor gives consumers an unprecedented access to information concerning the quality of a vital good: water. What is the fairest and most accurate way to manage this information?

7.1.4 Introduction to LCA

Among the three bottom lines presented on Figure 7.1, one key concept to manage the environmental performance is the life cycle thinking. This refers to the need of assessing the burden of products or services from cradle to grave; from raw materials extraction to end-of-life. The life cycle assessment (LCA) is a support and a tool for systematic evaluation of the environmental aspects of a product or service system through all stages of its life cycle. LCA studies are carried out in conformity with the ISO 14040 series. This is now accepted as effective approach to provide an adequate instrument for environmental

[1] https://sustainabilityguide.eu/

decision support by analysing scientifically energy consumption and environmental impact associated with a product or service. LCA is based on the product (or service) life cycle stages (see Figure 7.2) and includes 3 steps, the life-cycle inventory, the life cycle impact assessment and the life-cycle improvement analysis (see Figure 7.3). The first step determines the emissions that occur and the raw materials and energy that are used during the life-cycle of a product. The life-cycle impact assessment assess what the impacts of these emissions and raw material depletions are. For that step environmental indicators are aggregated to generate indices for environmental and economic sustainability such as global warming potential, acidification potential... [172] The last step interprets the results of the impact assessment in order to suggest improvements. When LCA is conducted to compare products this step may consist of recommending the most environmentally desirable product [173][174].

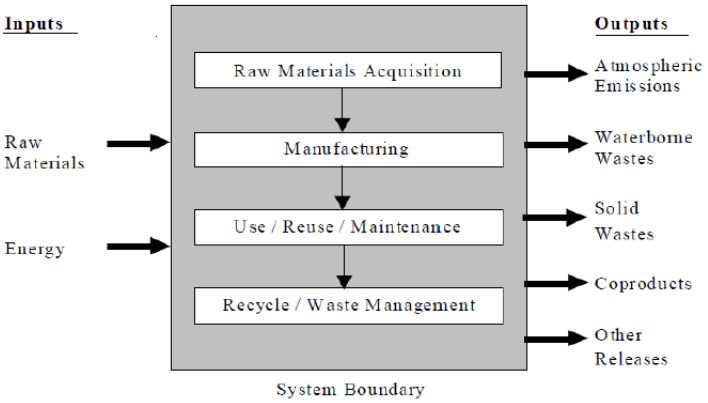


Figure 7.2: Product Life Cycle Stages [174].

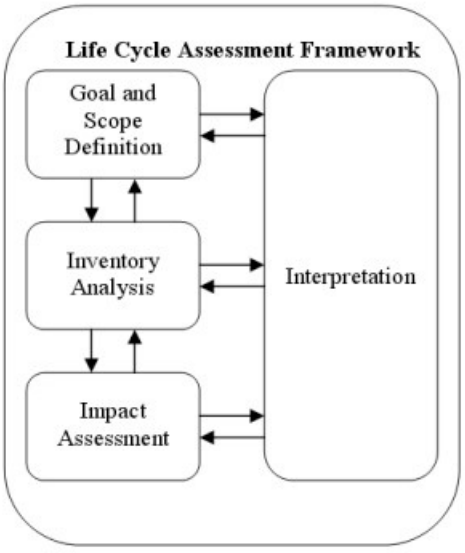


Figure 7.3: Life Cycle Assessment [174].

Legislations and convention also help to have guidelines, objectives and clear goals.

The United Nations Framework Convention on Climate Change (UNFCCC) includes 195 Parties. Its secretariat supports all institutions involved in the international climate change negotiations as the Conference of the Parties (COP) The Kyoto Protocol was adopted in 1997 and is what "operationalizes" the Convention. It legally binds developed countries to emission reduction targets based on the principles of the Convention. There are now 192 parties to the Kyoto Protocol. Three main mechanisms defined in articles of the Protocol are the International Emissions Trading (the allowed emissions are divided into "assigned amount units"), the Joint Implementation (a join implemented project must provide a reduction in emissions by sources, or an enhancement of removals by sinks) and the Clean Development Mechanism (implementation of an emission-reduction project in developing countries).
The 2030 agenda for sustainable development is a call for action to change our world. This integrates in a balanced manner the three dimensions of sustainable development (economic, social and environmental) and was adopted by all United Nations member states in 2015. The 17 global sustainable development goals (SGDs) are the world's best plan to build a better world for people and our planet by 2030 (see Figure 7.4). The follow-up of these SDG's is made by the high-level political forum (HLPF) which is the main United Nations platform on sustainable development engaging 197 member states.



Figure 7.4: Sustainable development goals [175].

Among others, the REACH legislation regulates chemicals on the market. It involves a clear legislative framework to place chemicals on the market. The legislation is hierarchized in international, European, national and regional legislations [174].

7.2 Comparative Life Cycle Assessment

7.2.1 Introduction

Paper-based technologies are emerging because of their numerous advantages such as their low cost, flexibility and light weight. One of the main motivations of such devices is their disposability and in microfluidic applications, their ability of being self-sufficient thanks to the capillarity taking place into porous material.

The performances of biosensors are of high importance and they have been studied and discuted for the nitrocellulose earlier in the last chapters of this master thesis. To obtain a sensor with high performances, the targeted design gathers the advantages of the porous and disposable material to an high sensitivity and selectivity by the implementation of an impedance measurement.

The polydimethylsiloxane (PDMS) is a silicon-based organic polymer and it is the most used elastomer in biosensors application. Its main advantages are its elasticity, its optical transparency, its low fluorescence, its cost and its fast process. However on the contrary of paper materials PDMS such as other polymers require complex fabrication techniques and micromachined devices to induce microflow in their microfluidic channels [34][30].

While the performances are important, in the current century the sustainability of new designed product can not be neglect anymore. That actually takes place in the main global challenges of today focusing notably on local and global pollution as well as on natural resources depletion. "Environmental-friendly" products are filling the market more and more because of the increasing demand and regulation.
In this context two microfluidic devices are going to be compared in this study through a Life Cycle Assessment (LCA) taken into account different parameters influencing their environment impact: a nitrocellulose strip and a PDMS chip.
The general frame of LCA is given by International Standards ISO 14040 and ISO 14044. The following simplified LCA is based on the global life cycle of each microfluidic device by using primary and generic data. Most of generic data come from the EduPack database.

A rigorous quantitative assessment of all burdens is a time-consuming task and requires deep skills of those involved, leading many companies to abandon this approach. In this study, the embodied energy and carbon footprint will be used for assessing the environmental burden, not for replacing a complete LCA, but for providing fast and reliable information to those involved in the design of a new product [176].

7.2.2 Goal and scope definition

The goal of this LCA is to compare two different microfluidic support materials: nitrocellulose and PDMS.
The function of both devices is to support a microfluidic flow in order to transport a certain amount of liquid media. To fulfil this function a rectangular strip and a die are needed respectively in the nitrocellulose and in the PDMS case. In both cases it is assumed that the microfluidic device has an single use because of the biological nature of the liquid sample which is going to flow into it. The functional unit is chosen to be 1000 microfluidic devices each one able to transport 30 μL of a liquid media in 90 seconds. That corresponds to 1000 strips of 1cm x 3.5 cm of nitrocellulose and 1000 microfluidic caps of about 1 cm^3 of PDMS with a flow rate of 20 $\mu L/min$ going through the microfluidic channel of a volume of 1-1.5 μL.

The system boundaries considered are presented on Figure 7.5. The impacts selected to be compared are the energy $[MJ/kg]$ and the carbon footprint $[kg_{CO_2,eq}/kg]$. The infrastructures production, the transport, the use and the end-of-life phases as well as the eventual reuse and recycling of input materials are excluded from the study.

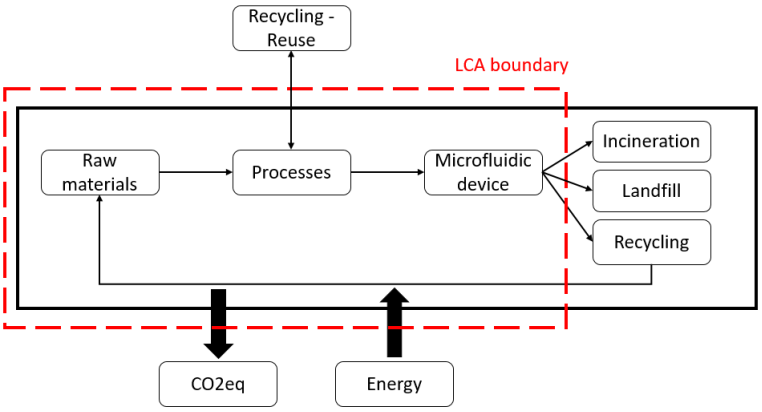


Figure 7.5: System boundaries for both microfluidic devices.

7.2.3 Data inventory

Figure 7.6 presents the processes from raw materials to the final device for the nitrocellulose microfluidic device. It includes as well the used chemicals in the different steps. Such membranes are manufactured by dissolving cellulose nitrate (or a mixture of cellulose nitrate and cellulose acetate) in a solvent and casting the resulting viscous solution on an endless steel belt. By controlling the conditions of solvent evaporation, controlled pores are formed in the resulting polymer membrane [177].

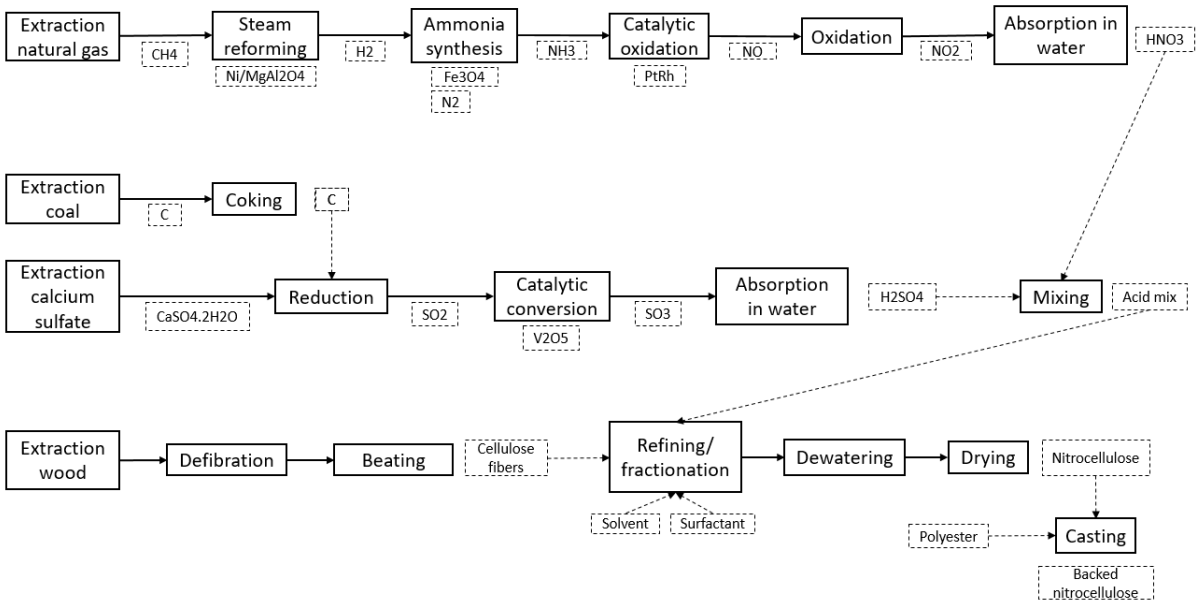


Figure 7.6: Flowsheet of the manufacturing of nitrocellulose from raw materials to the microfluidic device.

Table 7.1 presents the input mass flows for the manufacturing of the nitrocellulose microfluidic device and Table 7.2 gathers secondary and generic data of energy and carbon footprint for these chemicals and processes used in the nitrocellulose process.

Table 7.1: Materials consumption (inputs and intermediate products) for the manufacturing of 1000 membranes made each one of 0.079625 grams of nitrocellulose.

Material	Mass consumption [g]
CH_4	6.80
$Ni/MgAl_2O_4$	7.09e-7
H_2	2.55
Fe_3O_4	4.05e-6
N_2	11.89
NH_3	14.44
PtRh	1.42e-5
HNO_3	50.67
C	6.20
$CaSO_4.2H_2O$ (gypse)	140.64
V_2O_5	2.84e-4
H_2SO_4	101.34
Solvent (assumption same volume than final membrane)	62.47
Surfactant	3.2e-4
Cellulosic fibers	43.43 (2.63e-4 m^3 ub wood)
Polyester	0.05

Table 7.2: Embodied energy and carbon footprint for chemicals and processes used in the nitrocellulose (CN) process, from EduPack and [137, 178–186].

Chemical/Process	Embodied energy [MJ/kg]	Carbon footprint [$kg_{CO_2,eq}/kg$]
CH_4	45	3.3
$Ni/MgAl_2O_4$	1.47e3	100
Steam reforming	8.5	67
Fe_3O_4	3.92	0.3
N_2	0.66	0.06
NH_3 synthesis	31	2.7
PtRh	3.2e5	16.5e4
HNO_3 synthesis from NH_3	-1.6	2.79
C	24.5	0.265
$CaSO_4.2H_2O$	2.2	0.2
V_2O_5	35	?
H_2SO_4 synthesis from gypse	0.69	0.14
Solvent (assumed C_3H_6O)	61.87	2
Surfactant	17	1.4
CN synthesis from acids and wood	50	1.2
Polyester	80	2.7
Polyester film manufacture	6	0.46

On the contrary to porous materials simply offering their small pores as microfluidic

channels, other materials require more complex processes to be considered as microfluidic support. Different techniques for microfluidic devices fabrication exist. They may be classified into direct techniques such as laser ablation or laser micromachining of polymers, photolithography or optical lithography, X-ray lithography and prototyping techniques, including hot embossing, injection molding, and soft lithography. The analysed method in the LCA study is the photolithography of PDMS which is a technique based on the exposure of light on a photoactive material that undergoes a chemical reaction to form a liquid-solid transition. The advantages of photolithography are mainly the spatial control of light and the high resolution of the microstructured fluidic devices or molds produced [30].
Figure 7.7 presents the processes from raw materials to PDMS monomer.

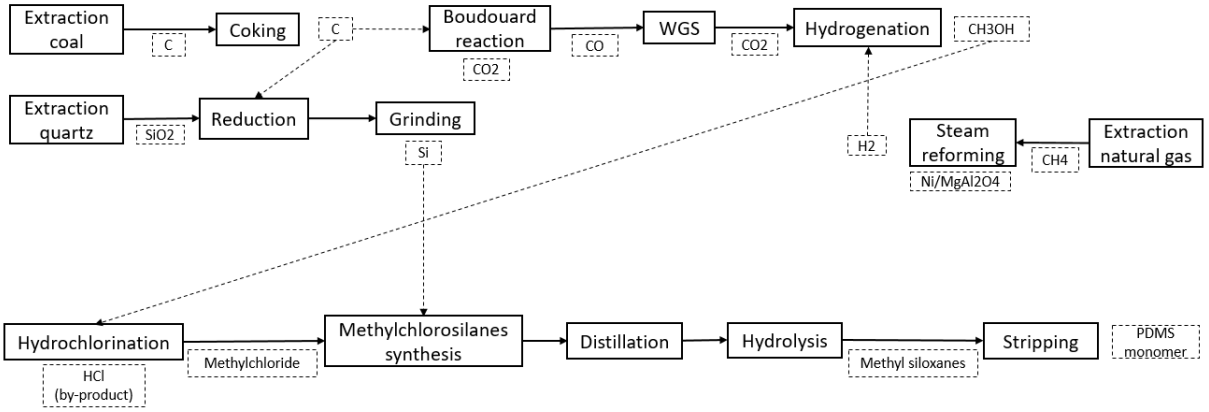


Figure 7.7: Flowsheet of the manufacturing of PDMS from raw materials to the PDMS monomer.

The wafer fabrication presented on Figure 7.8 accounts for a non-negligible part of the microfluidic fabrication process in terms of energy and carbon footprint as it can be seen from Tables 7.3 and 7.4.

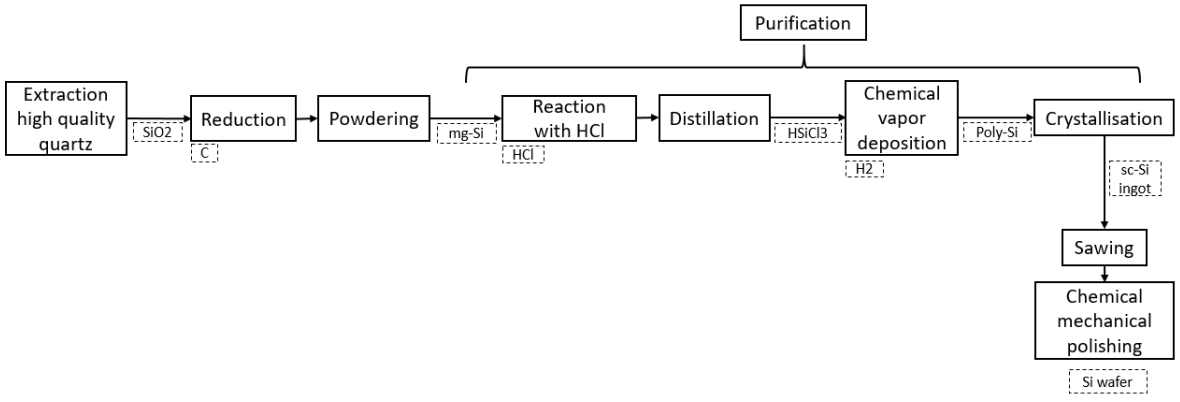


Figure 7.8: Flowsheet of the wafer manufacturing, from [187].

Table 7.3: Materials consumption for the manufacturing of one silicon wafer of 6.03 grams.

Material	Mass consumption [g]
SiO_2	12.92
C	5.17
HCl	23.25
H_2	0.43

Table 7.4: Embodied energy and carbon footprint for chemicals and processes used in the silicon wafer process, from [187] and [184].

Chemical/Process	Embodied energy [MJ/kg]	Carbon footprint [$kg_{CO_2,eq}/kg$]
SiO_2 of high quality	40.45	2.37
C	24.5	0.265
HCl	0.91	0.08
H_2	8.5	67
Fabrication processes	22.3e3	950.77

Figure 7.9 presents the processes from PDMS monomer and silicon wafer to the final PDMS microfluidic device followed by the Winfab lab. The used machines and their specifications are gathered in Table 7.5. Thanks to the PTFE coating step the silicon wafer may be used several times because this layer will prevent PDMS adhesion to the mold [188]. In this study it will be assumed that each wafer can be used 6 times and that one use of the wafer produce 22 PDMS microfluidic devices.
The corresponding primary data are presented on Tables 7.6 and 7.7.

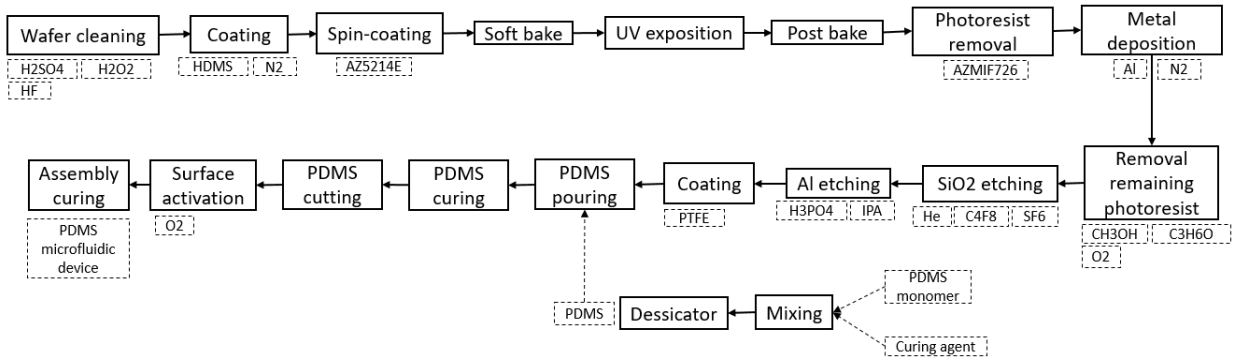


Figure 7.9: Flowsheet of the Winfab manufacturing of PDMS from PDMS monomer to the microfluidic device.

Table 7.5: Winfab machines specification for each machining step of the manufacturing of the PDMS microfluidic device. Assumptions are written in italic.

Step	Machine	Specifications
Coating HDMS	LPII oven	23 minutes, 120°C, 1.2kW, *5 wafers a time*
Spin-coating	SUSS Gamma 80	30 minutes, 21°C, 1000-4000 rpm/sec
Soft bake	SUSS Gamma 80	90 seconds, 110°C
UV exposition	SUSS MA6	0.6 seconds of exposition but +- 30 minutes of use, 1.5kW for light and 3kW for machine
Post bake	SUSS Gamma 80	90-120 seconds, 118°C
Metal deposition	VACOTEC	5h30, 15kW for machine and 3.68kW for water heater, *5 wafers a time*
Removal remaining photoresist	EmiTech K1050X	20 minutes, 2.5kW
SiO_2 etching	Deep-RIE	19 seconds per cycle (etching+deposition), 3h10 of use, 2.5kW
Coating PTFE	LPII oven	30 minutes, 120°C, 1.2kW, *5 wafers a time*
PDMS curing	Oven	10 minutes, 150°C, 700W
Surface activation	EmiTech K1050X	1 minutes, 2.5kW
Assembly curing	Oven	12h, 120°C, 700W

Table 7.6: Winfab materials consumption for the manufacturing of 1000 PDMS microfluidic devices.

Material	Mass consumption [kg]	Comments
H_2SO_4	9.503	2 baths of piranha solution H_2O_2 : H_2SO_4 (2:5) (1 bath = 2L for 25 wafers)
H_2O_2	2.995	
HF	0.07	1 bath of 2L of 2% HF solution for 25 wafers
HDMS	0.035	0.005mL/wafer
N_2	0.2383	
AZ5214E	0.182	Approximated as PMMA
AZMIF726 (developer)	0.045	Approximated as TMAH, litterature value for mass of developer
Al	5.4e-4	Assuming 1μm on all the chamber ($1m^2$) and 5 wafers a time (efficiency 2.28%)
N_2	1.408	Assuming needed amount N_2 = volume of chamber
CH_3OH	7.2e-3	5cl/bath
C_3H_6O	0.05	35cl/bath
O_2	0.0242	20' at 20L/min
He	0.4788	
C_4F_8	7.56	
SF6	11.96	
H_3PO_4	4.374	1 bath of 2L solution H_3PO_4 85% : IPA (5:2) for 25 wafers
IPA	0.817	
PTFE	0.1	0.005mL/wafer
PDMS	1.25	4mm of thickness per wafer
O_2	7.058e-4	35" at 20L/min

Table 7.7: Embodied energy and carbon footprint for chemicals and processes used in the PDMS process, from EduPack and [183, 184, 189–191].

Chemical/Process	Embodied energy [MJ/kg]	Carbon footprint [$kg_{CO_2,eq}/kg$]
Electricity	10.5 [MJ/kWh]	0.447 [$kg_{CO_2,eq}/kWh$]
H_2SO_4	4.55	0.4
H_2O_2	12	1
HF	18	1.5
N_2	0.66	0.06
HDMS	3.1	0.26
AZ5214E	102	4.875
AZMIF726	3.1	0.26
Al	260	22
CH_3OH	18.6	10.4
C_3H_6O	61.87	2
O_2	1.8	0.15
He	0.83	0.07
C_4F_8	0.8	0.07
SF6	1.93	22800
H_3PO4	3.1	0.26
IPA	3.1	0.26
PTFE	297.5	16.2
PDMS	120	8.58

7.2.4 Results and discussion

7.2.4.1 Polyester backing

In order to give strength to the nitrocellulose membrane which is very fragile, this one is cast onto a baking in polyester. In addition to this improvement of the mechanical strength and the easiness to handle it, the polyester film acts as a barrier to chemical contamination from adhesive cards that are used to mount the membrane during test strip manufacture for the ease of handling. Adhesives were shown to not penetrate into a microporous membrane more than a few microns but volatile organic solvents released from the adhesive during long-term storage may be adsorbed to the nitrocellulose. This can alter the wetting properties of the membrane and therefore affect its lateral flow properties. For these reasons, most lateral flow tests are produced using backed membranes [83][132]. This addition of a polyester film is discussed in order to larger the scope of the study and measure its environmental influence. Table 7.2 gives the energy and the carbon footprint of this film addition. The casting of the nitrocellulose membrane onto the polyester backing is assumed to be included in the nitrocellulose synthesis where the energy for lamination steps is already taken into account. Figure 7.10 shows the impact of the polyester film backing on both embodied energy and carbon footprint of the microfluidic device. It is observed that the polyester backing has a non-negligible negative impact on the environmental point of view. Moreover the recyclability of the device is impacted as well.

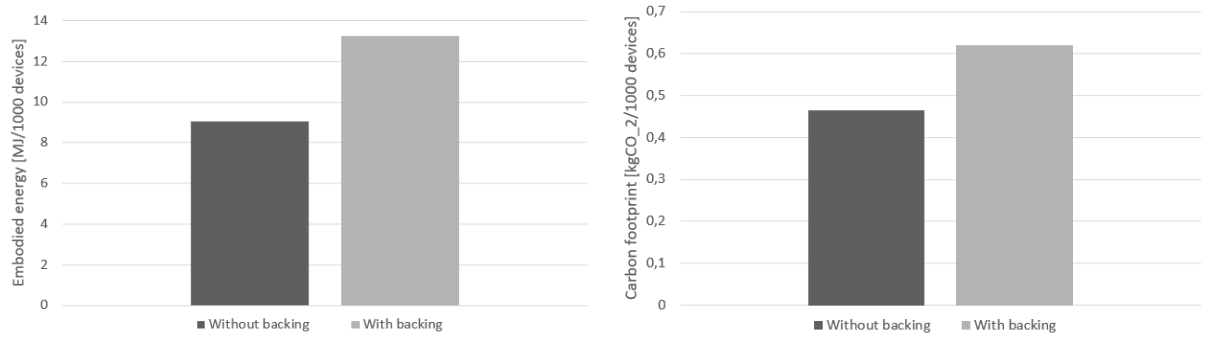


Figure 7.10: Embodied energy and carbon footprint of nitrocellulose device with and without polyester backing.

An uncertainity for the processes energy value for the nitrocellulose device should still be mentioned as no specific data were found.

7.2.4.2 Comparison nitrocellulose and PDMS microfluidic devices

Figure 7.11 compares the environmental impacts of the materials and the manufacturing processes required to produce 1000 microfluidic devices, each one able to transport 30 μL of a liquid media in 90 seconds, of nitrocellulose and PDMS.

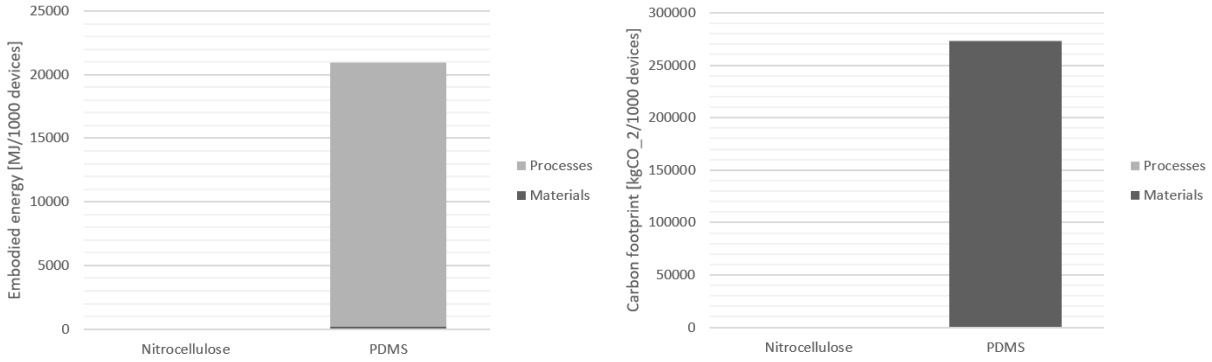


Figure 7.11: Comparison of embodied energy and carbon footprint of 1000 microfluidic devices made in nitrocellulose and made in PDMS.

On the light of embodied energy and carbon footprint and in these circumstances, the nitrocellulose device seems clearly to be the best choice in term of environmental impact compared to the PDMS device.

From the study it can be seen that the processes required to manufacture the PDMS device are very energy consuming. Actually, as it is highlighted by Figure 7.9, a lot of processes are needed and some requires high amount of electricity, sometimes for several hours of use. Figure 7.12 presents the impact of each step on the total embodied energy for the PDMS device manufacturing. The most impacting steps are the metallization, the SiO_2 etching and the last curing for the assembly.

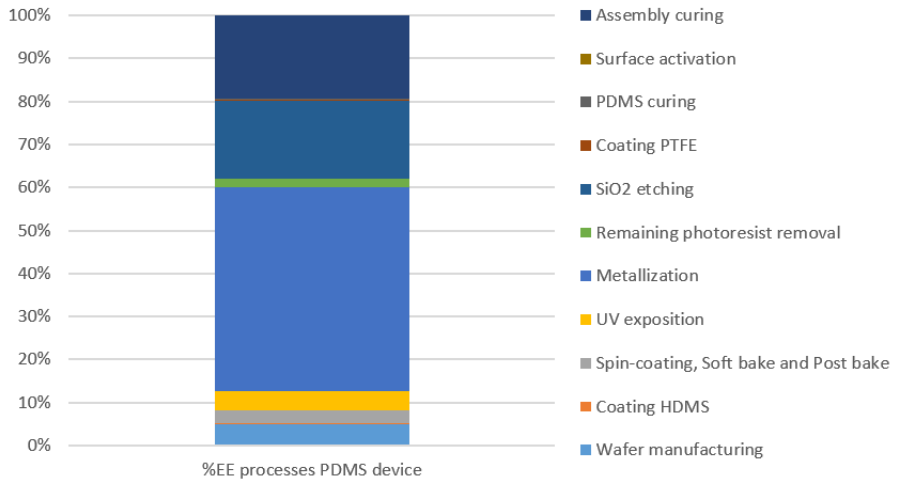


Figure 7.12: Ccontribution of each process to the total process energy value for the PDMS microfluidic device manufacturing.

While the processes are the most impacting for the energy point of view, the materials consumed for the PDMS device manufacturing are the ones impacting the most the carbon footprint of the device. This is essentially due to the SF6 gas having a very high carbon footprint (see Table 7.7).
The impact of materials can not easily be decreased but the one of the processes can be lowered by optimizing the use of the different machines. Each step should be started only when the maximal number of wafers/devices that the corresponding machine can handle is reached.

Scarcity and criticality of some raw materials
From the Edupack data source, the catalyst platinum rhodium (PtRh) contains more than $5_{wg}\%$ of critical elements. Rhodium has an abundance of 0.0002 ppm in the Earth's crust, making it the second rarest element in Earth. The metal's extremely low occurrence means actually there are no primary rhodium mines. Rhodium is produced entirely as a by-product, mostly as a by-product of platinum mining, being considered as a critical element as well. There are fewer than 10 significant rhodium-producing mines in the world and most are located in South Africa [192].

Silicon wafer is made of quartz. While quartz is the second most abundant mineral in Earth's continental crust as found in most of the world's sand grains, the one used for high quality electronics must be of high purity and is not found anywhere. High-purity silicon dioxide particles are currently extracted for the Spruce Pine in North Carolina in USA. In addition to the high impact of the silicon wafer manufacturing (see Table 7.4), its main raw material is therefore not abundant at all and its current source is not renewable as it took some 100 million years in specific conditions to form rocks almost without impurities [193].

End of life strategies
The way in which waste materials and products are disposed of has an important bearing on the sustainability of society.

The **waste hierarchy** as laid down in the Waste Framework Directive (2008/98/EC) defines the preferred approach to waste treatment (see Figure 7.13). The preferred option is to reduce the amount of waste generated. If this is not possible then the hierarchy ensures that no down-cycling takes place and that disposal/landfilling is limited as much as possible [143].



Figure 7.13: Waste hierarchy [143].

Nowadays a lot of objects (mainly packagings) are sold and said to be "compostable". It is interesting to mention that legally speaking, an object can be said compostable if it meets four criteria:

- The amount of heavy metals has to be below given maximum values, and the final compost must not be affected negatively.
- It has to be biodegradable, meaning that >90% of the original material have to be converted into CO_2, water and minerals by biological processes within 6 months.
- After 3 months, the mass of residues has to be less than 10% of the original mass and the residues have to be able to pass through a 2x2 mm sieve.
- The absence of toxic substances and other substances that negatively affect composting.

Health-care activities protect, restore health and save lives but they also generate waste and by products. About 85% of them are considered as non-hazardous waste while the remaining 15% may be infectious, chemical or radiactive hazardous waste. Treatment and disposal of healthcare waste may pose health risks indirectly through the release of pathogens and toxic pollutants into the environment. The management of health-care waste requires increased attention and diligence to avoid adverse health outcomes associated with poor practice, including exposure to infectious agents and toxic substances.
The World Health Organization (WHO) developed the first global and comprehensive guidance document, *Safe management of wastes from health-care activities*, which addresses aspects such as regulatory framework, planning issues, waste minimization and recycling, handling, storage and transportation, treatment and disposal options, and training. Among others, infectious wastes must be collected in leak-proof containers carefully sealed and

transported to a central storage facility/delivery point in a way that precludes direct contact. They must either be incinerated or be disinfected prior to final disposal using a recognized method, preferably treatment with saturated steam (autoclaving). The method must be verified by a recognized institution before first operation and at regular intervals [194].

PDMS is not biodegradable and is not recycled but it can be incinerated for energy recovery. Its heat of combustion is 13.1-14.2 MJ/kg. A certain share of the calorific value of the waste input is often utilised for the production of electricity and/or heat (mostly district heat), or the incinerated waste directly replaces fossil fuels (industrial plants). While energy is recovered, the fossil carbon content of this silicone-based product is transformed into CO_2. About 1.3 kilograms of CO_2 per kilograms of incinerated matter is released to the atmosphere.
Another end of life strategy for the PDMS is the waste disposable. In this case and because of physical and chemical degradation processes (due to conditions in the landfills) carbon in the silicone products can also be converted to CO_2.

Cellulose based papers are biodegradable and can be recycled, incinerated or disposed. Nitrocellulose is mainly composed of cellulose fibers, sulfuric acid and nitric acid.
Sulfuric acid dissolves readily in water to form sulfate ions and hydrated protons. Its toxicity in aquatic life is moderate acute (short-term) and it is very corrosive so that it would burn any living species exposed to it. Large quantities of sulfuric acid may lower the pH of aquatic systems for extended periods of time. However small quantities will be neutralised by the natural alkalinity in such systems [195]. Nitric acid is highly corrosive and a strongly oxidizing acid. Strong solutions of nitric acid can also cause burn to any living species put in contact with and inhalation of this compound can cause severe health effect [196]. Nitric acid will be gradually neutralized by hardness minerals (calcium and magnesium) in water. The nitrate ion may persist longer but will ultimately be consumed as a plant nutrient. If acid particles dissolve in clouds, fog, rain or snow it will result in very dilute acid solutions causing environmental damage as wet acid deposition, usually known as acid rain.
Recycling is not a possibility as the membrane, in addition to its microfluidic role, will be used as a biological support.
The "Centers for Disease Control and Prevention" based in Atlanta published one report concerning the recommended guidelines for disposing of nitrocellulose membrane [177]. The first recommendations in this is to suitably decontaminated the membrane by approved methods to eliminate any possibility of a biohazard. One way is to sterilize the membrane by steam sterilization. Then the easiest, safest, and least expensive method of disposing of NC membranes is burial in an approved sanitary landfill. Because of both acids included in the membrane, the biodegradation will not have a non-zero impact on environment due to chemicals found into it but nitrocellulose device may considered as biodegradable if not coated with polyester. The website "Bioplastics NEWS" notably classes the cellulose nitrate as a biodegradable polymer. More specifically it needs 1 month in fresh water and 6-12 months in marine or landfill environment to be degraded by bacteria [197].
If coated, the end of life strategy of the nitrocellulose membrane should be the incineration. That also would be the best solution if the decontamination step wants to be avoided.

In the case where these microfluidic devices are also the support of electronics, extra directives for WEEE must be considered.
Waste of electrical and electronic equipment (WEEE) is a complex mixture of materials and components that because of their hazardous content, and if not properly managed, can cause major environmental and health problems. To address these problems two pieces of legislation have been put in place: the Directive on waste electrical and electronic equipment (WEEE Directive) and the Directive on the restriction of the use of certain hazardous substances in electrical and electronic equipment (RoHS Directive). The first one aims to increase the recycling and/or re-use of WEEE and the second one requires some hazardous substances to be substituted by safer alternatives [198].

7.2.5 Conclusions

The main limitation of this study is the choice of only two environmental sustainability indicators. In order to completely evaluate impacts of each devices, other environmental indicators such as acidification potential, eutrophication potential, smog potential, ozone depletion potential, human health particulate and toxicity should have been discussed as well. That may be the goal of further research.

Thanks to the conduction of this simplified life cycle assessment it has been shown that, in the light of the embodied energy and the carbon footprint indicators and compared to a PDMS microfluidic device, the nitrocellulose microfluidic device is more environmental friendly. The polyester backing of the nitrocellulose impacts both indicators and take the biodegradability away from the membrane. This backing providing positive and sometimes essential characteristics to the nitrocellulose strip, the idea of replacing the polyester by another less impacting polymer should be pursued. Bioplastics may be an interesting alternative [199][200][201].
PLA is a bioplastic made from cornstartch. It is much cheaper than other bioplastics and is easily shaping into small rigid supports. This polymer is only industrially biodegradable because it needs specific conditions and specific bacteria. PHA could be another possible substitute of polyester. These possibilities as well as their impacts and properties should be discussed in a following study.

Chapter 8

Conclusions and perspectives

The project of this paper-based biosensor for water monitoring takes place in the context of the growing need to improve the assessment and management of water quality in developing countries in order to reduce water pollution and infectious diseases that are still woefully prevalent in these regions. On the other hand, the emergence of SARS-CoV-2 infection in 2019 has highlighted other possible uses of these types of PoC devices for health and medical helps.

In this master thesis the different design parameters impacting the biosensor response through microfluidics means have been highlighted and discussed. Phages RBPs and CBDs have been found to possibly be good candidates to be used as bioreceptors thanks to an approach "proof-of-concept" with such specific proteins to the *Bacillus* cereus group.
Technical results and research have led to the drawing of general guidelines for the design of the biosensing device but further work will be required to get closer to the final sensor. Within this scope, this master thesis also served to identify the next steps related to microfluidic and biological studies. It should be mentioned that the biological issues in this work have been confined to a very early stage compared to microfluidic analysis.

To finalize the microfluic study, further experiments studying the influence of the relative humidity on the capillary flow rate should be conducted in order to complete and conclude the discussion started in this work.
Once the biofunctionalization step of the nitrocellulose membrane by RBPs and CBDs will be optimized, the location of the test line should be determined. For this purpose and through the observation of interaction between bioreceptors and bacteria, different locations have to be compared by means of capillary flow of a liquid media including fluorescent bacteria. In the meantime it may be checked that the sensitivity is inversely related to the square of the flow rate [83]. The sensitivity could be qualitatively measured by colorimetric observation as done in [131] and [202] while waiting for the amperometric measurement to be developed.
Thanks to fluorescent imaging it will be possible to observe eventual non-specific adsorption of bacteria into the nitrocellulose membrane out of the test line.
The two different bioreceptors may be compared in order to be draw conclusions about the use of one or the other. The main comparison factor is their interaction stability. The force of interaction can be observed the fluorescent intensity of the biofunctionalized line before and after rinsing the membrane with an adapted wash buffer. In addition this rinse

will allow non-immobilized biomolecules to be cleared, which will be useful in practice because of the complex media where the sample will come from.
Finally further experiments could have the aim to determine and optimize of the capture reagent buffer as well as the sample buffer solutions by testing different possibilities suggested in the literature [83][170].

The life cycle assessment presented in the last chapter confirms the low environmental impact of the nitrocellulose support of the biosensor regards to embodied energy and carbon footprint and compared to a conventional substrate material for such application, i.e. PDMS. Despite this positive result, this paper-based biosensor will not simply be biodegradable due to the bio-contamination concerns that are subject to directives but also due to the need for a polymer support to ensure the sensor is well maintained and easy to use. However biodegradable bioplastics may be further studied as a possible suitable alternative to the current polyester backing.

It has not be confirmed in this work but from research, lateral flow assay such as the studied biosensor is expected to have a relatively low sensitivity. Treatments and methods may be applied to improve performance but that will limit its applications. This technique, on the other hand, is small, portable, inexpensive compared to other ones and provides near real-time data. In addition, its low environmental impact makes its single use acceptable. It is a matter of compromise and in this context, this sensor should preferably be used as an early warning detection system able to efficiently and accurately detect suspicious sources of harmful bacteria or viruses without the need of centralized laboratories.

Bibliography

[1] K. Mao, H. Zhang, and Z. Yang. Can a paper-based device trace covid-19 sources with wastewater-based epidemiology? *Environmental Science & Technology*, 54(7):3733–3735, 2020. PMID: 32202421.

[2] O. Lazcka, F. Javier Del Campo, and F. Xavier Munoz. Pathogen detection: A perspective of traditional methods and biosensors. *Elsevier*, 2006.

[3] Lumen. Counting bacteria - boundless microbiology. `https://courses.lumenlearning.com/boundless-microbiology/chapter/counting-bacteria/`. Accessed: 2020-02-05.

[4] Pcr cycling parameters–six key considerations for success. `https://www.thermofisher.com/be/en/home/life-science/cloning/cloning-learning-center/invitrogen-school-of-molecular-biology/pcr-education/pcr-reagents-enzymes/pcr-cycling-considerations.html`. Accessed: 2020-05-14.

[5] An introduction to elisa (part 2). `https://www.antibodies-online.com/resources/17/1464/an-introduction-to-elisa-part-2/`. Accessed: 2020-05-14.

[6] L. Váradi, J. Lin Luo, D. E. Hibbs, J. D. Perry, R. J. Anderson, S. Orenga, and P. W. Groundwater. Methods for the detection and identification of pathogenic bacteria: past, present, and future. *Chem. Soc. Rev.*, 46:4818–4832, 2017.

[7] M. Eshrat, E. Alahi, and S. Chandra Mukhopadhyay. Detection methodologies for pathogen and toxins: A review. *Sensors*, 17, 2017.

[8] M. Asal, Ö. Özen, M. Şahinler, H. Tahsin Baysal, and İ. Polatoğlu. An overview of biomolecules, immobilization methods and support materials of biosensorss. *Sensor Review*, 2018. Accessed: 2019-11-19.

[9] ElProCus. What is a biosensor, types of biosensors and applications. `https://www.elprocus.com/what-is-a-biosensor-types-of-biosensors-and-applications/`. Accessed: 2020-03-30.

[10] V. Perumal and U. Hashim. Advances in biosensors: principle, architecture and applications, 2019.

[11] M. Marazuela and M. Moreno-Bondi. Fiber-optic biosensors – an overview. *Anal Bioanal Chem*, 372:664–682, 2002.

[12] A. Leprince. Group meeting spring session 2020 - phages infecting the bacillus cereus group : Rbps identification, 2020.

[13] G. P. Salmond and P. C. Fineran. A century of the phage: past, present and future. *Nature reviews microbiology*, page 777–786, 2015.

[14] M. Nuytten. Molecular characterization of phage deep-purple infecting the bacillus cereus group, 2020.

[15] M. Tolba, M. Uddin Ahmed, C. Tlili, F. Eichenseher, M. J. Loessner, and M. Zourob. A bacteriophage endolysin-based electrochemical impedance biosensor for the rapid detection of listeria cells. *Analyst*, 137:5749–5756, 2012.

[16] Wikipedia. Antibody. `https://en.wikipedia.org/wiki/Antibody`. Accessed: 2020-02-06.

[17] Y. He, J. E. Keen, R. B. Westerman, E. T. Littledike, and J. Kwang. Monoclonal antibodies for detection of the h7 antigen of escherichia coli. *Applied and Environmental Microbiology*, 62(9):3325–3332, 1996.

[18] Q. Shi, J. Huang, Y. Sun, M. Yin, M. Hu, X. Hu, Z. Zhang, and G. Zhang. Utilization of a lateral flow colloidal gold immunoassay strip based on surface-enhanced raman spectroscopy for ultrasensitive detection of antibiotics in milk. *Spectrochimica Acta Part A: Molecular and Biomolecular Spectroscopy*, 197:107 – 113, 2018. Festschrift in honor of Prof. Yukihiro Ozaki.

[19] S. Kumar, P. Bhushan, V. Krishna, and S. Bhattacharya. Tapered lateral flow immunoassay based point-of-care diagnostic device for ultrasensitive colorimetric detection of dengue ns1. *Biomicrofluidics*, 12(3):034104, 2018.

[20] Fu Q. Xie J. et al. Chen, Y. Development of a high sensitivity quantum dot-based fluorescent quenching lateral flow assay for the detection of zearalenone. *Anal Bioanal Chem*, 411:2169–2175, 2019.

[21] G. Le Brun. Proposal application form [fria-b1 2019], 2019.

[22] F. Cui, Y. Xu, R. Wang, H. Liu, L. Chen, Q. Zhang, and X. Mu. Label-free impedimetric glycan biosensor for quantitative evaluation interactions between pathogenic bacteria and mannose. *Biosensors and Bioelectronics*, 103:94 – 98, 2018.

[23] A. Ahmed, J. V. Rushworth, N. A. Hirst, and P. A. Millner. Biosensors for whole-cell bacterial detection. *Clinical Microbiology Reviews*, 27(3):631–646, 2014.

[24] V. Cantale. *Towards label-free biosensors based on localized surface plasmon resonance.* PhD thesis, 03 2011.

[25] Markets and Markets. Microfluidics market worth $63.05 billion by 2027, at a cagr of 22.6%. `https://www.marketsandmarkets.com/PressReleases/microfluidics.asp`. Accessed: 2020-02-22.

[26] A. Borbath, M. Gonzalez, and E. Masarweh. Digital microfluidic biochips for single-cell applications in diagnostics, 2019.

[27] ElveFlow. How to generate droplets with a glass microfluidic droplet generation pack. https://www.elveflow.com/microfluidic-applications/setup-droplet-and-digital-microfluidics/microfluidic-droplet-chip/. Accessed: 2020-03-30.

[28] InSITE. Microfluidics – small devices with big potential. https://www.insitefellows.org/microfluidics-small-devices-with-big-potential/. Accessed: 2020-05-23.

[29] Instructables. Paper microfluidic devices. https://www.instructables.com/id/Paper-Microfluidic-Devices/. Accessed: 2020-05-23.

[30] A. Alrifaiy, O. A. Lindahl, and K. Ramser. Polymer-based microfluidic devices for pharmacy, biology and tissue engineering. *Polymers*, 4(3):1349–1398, 2012.

[31] M. A. Lake, C. E. Narciso, K. R. Cowdrick, T. J. Storey, J. J. Zartman S. Zhang, and D. J. Hoelzle. Microfluidic device design, fabrication, and testing protocols, 2015.

[32] D. Gosselin. Vers un dispositif de diagnostic point of care intégré: utilisation de la capillarité ainsi que des procédés de thermoformage et de sérigraphie, October 2017.

[33] T-F. Hong, W-J. Ju, M-C. Wu, C-H. Tai, C. Tsai, and L-M. Fu. Rapid prototyping of pmma microfluidic chips utilizing a co2 laser. *Microfluidics and Nanofluidics*, 9:1125–1133, 12 2010.

[34] C-W. Tsao. Polymer microfluidics: Simple, low-cost fabrication process bridging academic lab research to commercialized production. *Micromachines*, 7, 2016.

[35] C. Iliescu, H. Taylor, M. Avram, J. Miao, and S. Franssila. A practical guide for the fabrication of microfluidic devices using glass and silicon. *Biomicrofluidics*, 2012.

[36] ElveFlow. Materials for microfluidic chips fabrication: a review 2017. *ElveFlow*, 2017.

[37] Y. Ma, X. Cao, X. Feng, Y. Ma, and H. Zou. Fabrication of super-hydrophobic film from pmma with intrinsic water contact angle below 90°. *Elsevier*, 2007.

[38] Kayaku Advanced Materials. Su-8. https://kayakuam.com/products/su-8-photoresists/. Accessed: 2019-12-05.

[39] Z. Gao, D. B. Henthorn, and C-S. Kim. Enhanced wettability of su-8 photoresist through a photografting procedure for bioanalytical device applications. *J Micromech Microeng.*, 2009.

[40] Elveflow. Pdms: A review. https://www.elveflow.com/microfluidic-tutorials/microfluidic-reviews-and-tutorials/the-poly-di-methyl-siloxane-pdms-and-microfluidics/. Accessed: 2019-11-19.

[41] T. Fujii. Pdms-based microfluidic devices for biomedical applications. *Microelectronic Engineering*, 2002.

[42] Fluigent. How to choose a microfluidic chip? `https://www.fluigent.com/microfluidic-expertise/what-is-microfluidic/how-to-choose-a-microfluidic-chip/`. Accessed: 2019-11-19.

[43] A. Sabbah, A. Youssef, and P. Damman. Superhydrophobic surfaces created by elastic instability of pdms. *Applied Sciences*, 2016.

[44] A. E. Ismail, G. S. Grest, D. R. Heine, Mark J. Stevens, and Mesfin Tsige. Interfacial properties of pdms-water systems, 2006.

[45] J. E. Mark. *Polymer Data Handbook*. 1999.

[46] K. Ren, J. Zhou, and H. Wu. *Materials for Microfluidic Chip Fabrication*, volume 46. Accounts of Chemical Research, 11 2013.

[47] S. Bhattacharya, A. Kumar Agarwal, N. Chanda, A. Pandey, and A. Kumar Sen. *Environmental, Chemical and Medical Sensors*. Springer, 2018.

[48] L. Winandy, F. Hilpert, O. Schlebusch, and R. Fischer. Comparative analysis of surface coating properties of five hydrophobins from aspergillus nidulans and trichoderma reseei. *Scientific Reports*, 8, 12 2018.

[49] C.M.S Vicente, P.S. André, and R.A.S. Ferreira. Simple measurement of surface free energy using a web cam. *Revista Brasileira de Ensino de Fisica*, 34:1 – 5, 09 2012.

[50] Y. Xu, X. Hu, S. Kundu, A. Nag, N. Afsarimanesh, S. Sapra, S. Chandra Mukhopadhyay, and T. Han. Silicon-based sensors for biomedical applications: A review. *Sensors*, 19, 2019.

[51] F. Karbassian. *Porous Silicon*. IntechOpen, 2018.

[52] Y. He. Lateral porous silicon membranes for planar microfluidic applications, 2016.

[53] S. Dhanekar and S. Jain. Porous silicon biosensor: Current status. *Elsevier, Biosensors and Bioelectronics*, 41, 2013.

[54] K. Rahmouna, H.I. Faraouna, G. Bassoub, C. Mathieuc, and N.E. Chabane Sari. Determination of mechanical properties of porous silicon with image analysis and finite element. *Elsevier*, 2014.

[55] S. Azimi, Z. Dang, C. Zhang, J. Song, M. Breese, C. H. Sow, J. van Kan, and J. van der Maarel. Buried centimeter-long micro- and nano-channel arrays in porous silicon and glass. *Lab on a Chip*, 2014.

[56] L. Jiang, S. Li, J. Wang, L. Yang, Q. Sun, and Z. Li. Surface wettability of oxygen plasma treated porous silicon. *Journal of nanomaterials*, 01 2014.

[57] Y-S. Lin, C-H. Yang, C-Y. Wang, R-R. Chang, K-S. Huang, and W-C. Hsieh. An aluminum microfluidic chip fabrication using a convenient micromilling process for fluorescent poly(dl-lactide-co-glycolide) microparticle generation. *Sensors*, 2012.

[58] Bhattacharya J., Kisner A., Offenhäusser A., and Wolfrum B. Microfluidic anodization of aluminum films for the fabrication of nanoporous lipid bilayer support structures. *Beilstein J Nanotechnol.*, 2011.

[59] P. R. Solanki, A. Kaushik, V. Agrawal, and B. D. Malhotra. Nanostructured metal oxide-based biosensors. *NPG Asia Mater*, 2011.

[60] The Engineering Toolbox. Young's modulus - tensile and yield strength for common materials. `https://www.engineeringtoolbox.com/young-modulus-d_417.html`. Accessed: 2020-01-16.

[61] K. D. Sattler. *Nanotubes and Nanowires*. 2010.

[62] S. Gim, K.J. Cho, H. Lim, and et al. Structure, dynamics, and wettability of water at metal interfaces. *Sci Rep*, 9, 2019.

[63] P. Mostafalu, M. Akbari, K. Alberti, and et al. A toolkit of thread-based microfluidics, sensors, and electronics for 3d tissue embedding for medical diagnostics. *Microsyst Nanoeng*, 2, 2016.

[64] A. Nilghaz, D. R. Ballerini, and W. Shen. Exploration of microfluidic devices based on multi-filament threads and textiles: A review. *Biomicrofluidics*, 2013.

[65] G. Kharkova, O. Kononova, A. Krasnikovs, M. Eiduks, E. Machanovskis, and K. Dzelzitis. Elastic properties of cotton fabric based polymer composities. *Engineering for Rural Development*, 2011.

[66] H. Dave, L. Ledwani, N. Chandwani, N. Chauhan, and S. Nema. The removal of impurities from gray cotton fabric by atmospheric pressure plasma treatment and its characterization using atr-ftir spectroscopy. *Journal of the Textile Institute*, 105, 09 2013.

[67] B. Cortese, D. Caschera, F. Federici, G. Ingo, and G. Gigli. Superhydrophobic fabrics for oil/water separation through a diamond like carbon (dlc) coating. *Journal of Materials Chemistry A*, 2:6781, 03 2014.

[68] Ryan P. Tortorich, H. Shamkhalichenar, and J-W. Choi. Inkjet-printed and paper-based electrochemical sensors. *Applied Sciences, An Open Access Journal from MDPI*, 8(288), 2018.

[69] Elveflow. Paper microfluidic devices : A review 2017. `https://www.elveflow.com/microfluidic-tutorials/microfluidic-reviews-and-tutorials/paper-microfluidic-devices-a-review-2017/`. Accessed: 2019-11-19.

[70] PrintWiki – the Free Encyclopedia of Print. Porosity. `http://printwiki.org/Porosity?viewType=Print&viewClass=Print`. Accessed: 2019-11-19.

[71] A. Tribhuwan Singh, D. Lantigua, A. Meka, S. Taing, M. Pandher, and G. Camci-Unal. Paper-based sensors: Emerging themes and applications. *Lab Chip*, 2018.

[72] A. Liukkonen. Contact angle of water on paper components: Sessile drops versus environmental scanning electron microscope measurements. *Applications*, 19:411–415, 1997.

[73] J. Qin Y. Lu, W. Shi and B. Lin. Fabrication and characterization of paper-based microfluidics prepared in nitrocellulose membrane by wax printing. *Analytical Chemistry*, 82(1), 2010.

[74] F. allah, M. Khorasani, and M. Ebrahimi. Improving the mechanical properties of waterborne nitrocellulose coating using nano-silica particles. *Elsevier*, 109:110–116, 2017.

[75] P. He, I.N. Katis, R.W. Eason, and C.L. Sones. Rapid prototyping of microfluidic channels in nitrocellulose using laser-direct-write patterning. In *SPIE Photonics West - Microfluidics, BioMEMS, and Medical Microsystems XIII (12/02/15)*, February 2015. BO208-2.

[76] M. Ferrari, L. Liggieri, and R. Miller. *Drops and Bubbles in Contact with Solid Surfaces*. 04 2016.

[77] K. V. Nemani, K. L. Moodie, J. B. Brennick, A. Su, and B. Gimi. In vitro and in vivo evaluation of su-8 biocompatibility. *Elsevier*, 33, 2013.

[78] B. A. Morris. 8 - barrier. In Barry A. Morris, editor, *The Science and Technology of Flexible Packaging*, Plastics Design Library, pages 259 – 308. William Andrew Publishing, Oxford, 2017.

[79] A. M. López-Marzoa and A. Merkoçi. Paper-based sensors and assays: a success of the engineering design and the convergence of knowledge areas. *Lab Chip*, 16, 2016.

[80] A. Goel, M. Tzanakakis, S. Huang, S. Ramaswamy, D. Choi, and B. Ramarao. Characterization of the three-dimensional structure of paper using x-ray microtomography. *TAPPI Engineering Conference*, 84:407–411, 01 2000.

[81] The Fiber Wire. The three p's: Porosity, permeability and permeance. `https://thefiberwire.com/2016/04/07/the-three-ps-porosity-permeability-and-permeance/`. Accessed: 2020-05-03.

[82] G. E. Fridley, C. A. Holstein, S. B. Oza, and P. Yager. The evolution of nitrocellulose as a material for bioassays. *MRS BULLETIN*, 38, 2013.

[83] EMD Millipore. Rapid laterial flow test strips - considereations for product development, 2013.

[84] A. Riau, D. Mondal, G. Yam, M. Setiawan, B. Liedberg, S. Venkatraman, and J. Mehta. Surface modification of pmma to improve adhesion to corneal substitutes in a synthetic core–skirt keratoprosthesis. *ACS applied materials interfaces*, 7, 09 2015.

[85] S. Devikala, P. Kamaraj, and M. Arthanareeswari. Conductivity and dielectric studies of pmma composites. *Chemical Science Transactions*, 2013.

[86] H. Q. Zhang et al. The optical and electrical characteristics of pmma film prepared by spin coating method. *IOP Conference Series: Materials Science and Engineering*, 87, 2015.

[87] A. Altuna, L. Menendez de la Prida, E. Bellistri, G. Gabriel, A. Guimera, J. Berganzo, R. Villa, and L. J. Fernandez. Su-8 based microprobes with integrated planar electrodes for enhanced neural depth recording. *Elsevier*, 37, 2012.

[88] T. A. Anhøj. Fabrication of high aspect ratio su-8 structures for integrated spectrometers., 2007.

[89] J. Nicolás Cabrera, M. M. Ruiz, M. Fascio, N. D'Accorso, R. Mincheva, L. Lizarraga P. Dubois, and R. Martín Negri. Increased surface roughness in polydimethylsiloxane films by physical and chemical methods. *Polymers*, 9, 08 2017.

[90] P. Du, X. Lin, and X. Zhang. Characterization on the electrical properties of pdms nanocomposites by conducting polymer nanowires. *MRS Proceedings*, 1312, 11 2010.

[91] E. Pereira da Silva, M. Chaves, G. Junior da Silva, L. Baldo de Arruda, P. Noronha Lisboa-Filho, S. Frederick Durrant, and J. Roberto Ribeiro Bortoleto. Al-doping effect on the surface morphology of zno films grown by reactive rf magnetron sputtering. *Materials Sciences and Applications*, 4, 2013.

[92] The Physics Factbook. Resistivity of glass. `https://hypertextbook.com/facts/2004/JaneGolubovskaya.shtml`. Accessed: 2020-01-24.

[93] CsgNetwork. Dielectric constants of various materials table. `http://www.csgnetwork.com/dieconstantstable.html`. Accessed: 2020-01-28.

[94] Dielectric constants of common materials. `https://www.kabusa.com/Dilectric-Constants.pdf`. Accessed: 2020-01-28.

[95] Wikipedia. Silicon. `https://en.wikipedia.org/wiki/Silicon`. Accessed: 2020-01-24.

[96] Virginia Semiconductor. The general properties of si, ge, sige, sio2 and si3n4, 2002.

[97] Karim M., Martini R., Radhakrishnan HS., and et al. Tuning of strain and surface roughness of porous silicon layers for higher-quality seeds for epitaxial growth. *Nanoscale Res Lett.*, 9, 2014.

[98] P. Sarafis and A. Galiouna Nassiopoulou. Dielectric properties of porous silicon for use as a substrate for the on-chip integration of millimeter-wave devices in the frequency range 140 to 210 ghz. *Nanoscale Res Lett*, 2014.

[99] E Lee et al. A study on the surface shape and roughness of aluminum alloy for heat exchanger using ball end milling. *IOP Conf. Ser.: Mater. Sci. Eng.*, 88, 2015.

[100] CPLabSafety. Aluminum chemical compatibility. `https://www.calpaclab.com/aluminum-chemical-compatibility-chart/`. Accessed: 2020-05-03.

[101] Dr. Helmenstine. Table of electrical resistivity and conductivity. `https://www.thoughtco.com/table-of-electrical-resistivity-conductivity-608499`. Accessed: 2020-01-24.

[102] D. Tobjörk and R. Österbacka. Paper electronics. *Advanced Materials*, 23, 2011.

[103] P. Sirviö. Electrical and dielectric properties of uncoated and coated wood-free paper for electrophotography. 2016.

[104] The Engineering ToolBox. Relative permittivity - the dielectric constant. https://www.engineeringtoolbox.com/relative-permittivity-d_1660.html. Accessed: 2020-01-28.

[105] J. Italo, L. Amaro, D. Caina, C. Cakmak, N.Marchal, S. Massar, and T. Bertrand. Fabrication of low-cost biosensor on paper substrate by inkjet printing, May 2019.

[106] Sciencemadness. Nitrocellulose. http://www.sciencemadness.org/smwiki/index.php/Nitrocellulose. Accessed: 2019-12-19.

[107] M. Hauwaert. Towards the design of a paper-based electrical sensor for water quality monitoring and usage perspectives, 2020.

[108] Cefic. Poly methyl methacrylate (pmma): Eco-profiles and environmental product declarations of the european plastics manufacturers, 2016.

[109] PMMA online. Pmma, sustainability. https://www.pmma-online.eu/sustainability/. Accessed: 2019-12-19.

[110] Boustead for PlasticsEurope. Liquid epoxy resins, 2005.

[111] A.D. La Rosa. 4 - life cycle assessment of biopolymers. In Fernando Pacheco-Torgal, Volodymyr Ivanov, Niranjan Karak, and Henk Jonkers, editors, *Biopolymers and Biotech Admixtures for Eco-Efficient Construction Materials*, pages 57 – 78. Woodhead Publishing, 2016.

[112] B. Brandt, E. Kletzer, H. Pilz, D. Hadzhiyska, and P. Seizov. Silicon-chemistry carbon balance an assessment of greenhouse gasemissions and reductions, 2012.

[113] Eco USA. Polydimethylsiloxane. http://www.siliconerecycling.com/polydimethylsiloxane/. Accessed: 2019-11-19.

[114] Silicones Health and Silicone Industry Association of Japan Safety Council of North America, Centre Europeen Des Silicones. Environmental fate and effects of pdms, Undated.

[115] AGC Glass Europe. Our environmental impact. https://www.agc-glass.eu/en/sustainability/environmental-achievements/environmental-impact. Accessed: 2019-11-19.

[116] V. Carrillo Usbeck, J. Pflieger, T. Sun, and PE International AG. Life cycle assessment of float glass, 2010.

[117] Glass Alliance Europe. Glass sustainability the environment. http://www.siliconerecycling.com/polydimethylsiloxane/. Accessed: 2019-11-19.

[118] EGTEI. Guidance document on control techniques for emissions of sulphur, nox, vocs, dust (including pm10, pm2.5 and black carbon) from stationary sources, 2012.

[119] T. Norgate, S. Jahanshahi, and W. Rankin. Assessing the environmental impact of metal production processes. *Journal of Cleaner Production*, 15:838–848, 10 2006.

[120] A. Margrét Kornelíusdóttir. A cradle-to-gate life cycle assessment of primary aluminium production at norðurál, 2014.

[121] Wise Geek. How is nylon made. `https://www.wisegeek.com/how-is-nylon-made.htm`. Accessed: 2020-02-11.

[122] Nitro Quimica. Sustainability report 2016, 2016.

[123] Y. Fan. Low-cost microfluidics: Materials and methods. *Micro Nano Letters*, 2016.

[124] Euroscientist. Paper biosensors: towards eco-friendly diagnosis. `https://www.euroscientist.com/paper-biosensors/`. Accessed: 2020-04-30.

[125] J. Zdarta, A. Meyer, T. Jesionowski, and M. Pinelo. A general overview of support materials for enzyme immobilization: Characteristics, properties, practical utility. *Catalysts*, 8:92, 02 2018.

[126] R. Cao, L. Guan, M. Li, J. Tian, and W. Shen. A zero-step functionalization on paper-based biosensing platform for covalent biomolecule immobilization. *Sensing and Bio-Sensing Research*, 6:13 – 18, 2015.

[127] A. Böhm, S. Trosien, O. Avrutina, H. Kolmar, and M. Biesalski. Covalent attachment of enzymes to paper fibers for paper-based analytical devices. *Frontiers in Chemistry*, 6:214, 2018.

[128] A. W. Martinez, S. T. Phillips, G. M. Whitesides, and E. Carrilho. Diagnostics for the developing world: Microfluidic paper-based analytical devices. *Analytical Chemistry*, 82(1):3–10, 2010. PMID: 20000334.

[129] Recent advances in high-sensitivity detection methods for paper-based lateral-flow assay. *Biosensors and Bioelectronics*, 152:112015, 2020.

[130] R. Tang, H. Yang, J. Ru Choi, Y. Gong, J. Hu, S. Feng, B. Pingguan-Murphy, Q. Mei, and F. Xu. Improved sensitivity of lateral flow assay using paper-based sample concentration technique. *Elsevier*, 2016.

[131] S-F. Zhang, L-N. Liu, R-H. Tang, Z. Liu, X-C. He, Z-G. Qu, and F. Li. Sensitivity enhancement of lateral flow assay by embedding cotton threads in paper. *Springer*, 2019.

[132] Inc. TechNote 303 Bangs Laboratories. Lateral flow tests. 2013.

[133] X. Zhu, P. Shah, S. Stoff, H. Liu, and C-Z. Li. A paper electrode integrated lateral flow immunosensor for quantitative analysis of oxidative stress induced dna damage. *Analyst*, 139:2850–2857, 2014.

[134] Sudeshna P., Evangelyn C. A., and Frances P. D. Nanowire labeled direct-charge transfer biosensor for detecting bacillus species. *Biosensors and Bioelectronics*, 22(9):2329 – 2336, 2007. Selected Papers from the Ninth World Congress On Biosensors. Toronto, Canada 10 - 12 May 2006.

[135] Xun M., Meenu B., Anant S. G., Yuehe L., and Guodong L. Multiplex electrochemical immunoassay using gold nanoparticle probes and immunochromatographic strips. *Electrochemistry Communications*, 10(10):1636 – 1640, 2008.

[136] Y. Luo, S. Nartker, M. Wiederoder, H. Miller, D. Hochhalter, L. Drzal, and E. Alocilja. Novel biosensor based on electrospun nanofiber and magnetic nanoparticles for the detection of e. coli o157:h7. *IEEE Transactions on Nanotechnology*, 11:676–681, 07 2012.

[137] Prof M. Lindström. Pulp and paper production, lecture ke2310, kth, 2019.

[138] M. A. Mansfield. Chapter 6: Nitrocellulose membranes for lateral flow immunoassays: A technical treatise. *Lateral Flow Immunoassay*, 2009.

[139] R. Leenaerts. *La filtration industrielle des liquides: Chapitre Deuxième - La porosité*. Société belge de filtration.

[140] A. El Ghouch. Lfsab1105 - probabilité et statistiques, 2017-2018.

[141] J. Vanderschuren. *La filtration industrielle des liquides: Chapitre Troisième - Ecoulement des fluides dans les milieux poreux*. Société belge de filtration.

[142] ThoughtCO. Capillary action: Definition and examples. `https://www.thoughtco.com/definition-of-capillary-action-604866`. Accessed: 2019-11-19.

[143] P. Luis. Lmapr 2647 - sustainable treatment of industrial and domestic waste - composition wastewater presentation, 2015.

[144] M. M. Gong and D. Sinton. Turning the page: Advancing paper-based microfluidics for broad diagnostic application. *Chemical Reviews*, 117, 2017.

[145] G. Le Brun and Pr. J-P. Raskin. Disposable paper-based bacteria sensor for water quality monitoring, 2019.

[146] Wikipedia. Young-laplace equation. `https://en.wikipedia.org/wiki/Young%E2%80%93Laplace_equation`. Accessed: 2019-12-02.

[147] C. K. Camplisson, K. M. Schilling, W. L. Pedrotti, H. A. Stone, and A. W. Martinez. Two-ply channels for faster wicking in paper-based microfluidic devices. *Lab Chip*, 15:4461–4466, 2015.

[148] E. Elizalde, R. Urteaga, and C. L. A. Berli. Rational design of capillary-driven flows for paper-based microfluidics. *Lab Chip*, 15:2173–2180, 2015.

[149] S. Hong and W. Kim. Dynamics of water imbibition through paper channels with wax boundaries. *Microfluidics and Nanofluidics*, 19:845–853, 10 2015.

[150] M. Rasi. Permeability properties of paper material, 2013.

[151] R. Masoodi and K. M. Pillai. Darcy's law-based model for wicking in paper-like swelling porous media. *AIChE Journal*, 56(9):2257–2267, 2010.

[152] COMSOL Multiphysics 5.5. Wicking in a paper strip.

[153] H. Brooks and A. T. Corey. Properties of porous media affecting fluid flow. *Journal of the Irrigation and Drainage Division Proceedings of the American Society of Civil Engineers*, pages 61–88, 1966.

[154] C. Belleudy, M. Woloszyn, M. Chhay, and M. Cosnier. A 2d model for coupled heat, air, and moisture transfer through porous media in contact with air channels. *International Journal of Heat and Mass Transfer*, 95:453 – 465, 2016.

[155] C-H. Ku and R-J. Yang. A new method for paper porosity estimation. *TechConnect Briefs*, pages 194–197, 2018.

[156] Y. Basso-Bert and Q. Perrin. Par 135 : Microtechnologies souples intégrées sur papier. génération de capteurs chimiques flexibles bas coût, 2019.

[157] L. Greenspan. Humidity fixed points of binary saturated aqueous solutions. *JOURNAL OF RESEARCH of the National Bureau of Standards*, 81A:89–96, 10 1976.

[158] G. Le Brun. Compte-rendu - observation d'une membrane de nitrocellulose fonctionnalisée avec des anticorps and expériences sem, 2019.

[159] R. Y. Tsien. The green fluorescent protein. *Annu. Rev. Biochem.*, pages 509–544, 1998.

[160] Thorlabs. Laser scanning microscopy tutorial. `https://www.thorlabs.com/tutorials.cfm?tabID=8ed9f76d-3bbd-4e6c-b2f5-f6a89a2c4fc9`. Accessed: 2020-03-08.

[161] KRÜSS. Confocal microscopy. `https://www.kruss-scientific.com/services/education-theory/glossary/confocal-microscopy/`. Accessed: 2020-03-09.

[162] R. Deegan, O. Bakajin, T. Dupont, and et al. Capillary flow as the cause of ring stains from dried liquid drops. *Nature*, 389:827–829, 1997.

[163] Y. Ooi, I. Hanasaki, D. Mizumura, and Y. Matsuda. Suppressing the coffee-ring effect of colloidal droplets by dispersed cellulose nanofibers. *Science and Technology of Advanced Materials*, 18(1):316–324, 2017. PMID: 28567177.

[164] H. Hu and R. G. Larson. Marangoni effect reverses coffee-ring depositions. *The Journal of Physical Chemistry B*, 110(14):7090–7094, 2006. PMID: 16599468.

[165] N. Walji and B. MacDonald. Influence of geometry and surrounding conditions on fluid flow in paper-based devices. *Micromachines*, 7(5):73, Apr 2016.

[166] E. Fua, S. A. Ramseyb, P. Kauffmana, B. Lutza, and P. Yagera. Transport in two-dimensional paper networks. *Microfluid Nanofluidics*, 10, 2011.

[167] A. Böhm, F. Carstens, C. Trieb, S. Schabel, and M. Biesalski. Engineering microfluidic papers: Effect of fiber source and paper sheet properties on capillary-driven fluid flow. *Microfluidics and Nanofluidics*, 16:789–799, 05 2014.

[168] S. Hong and W. Kim. Dynamics of water imbibition through paper channels with wax boundaries. *Microfluidics and Nanofluidics*, 19:845–853, 2015.

[169] E. Fu, T. Liang, J. Houghtaling, S. Ramachandran, S. A Ramsey, B. Lutz, and P. Yager. Enhanced sensitivity of lateral flow tests using a two-dimensional paper network format. *Analytical chemistry*, 83(20):7941—7946, October 2011.

[170] J. Li, D. McMillan, and J. Macdonald. Enhancing the signal of lateral flow immunoassays by using different developing methods. *Sensors and Materials*, 27:549–561, 06 2015.

[171] X. Yan and K. Persaud. The optimization of a lateral flow immunoassay for detection of aflatoxin b 1 in potable water samples. *IEEE Sensors Journal*, PP:1–1, 10 2018.

[172] A. Umer, K. Hewage, H. Haider, and R. Sadiq. Sustainability evaluation framework for pavement technologies: An integrated life cycle economic and environmental trade-off analysis. *Elsevier*, 2017.

[173] M. Vervaeke. Life cycle assessment software for product and process sustainability analysis. *Journal of Chemical Education*, 2012.

[174] P. Luis. Lmapr 2648 - case studies of sustainable treatment of industrial and domestic waste, 2015.

[175] United Nations. Sustainable development goals. `https://sustainabledevelopment.un.org/sdgs`. Accessed: 2020-03-31.

[176] A. Augusto Morini, M. J. Ribeiro, and D. Hotza. Early-stage materials selection based on embodied energy and carbon footprint. *Materials Design*, 178:107861, 2019.

[177] Morbidity and Mortality Weekly Report. Current trends recommended guidelines for disposing of nitrocellulose membranes. `https://www.cdc.gov/mmwr/preview/mmwrhtml/00000630.htm`. Accessed: 2020-05-13.

[178] M. Ndiaye, N. and Bernier and R. Zmeureanu. Evaluation of the embodied energy in building materials and related carbon dioxide emissions in senegal. 09 2005.

[179] K. Einar Rosendahl E. Gavenas and T. Skjerpen. Co2-emissions from norwegian oil and gas extraction, 2015.

[180] T. Brown. Round-trip efficiency of ammonia as a renewable energy transportation media. `https://www.ammoniaenergy.org/articles/round-trip-efficiency-of-ammonia-as-a-renewable-energy-transportation-media/`. Accessed: 2020-05-13.

[181] Emission factors in kg co2-equivalent per unit. `https://winnipeg.ca/finance/findata/matmgt/documents/2012/682-2012/682-2012_Appendix_H-WSTP_South_End_Plant_Process_Selection_Report/Appendix%207.pdf`. Accessed: 2020-05-13.

[182] J. Adetayo Adeniran, R. Olasunkanmi Yusuf, and M. A. L. Adetoro. Life cycle engineering case study: Sulphuric acid production. *Journal of Engineering and Technology*, 8, 2017.

[183] J. Dewilde. Lmapr2430: Basic industrial chemical processes, 2018.

[184] S. Boyd. *Life-Cycle Assessment of Semiconductors*. 03 2011.

[185] E. R. Monazam, R. W. Breault, and R. Siriwardane. Reduction of hematite (fe2o3) to wüstite (feo) by carbon monoxide (co) for chemical looping combustion. *Chemical Engineering Journal*, 242:204 – 210, 2014.

[186] Abstracts of lci's. `http://esu-services.ch/data/abstracts-of-lcis/`. Accessed: 2020-05-13.

[187] E. D. Williams, R. U. Ayres, and M. Heller. The 1.7 kilogram microchip: energy and material use in the production of semiconductor devices. *Environmental Science & Technology*, 36(24):5504–5510, 2002. PMID: 12521182.

[188] V. Rossi and M. Carpenter. Reusable polystyrene wafer coating as an antiadhesive layer for pdms thin film production. *Materials Letters*, 262:127045, 11 2019.

[189] WBCSD chemicals. Life cycle metrics for chemical products, 2015.

[190] Phenol and Acetone Sector Group. Phenol and acetone cefic petrochemicals europe, 2016.

[191] M. Branham. Semiconductors and sustainability : energy and materials use in integrated circuit manufacturing. 06 2009.

[192] L. Burgess for Energy and Capital. Special report: The 5th precious metal: Rhodium. `https://www.energyandcapital.com/report/the-5th-precious-metal-rhodium/1711`. Accessed: 2020-05-13.

[193] V. Beiser. The ultra-pure, super-secret sand that makes your phone possible. `https://www.wired.com/story/book-excerpt-science-of-ultra-pure-silicon/`. Accessed: 2020-05-13.

[194] World Health Organization. Health-care waste. `https://www.who.int/news-room/fact-sheets/detail/health-care-waste`. Accessed: 2020-05-23.

[195] Water Australian Governement Department of Agriculture and the Environment. Sulfuric acid. `http://www.npi.gov.au/resource/sulfuric-acid`. Accessed: 2020-05-13.

[196] Public Health England. Nitric acid. `https://assets.publishing.service.gov.uk/government/uploads/system/uploads/attachment_data/file/659905/Nitric_acid_general_information.pdf`. Accessed: 2020-05-13.

[197] Biodegradable plastics. `https://bioplasticsnews.com/biodegradable-plastics/`. Accessed: 2020-05-16.

[198] European Commission. Waste electrical electronic equipment (weee). `https://ec.europa.eu/environment/waste/weee/index_en.htm`. Accessed: 2020-05-23.

[199] S. RameshKumar, P. Shaiju, K. E. O'Connor, and R. Babu P. Bio-based and biodegradable polymers - state-of-the-art, challenges and emerging trends. *Current Opinion in Green and Sustainable Chemistry*, 21:75 – 81, 2020. New Synthetic methods [U+25CF] Selected papers from the 4th Green and Sustainable Chemistry Conference.

[200] R. A. Gross and B. Kalra. Biodegradable polymers for the environment. *Science*, 297(5582):803–807, 2002.

[201] I. Vroman and L. Tighzert. Biodegradable polymers. *Materials*, 2(2):307–344, 2009.

[202] Q. Shi, J. Huang, Y. Sunc, M. Yinc, M. Huc, X. Huc, Z. Zhang, and G. Zhang. Utilization of a lateral flow colloidal gold immunoassay strip based on surface-enhanced raman spectroscopy for ultrasensitive detection of antibiotics in milk. *Elsevier*, 2017.

UNIVERSITÉ CATHOLIQUE DE LOUVAIN
École polytechnique de Louvain
Rue Archimède, 1 bte L6.11.01, 1348 Louvain-la-Neuve, Belgique | **www.uclouvain.be/epl**